Electronic Theses and Dissertations

2013

Development of a small scale tire for vehicle dynamics research

Sean M. Maloney

Follow this and additional works at: http://scholar.uwindsor.ca/etd

DEVELOPMENT OF A SMALL SCALE TIRE FOR VEHICLE DYNAMICS RESEARCH

by

SEAN M. MALONEY

A Thesis

Submitted to the Faculty of Graduate Studies and Research

through Mechanical, Automotive, & Materials Engineering

in Partial Fulfillment of the Requirements for

the Degree of Master of Applied Science at the

University of Windsor

Windsor, Ontario, Canada

2012

DEVELOPMENT OF A SMALL SCALE TIRE FOR VEHICLE DYNAMICS RESEARCH

by

SEAN M. MALONEY

APPROVED BY:

Dr. N. Kar

Electrical & Computer Engineering

Dr. D. Green

Mechanical, Automotive, & Materials Engineering

Dr. B. Minaker, Advisor

Mechanical, Automotive, & Materials Engineering

Dr. C. Novak, Chair of Defense

Mechanical, Automotive, & Materials Engineering

January 23, 2013

Author's Declaration of Originality

I hereby certify that I am the sole author of this thesis and that no part of this thesis has been published or submitted for publication.

I certify that, to the best of my knowledge, my thesis does not infringe upon anyone's copyright nor violate any proprietary rights and that any ideas, techniques, quotations, or any other material from the work of other people included in my thesis, published or otherwise, are fully acknowledged in accordance with the standard referencing practices. Furthermore, to the extent that I have included copyrighted material that surpasses the bounds of fair dealing within the meaning of the Canada Copyright Act, I certify that I have obtained a written permission from the copyright owner(s) to include such material(s) in my thesis and have included copies of such copyright clearances to my appendix.

I declare that this is a true copy of my thesis, including any final revisions, as approved by my thesis committee and the Graduate Studies office, and that this thesis has not been submitted for a higher degree to any other University or Institution.

Abstract

An approach for developing a tire suitable for performing small scale vehicle dynamics research is discussed. This will allow for physical verification of vehicle dynamics modelling and controls in environments where a full scale prototype is either not feasible or too large an investment. Currently, scale vehicle research is limited by the availability of tires on the desired scale, which are typically sourced from the radio controlled (RC) vehicle industry. Use of these tires, however, results in poor similitude between the representative scale vehicle and the full scale vehicle. This is due to variations in the behaviour of the scale tire to the full scale tire. An existing analytical tire model known as the cornering force self-aligning torque model (CF/SAT), is analyzed and modifications to the model are proposed to allow it to be used for non-dimensional tire parameterization. The model is then non-dimensionalized, using Buckingham Pi theory, to allow for comparison of small scale tire performance to large scale tire performance. A static load-deflection tire testing apparatus named the Windsor Automotive Tire Tester (WATT) is also developed. This machine is used to analyze if it is possible to determine the CF/SAT parameters for a given tire without the use of full scale tire dynamic studies and regression analysis. A DUBRO 5.00 T.V. RC airplane tire is then parameterized and modelled using relationships derived from the static tire data. The results of the tire model are compared with experimental data of the DUBRO 5.00 T.V. tire in order to analyze the effectiveness of the approach. It was found that it was possible to estimate some tire parameters using this method, however, more research is required to fully parameterize the tire using static load-deflection data.

To my parents, for always encouraging my insatiable curiosity.

Acknowledgements

I would like to thank my supervisor Dr. Bruce Minaker. The freedom and support provided by him allowed me to pursue my personal research interests unhindered. The experiences I had as a result of his efforts will have an everlasting effect on me personally and professionally. I am incredibly grateful.

I would also like to thank Dr. Daniel Green. He has been a mentor for me since my very first day in undergraduate education at the University of Windsor. The patience and guidance he provided for me at the early stages of my educational career are what ultimately lead to my decision to pursue graduate level education.

Additionally, I would like to extend my gratitude to my colleagues, Christopher Barks, Hart Honickman, Andre Levesque, and Michael Doody. The heated debates, invaluable guidance, and limitless modes of procrastination provided made this experience a very positive one.

Finally, I would like to thank all of my family, including the Maloneys, Boettgers, and Freunds. All of you have supported me to the fullest through out this time. Any success I have had is equally as much a success on your part. Everything from the kind words, financial assistance and even my various living accommodations have truly made this a possibility for me. I cannot imagine how I would have accomplished this without each of you supporting me. It is your unconditional love and support that inspires me to achieve all that is possible.

Contents

List of Tables

List of Figures

Notation

Label	Description
a_e	Effective tire slip angle
A_{x0}	Self-aligning torque stiffness of the rigid ring model
$c_f, C_{\alpha f}$	Front tire cornering stiffness
B	Pacejka tire model stiffness factor
C	Pacejka tire model shape factor
$c_r, C_{\alpha r}$	Front tire cornering stiffness
C_q	Compliance of front inclination in contact pressure
C_y	Lateral spring constant of tread element
C_z	Overall vertical stiffness of the tire
D	Pacejka tire model peak factor
$Dgsp(t; n, q)$	Generalized skew parabola function
D_ϕ	Effective roll dampening of the suspension in PURRS vehicle model
E	Pacejka model curvature factor
EI_z	Bending rigidity of the belt
f_f, f_r	Front and rear tire force response
F_y	Tire lateral force
F_z	Normal load on tire
g	Gravitational constant in Buckingham example

Label	Description
G_{mz}	Rotational stiffness of the sidewall
h	Mass center height for PURRS vehicle model
h_s	Height of the sprung mass in PURRS vehicle model
I_{xx_s}	Principle mass moment of inertia for sprung mass in the PURRS vehicle model
I_{xz_s}	Sprung mass product of inertia about the roll axis for the PURRS vehicle model
i_z, I_z	Vehicle mass moment of inertia about the vertical axis
I_{zz}, I_{yy}, I_{xx}	Principle mass moments of inertia for PURRS vehicle model
j	Number of Primary dimensions used to define a system
k	Number of non-dimensional parameters
k_y	Overall lateral tire stiffness
K_{y0}	Cornering stiffness of the rigid ring model
K_ϕ	Effective roll stiffness of the suspension in PURRS vehicle model
l	Length of tire contact patch
L	Vehicle wheelbase in IRS and PURRS vehicle model
l_f, a	Distance from front axle to vehicle center of mass
l_h	Boundary between static zone of contact patch to sliding zone
L_n	Dimension of length in Buckingham example
l_r, b	Distance from rear axle to vehicle center of mass
m	Vehicle mass
m_s	Sprung mass for PURRS vehicle model
M_z	Tire self-aligning torque
μ_d	Dynamic coefficient of friction
μ_s	Static coefficient of friction
n	Shoulder coefficient of the generalized skew parabola function
N	Number of parameters to define system response

Label	Description
q	Circumferential asymmetric coefficient of the generalized skew parabola function
r	Yaw rate
R	Radius of corner in IRS vehicle model
R_0	Free tire radius
R_e, r_e	Effective radius of the tire
t	Time
T	Wheel torque in IRS vehicle model
u, U, V_x	Forward vehicle velocity
v, V_y	Lateral vehicle velocity
w	Tire width
w_0	Initial velocity of an object in Buckingham example
x	Pacejka slip quantity
x_c	Steer axis location along length of contact patch
y	Pacejka generated force or moment
z	Vertical height of an object in buckingham pi example
z_0	Initial vertical height of an object in Buckingham example
α	Tire slip angle
α_f, α_r	Front and rear tire slip angle
δ_f, δ_r	Front and rear steer angles
ε	Deflection compliance of tire belt
κ	Slip ratio of the tire
Ω	Angular velocity of the tire
Ω_0	Angular velocity of a free rolling tire
ζ	Compliance of contact patch shift

Chapter 1

Introduction

1.1 Motivation and Purpose

While scale modelling of dynamic systems has found widespread adoption in the aerospace and marine industries, it is a largely under-utilized technique within the automotive industry. The large scale of aircraft and seafaring vessels makes physical experimentation with these vehicles a challenge, if not impossible. By using smaller, but dynamically similar, models of the vehicle to conduct physical verification, the cost associated with these studies is reduced greatly.

Ground vehicles, on the other hand, are much less difficult and costly to instrument in full scale. While OEMs (original equipment manufacturers) of automobiles undoubtedly have ample resources to construct, instrument, and test full size vehicles, academia is much less equipped to deal with this type of testing. Beyond the cost associated with obtaining a full size vehicle and instrumenting it, the availability of an appropriate proving ground and the risk involved with vehicle dynamics trials is typically too great for an academic association to bear. However, the need for these trials is unavoidable in the physical verification of vehicle dynamics models and control algorithms developed by academia. Scale modelling not only offers a cost effective solution, but also significantly reduced risk of injury to the analyst.

The application of scale modelling is not entirely new to the automotive industry; however,

the research that has been conducted in this area is minimal. One of the largest challenges when dealing with scaled ground vehicle models is proper treatment of the tire. The highly non-linear nature of tire response, coupled with the large variety of surfaces to which a tire is subjected, make precise mathematical modelling of the tire extremely challenging. A result of this the majority of studies conducted on the topic of scale vehicle modelling assume simplistic tire models, limiting the efficacy of the approach. The purpose of this research is to explore new avenues by which to treat the tire with respect to scale vehicle modelling, in such a way as to not reduce both the efficacy or practicality of the approach.

1.1.1   Objectives

There are three main objectives that are required in order to fully realize a method to properly develop a small scale tire for vehicle dynamics research. A set of criteria is required by which to evaluate the response characteristics of a tire. This can be accomplished through the selection or development of an appropriate tire model. Once this has been established, the model must be defined non-dimensionally to allow comparison of the dynamic response of the full scale tire to a small scale tire. This is the first objective of the research.

The second objective of this research is to establish a method by which to characterize the physical tire within the selected model. It is imperative the cost associated with this characterization remains low; otherwise, the practicality of a scale vehicle approach diminishes. This requirement prohibits the use of full scale dynamic tire studies due to the exceptional cost associated with such testing. To accomplish this objective the possibility of using a static tire testing approach was investigated.

The complete attainment of these two objectives would allow an analyst to ascertain whether the dynamic response of a small scale tire was similar to that of a desired full scale tire. With this information, a scaled vehicle based on a fully non-linear model can be developed without the limitations associated with linear scale models. New construction of a scale tire that is dynamically

similar to a specific full size tire; however, would further require a third objective, that a relationship is determined between the criteria outlined within the first objective to the specific design elements of the tire. While this final objective is required for the desired goal of this research, it is not attainable within the constructs of this study.

1.2   Structure of the Thesis

The thesis itself is broken up into six major sections. The first chapter introduces the topic of discussion and provides the motivation and objectives of the research. Chapter two discusses and presents the relevant work on the topic of scale vehicle modelling, as well as provides relevant background material for complete understanding of the work presented.

Chapter three deals primarily with the first stated objective, to establish a model by which to describe tire response. An appropriate model is selected and modifications are provided in order to improve its suitability for use as a scale vehicle model. The selected model is then non-dimensionalized to allow comparison of the performance of tires on various scales.

Chapter four details the work done on the development of a system to conduct the required static tire tests for characterization of the developed model. The mechanical design, as well as the electronic design of the machine are detailed. The calibration process and performance of the machine are finally assessed and presented.

Chapter five discusses the results obtained from the studies done with the static tire tester and the results of the estimation of tire parameters from these tests. The manner in which the results are treated to determine parameters for the tire model is presented along with details of the tire's response to the static tests. The results of the parameter estimation are then compared with results obtained from a dynamic tire testing system and manual fitting of the model to the dynamically obtained results.

Chapter six completes the thesis with a discussion of the contributions of the work derived from the results presented within it. The limitations of what can be concluded from these results and what

further research is required to fully realize the goals of this research is also presented.

Chapter 2

Background and Literature Review

2.1 Vehicle Modelling

The ability to model vehicle dynamic response mathematically has been of great interest over the last century, and has grown substantially since the introduction of the automobile. There are many models that exist today to model the behaviour of a vehicle in several contexts; straight line, handling, ride quality or a combination of all. The work presented in this thesis is a small step towards verification of the results predicted by these models through physical testing with scale vehicles. In order to understand that goal we must first look at how the vehicle can be modelled fundamentally. The enormity of this field alone is outstanding, and so, in the interest of brevity, a common vehicle handling model will merely be introduced, as it is referred to periodically throughout this work. The interested reader is encouraged to look at some of the excellent publications for more information on this model specifically, as well as other vehicle models [21, 10].

2.1.1 Vehicle Handling

Perhaps the most well known, and certainly the most common vehicle handling model, is the linear yaw-plane model or bicycle model. The term 'bicycle model' is derived from the simplification that the width of the vehicle has a negligible effect on the vehicle's handling response. Figure 2.1
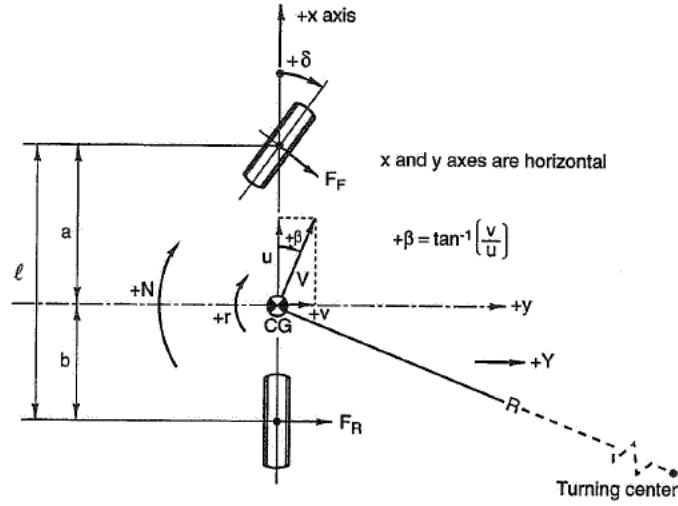
Figure 2.1: *The equivalent system representation of an automobile within the bicycle model.* Reproduced from Miliken [15].

depicts the equivalent system representation of a vehicle in the linear bicycle model.

This two degree of freedom model allows for variation in the vehicle's lateral velocity, v, and yaw rate, r. The forward speed of the vehicle, u, is fixed. The input forces to this system are solely a result of tire force acting at length l_f and l_r from the center of mass to the front and rear axles respectively; aerodynamic effects are ignored. The lumped tire response, f_f and f_r, is assumed to increase linearly with increased tire slip angle, α_f and α_r, as shown in equation (2.1),

$$f_f = -c_f \alpha_f$$
$$f_r = -c_r \alpha_r$$

(2.1)

where c_f and c_r are the front and rear tire 'cornering stiffness' respectively.

A small angle assumption is then applied, such that the tire slip angles can be expressed linearly

as

$$\alpha_f + \delta_f = \frac{v + rl_f}{u}$$
$$\alpha_r + \delta_r = \frac{v - rl_r}{u} \quad (2.2)$$

where δ_f and δ_r are the front and rear steer angles respectively.

Applying the preceding assumptions to Newton's equations results in the equations of motion shown below in equation (2.3) [22], where m is the mass and i_z is the moment of inertia about the vertical axis.

$$\begin{bmatrix} m & 0 \\ 0 & i_z \end{bmatrix} \begin{Bmatrix} \dot{v} \\ \dot{r} \end{Bmatrix} + \begin{bmatrix} \frac{(c_f + c_r)}{u} & \frac{(l_f c_f - l_r c_r)}{u} + mu \\ \frac{(l_f c_f - l_r c_r)}{u} & \frac{(l_f^2 c_f + l_r^2 c_r)}{u} \end{bmatrix} \begin{Bmatrix} v \\ r \end{Bmatrix} = \begin{bmatrix} c_f \\ l_f c_f \end{bmatrix} \begin{Bmatrix} \delta_f \end{Bmatrix} \quad (2.3)$$

Despite the large number of assumptions made during the formulation of this model, it has been found to be very accurate in predicting real world vehicle behaviour in certain situations. The two most important limitations of this model are the small angle assumption and negligence of vehicle width.

The small angle assumption is used to maintain the linearity of the model, as well as remain within the linear region of tire response. In later sections, a more realistic tire response will be presented. Although limited to operate within this regime, this model gives excellent insight into the fundamental handling behaviour of a vehicle.

The width of the vehicle begins to play a much more significant role as vehicle manoeuvres become more aggressive. This is due largely to the non-linear behaviour of the tire. The oversteer/understeer characteristics of the vehicle at high slip angles can be largely influenced by the roll stiffness of the vehicle. The reason for this behaviour will be looked at in more depth in Section 2.2.2

Much of the current research on scale vehicles utilizes this model for the development of the scale test beds, which is why this model was introduced. It is important for the reader to be aware

of their limitations due to this reliance as one reads the subsequent chapters.

2.2 Tires

The world's first pneumatic tire was invented by John Dunlop in 1888 for use on bicycles. It was later applied to an automobile by Andre Michelin in 1895 [1]. Over the next 100 plus years, the tire would undergo many revolutionary changes to become the cutting edge piece of engineering it is today. Aside from aerodynamic forces, the tire is the only available means by which a road vehicle may be controlled. As a result of this, the response of the tire is highly influential on the behaviour of the vehicle. Not only must the tire be capable of generating the required force to manoeuvre the vehicle under vastly different road conditions, but it also must do so in such a way as to not limit its useful service life, generate excessive noise, or transmit undesirable amounts of vibration to the occupants. These highly demanding and sometimes conflicting requirements make tire design a difficult task, and the selection of an appropriate tire for a given application is equally challenging. In order to better understand how the tire affects vehicle performance, the following sections will outline the typical construction of the common tire, tire force response characteristics, as well as various methods for modelling tire force responses.

2.2.1 Construction

In order to meet the desired dynamic performance, wear, and comfort requirements, the pneumatic tire is comprised of several layers, featuring various compounds of rubber, additives, and cords. These many layers work together to control how the tire deforms under various loads, maintain air pressure, and reduce noise and wear of the tire. Figure 2.2 depicts a cut away of a typical modern day radial tire.
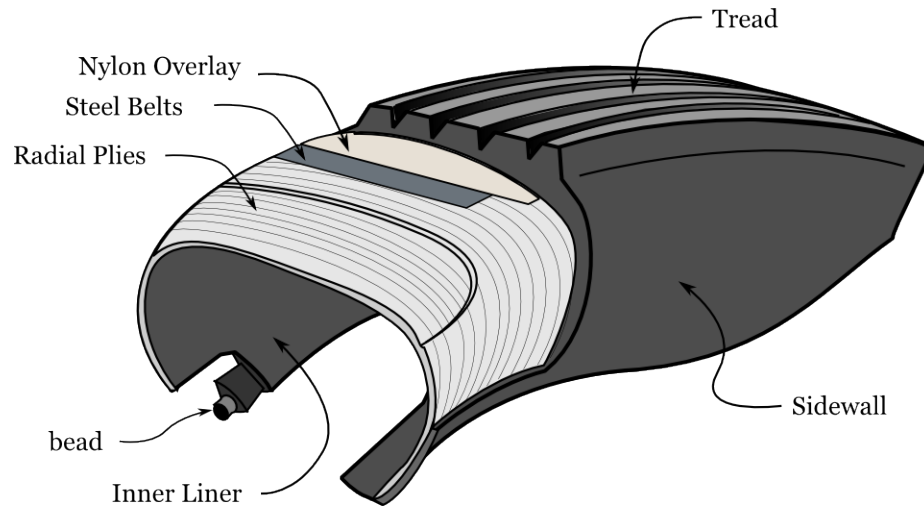
Figure 2.2: *Typical radial tire construction.* Reproduced from Rieveley [22]

Bead

The bead is constructed of several strands of high-tensile strength steel cord formed into a ring around the inner circumference of the tire. The bead provides the tire with hoop strength to seal the tire against the side of the wheel and prevent air leakage. It is typically coated with rubber in order to ensure adhesion between the bead and the tire carcass during construction [23].

Inner Liner

The inner liner is designed to prevent air from permeating out of the tire. It is constructed of a soft, fatigue resistant, durable rubber [23].

Ply Coat

The ply coat consists of rubber coated cords, made from nylon, textile or other high tensile strength material. The plies reinforce the tire and provide adequate resistance to inflation. A radial tire aligns the cords along the radial direction of the tire, while a bias tire runs the ply cords diagonally alternating the orientation by ninety degrees for each layer. The number of cords, their orientation,

and the material they are constructed from has a large influence on the tire's force response and comfort characteristics [23].

Belt Coat

The belts are used to stiffen the tread section of the tire, and are aligned circumferentially around the tire. They are typically made from steel or fiberglass. In most bias ply tires, the belt is absent since tread rigidity is supplied by the ply coat [23].

Sidewall

The sidewall transmits the torque applied by the wheel to the contact patch. It also supports the weight of the vehicle in conjunction with the inflation pressure. It is constructed of a rubber exhibiting high abrasion and tear resistance, as well as excellent weathering characteristics [23].

Tread

The tread is the area of the tire which contacts the road. It must provide good traction while also being highly durable, and provide low rolling resistance. In most applications it features deep grooves in order to facilitate the evacuation of water and increase wet traction [23].

2.2.2 Behaviour

The force response of the tire is largely governed by the manner in which the tire deforms. The stiffness of the tire under various loading conditions affects the pressure distribution at the contact patch, which ultimately determines the tire's response to slipping. The amount of slip the tire undergoes is the element that is actively, but indirectly, controlled in most vehicles through the steering wheel, or the accelerator. In order to determine the amount of slip the tire undergoes, the no slip condition of the tire must be defined. Since a tire rolling at a constant velocity must undergo a small amount of slip, due to the load it is bearing, there is no true zero slip condition. However,

in the case of road vehicles, the zero slip condition is assumed to occur when the relationship in equation (2.4) is maintained.

$$\Omega_0 r_e = V_x \tag{2.4}$$

Where, Ω_0 is the free rolling angular velocity, r_e is the effective radius, and V_x is the forward velocity of the vehicle [21].

This condition is referred to as the free rolling tire. Tire force generation is typically analyzed in lateral and longitudinal components individually in order to better understand the mechanisms involved in the generation of the component forces. Aside from the quantity of slip the tire undergoes, the force generation is highly dependent on the normal load the tire is withstanding. While the slip and normal load are not the only factors that affect tire response, they have the largest contribution.

Longitudinal Response

Tire force is generated in the longitudinal direction by the applied torque at the wheel from the powertrain or braking system. This wheel torque is opposed by the frictional contact at the ground, causing longitudinal acceleration of the vehicle. As the tire travels in the longitudinal direction, the material entering the contact patch tends to compress, while the material leaving the contact patch expands, causing slip relative to the ground. With increased driving torque, deflection in the tire increases, as well as the quantity of slip generated within the contact patch. The longitudinal force developed increases with an increased quantity of slip. The quantity of slip in the longitudinal direction is defined in equation (2.5)

$$\kappa = \frac{\Omega r_e}{V_x} - 1 \tag{2.5}$$

where κ is defined as the slip ratio, Ω is the angular velocity of the wheel, r_e is the effective tire radius, and V_x is the forward velocity of the vehicle [21].

The longitudinal force developed by the tire at a given normal load tends to increase quickly and linearly at low slip ratios until the limit of adhesion is reached. Once this point has been reached, the tire response reduces minimally and maintains a near constant value for increasing slip quantities.
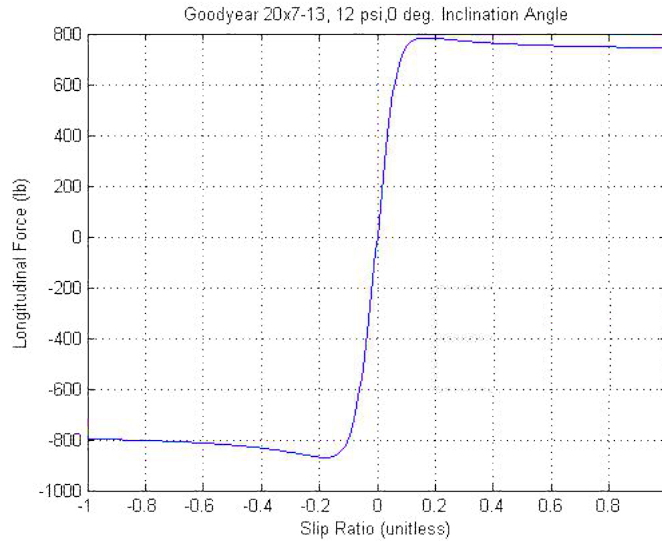
Figure 2.3: *Typical Longitudinal force response at a fixed normal load.* It should be noted that the slip ratio can be greater than 1 during extreme tire slip, however, the slip ratio is very rarely less than negative one as this would indicate a tire rolling in the opposite direction of the vehicle.

Figure 2.3 depicts the typical longitudinal response of a tire.

Lateral Response

In a similar fashion to the manner in which the longitudinal force was described, the lateral force a tire develops increases with increasing tire deflection and slip. The torque applied by the driver through the steering wheel causes the wheel to change its angle along an axis approximately perpendicular to the ground. The tire is now forced to follow a path that is not aligned with the forward direction of the wheel, which causes a shear force in the lateral direction at the contact patch as the tire rolls. The quantity of slip developed at the contact patch in the lateral direction is defined as the slip angle. The slip angle is given as the angle between the wheel heading and the wheel path. Figure 2.4 describes the slip angle more clearly. The slip angle is defined in equation (2.6)

$$\tan\alpha = -\frac{V_y}{V_x} \qquad\qquad (2.6)$$
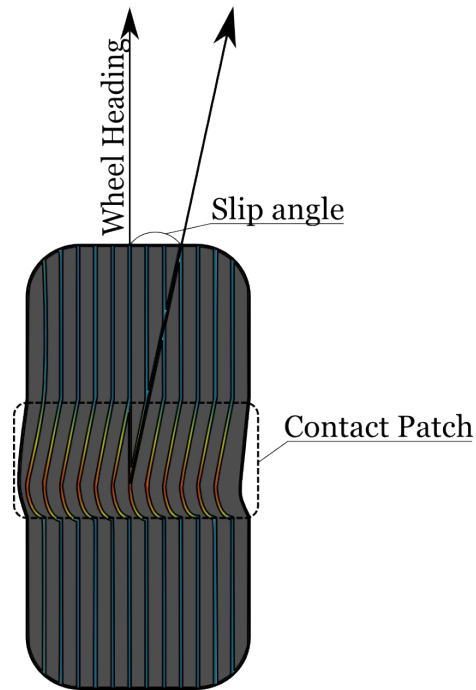
Figure 2.4: *Slip angle definition.*

where α is the slip angle, V_y is the lateral velocity, and V_x is the longitudinal velocity of the tire.

The lateral force developed by the tire, as a function of slip angle, increases steadily at low slip angles, and begins to drop off as the limit of adhesion is approached. This somewhat gradual drop off peaks as the majority of the contact patch reaches the limit of traction, then drops off to a steady value as the slip angle increases further. Figure 2.5 depicts a typical tire's lateral response.

Self-Aligning Torque

Along with the forces developed at the contact patch, a torque is also generated. This is typically referred to as the self-aligning torque, or SAT, due to its tendency to realign the tire with the forward direction. Both the longitudinal force and the lateral force contribute to the SAT; however, the lateral force is far more dominant due to the center of pressure being located much further from the center of the tire. The SAT is usually described in terms of the slip angle and not the slip ratio due to its
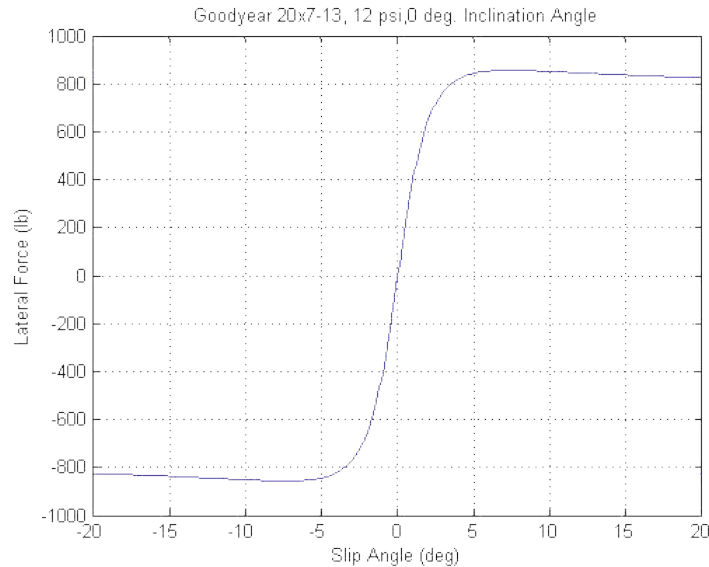
Figure 2.5: *Typical lateral force response at a fixed normal load.*

significantly larger impact. The SAT is an important feature of the tire's response since it contributes to driver feedback through the steering wheel, helping inform the driver of the tire's current state.

The SAT increases linearly with slip angle up to a peak, almost coinciding with the peak in lateral force. After the peak, the SAT quickly drops off and tends toward a zero moment as the center of lateral pressure approaches the center of the tire. To the driver, this will be interpreted as a reduction of steering effort and will alert them to the impending limit of lateral force. Figure 2.6 depicts the typical SAT response of a tire.

Contact Patch Phenomena

The behaviour of the tire within the contact patch has very important consequences to the tire's overall response. As the tire rolls along the ground, it compresses from the applied loads. As the material exits the contact area it expands. The energy released during expansion, however, is less than the required energy for compression. This tends to move the center of normal pressure within the contact patch forward of the center of the tire. The forward movement of the center of pressure
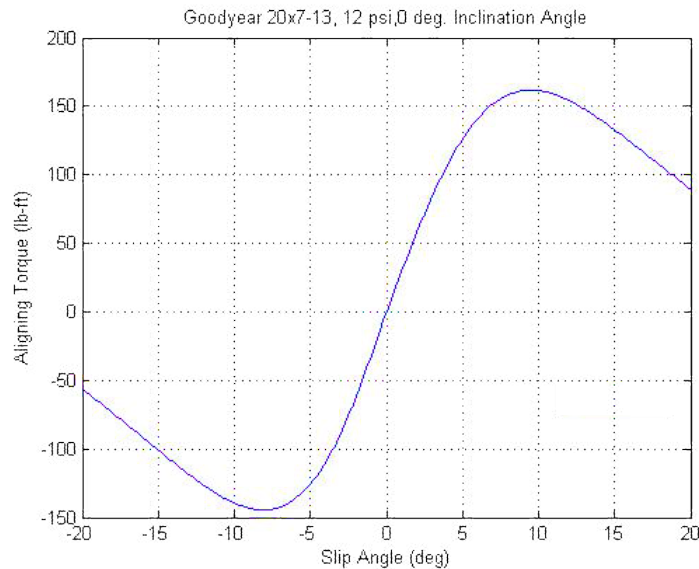
Figure 2.6: *Typical SAT response at a fixed normal load.*

of the normal force generates a moment against the rolling direction of the tire, contributing to the rolling resistance of the tire. Figure 2.7 depicts this effect.

In a similar fashion, the lateral force distribution within the contact patch changes as the slip angle is increased. As slip builds from zero, the center of pressure migrates away from the center of the tire. Once the tire begins to saturate and a greater portion of the tire is sliding along the ground, the center of pressure migrates back towards the center of the tire. This phenomena is the largest contributing factor for the behaviour observed in the self aligning torque response of the tire. The distance between the center of the tire and the center of pressure for the lateral force is defined as the pneumatic trail. This effect is described in Figure 2.8

State Sensitivity

The previous sections outlined how tire response varies with the quantity of slip, however, there are several other parameters that affect the response of the tire. Variations in normal load, forward speed, as well as camber angle also have an effect on tire response. Figure 2.9 shows a tire's lateral
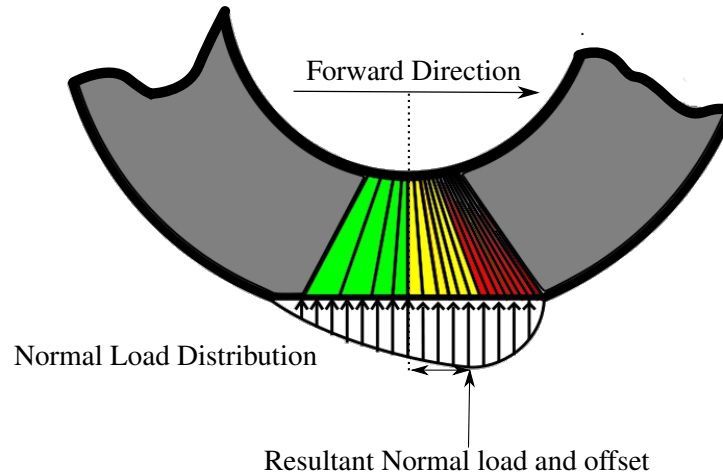
Figure 2.7: *Normal load variation with applied torque.*

response at various normal loads. Analyzing the figure, it can be seen that the lateral force a tire is capable of developing increases with increasing normal load. However, it does not do so linearly. Doubling the amount of normal load does not yield double the potential lateral force. It is due to this phenomena that the over/under steer behaviour of a vehicle can be affected by variation of the front and rear suspension roll stiffness distribution as mentioned in Section 2.1.1. The longitudinal force capabilities of the tire follow a similar trend.

Other considerations that affect tire response, such as forward velocity and camber angle have a much less dramatic effect on the tire's response. Increased negative camber, to an extent, tends to increase the lateral force capability of a tire through a phenomenon known as camber thrust. As the tire is tilted inwards, the deformation of the tire tends to pull the tread underneath it thereby increasing the contact patch area. However, increased negative camber tends to reduce the size of the contact patch under braking and acceleration, and therefore reduces the tires ability to apply force longitudinally.
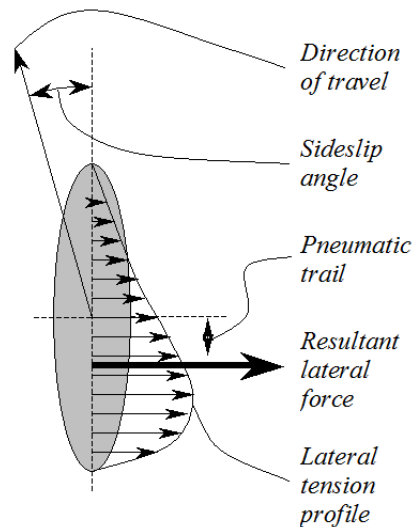
Figure 2.8: *Pneumatic trail.* Typical lateral force distribution within the contact patch. Reproduced from Dressel [7].

2.2.3 Tire Modelling

Due to the highly non-linear nature of the tire, modelling its behaviour is quite difficult. Despite this, many models exist, such as the Fiala model [9], the LuGre model [6], and the Dugoff model [8]. Although the method by which a tire can be modelled follows a continuum, there are typically three main categories in their mathematical treatment: finite element modelling (FEA), analytical modelling, and empirical modelling.

Tire designers use FEA models in order to better understand how the tire behaves prior to the production of the tire itself. An accurate FEA model is both very time consuming to produce and resource intensive to complete. It also requires the use of accurate material models. Since the tire is a composite structure featuring non-linear materials such as rubber, material modelling alone is quite challenging.

Empirical tire models use testing equipment in order to map the tire response under many different configurations. The data is then used to develop curve fits and interpolation is used to estimate
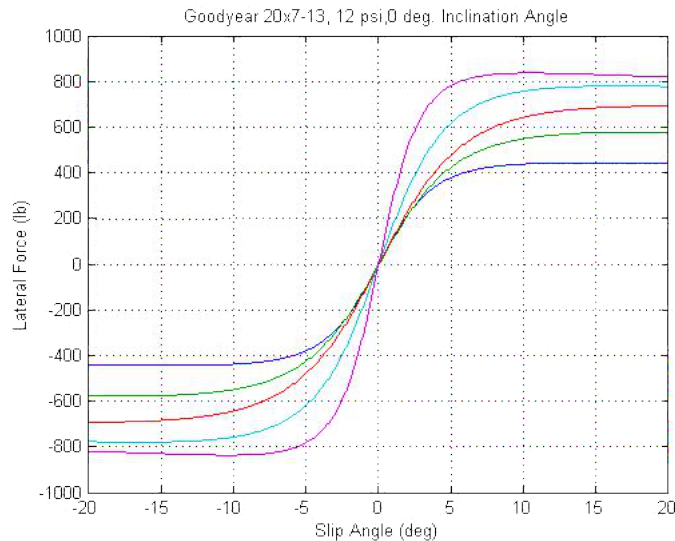
Figure 2.9: *Lateral force response at various loads.*

tire behaviour outside of the tested conditions. One of the most well known empirical tire models is the Pacejka [19], or 'magic tire model'. While empirical models give excellent results, as far as accuracy, the cost of fitting a specific tire to a model, such as the Pacejka model, is quite significant. Furthermore, they provide little, if any, insight as to what design aspect of the tire is responsible for the observed behaviour.

Analytical tire models attempt to predict tire behaviour through the analysis of a simpler representative dynamic system. Though this is likely the least utilized method of modelling a tire, it has some advantages over the previously discussed approaches. First, one analytical model should be capable of describing the behaviour of any tire, while FEA and empirical models only give information about the specific construction being analyzed. Secondly, parameterization of the tire theoretically should not require a full scale empirical test of the direct dynamic response of the tire. Unfortunately, the majority of analytical models encountered during this research used full scale dynamic testing and regression analysis to fit the developed model to the results measured. This undermines the significance of the model and there is no longer any guarantee the estimated

parameters from the regression analysis match the intended physical meaning.

To further contrast the difference between empirical and analytical modelling, an example of each will be given. First, the empirically based Pacejka tire model will be introduced. As stated earlier, this is the most utilized method and is more or less the industry standard for tire modelling. Next an analytical model known as the Cornering Force/Self-Aligning Torque Model (CF/SAT) will be introduced.

Pacejka Model

The Pacejka tire model uses empirically derived data to develop a series of coefficients representing the tire's response. The model is referred to as the 'magic tire model' because, while it has no physical basis for its form, it accurately predicts tire behaviour for a wide range of tire types and constructions. The Pacejka model has received wide adoption, not only because it is fairly accurate, but it is relatively simple to construct and allows for very fast estimation of tire response. One major drawback of the approach is the requirement of a fairly substantial dataset of dynamic tire response for each individual tire construction to be modelled.

The formulation for this model is given in equation (2.7),

$$y(x) = D \cdot \sin\{C \arctan\left[(1-E)x + E \cdot \arctan\left(Bx\right)\right]\} \tag{2.7}$$

where y is the force or moment generated, x is the slip quantity, B is the Stiffness factor, C is the Shape factor, D is the Peak factor, and E is the Curvature factor. Each of these factors are determined through analysis of the collected dataset. It should be noted that these factors are each functions of both normal load and camber angle. For more information on this method, please see [19].

CF/SAT

The CF/SAT model is an analytical model based on the Fiala tire model. The system is represented by a wheel assumed to behave as a rigid ring and the sidewall as a spring connecting the belts and
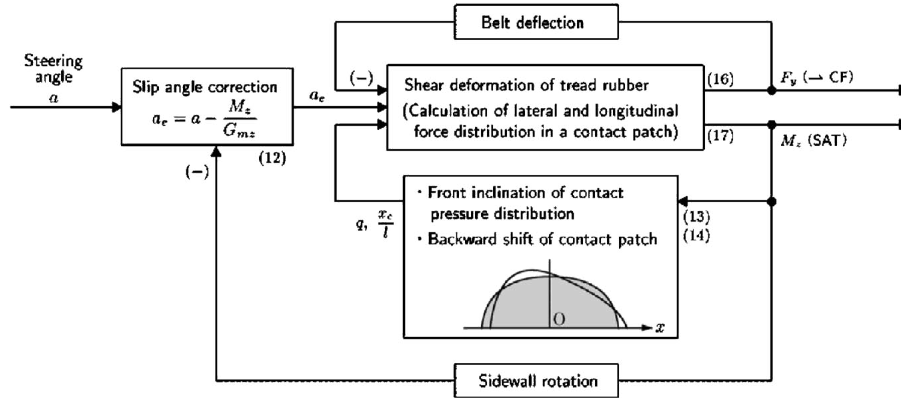
Figure 2.10: *CF/SAT block diagram.* Reproduced from Miyashita and Kabe[17]

tread to the wheel. The belts and tread are allowed to deform in plane based on the shear force *Fy*

and out of plane by a rotation caused by the self aligning torque M_z. These deflections are caused by

the generation of force by the tire. In turn the deflection of the tire affects the generation of force,

and so a feedback loop is introduced, allowing the deflection caused by the generation of force to

affect its own ability to further generate force. A block diagram outlining the various steps the

model uses is shown in Figure 2.10. The governing equations of the model are given in Table 2.1.

For a description of the variables used in the model, please refer to the notation section. For a more

complete description of this model, please see Miyashita and Kabe [17].

The contact pressure distribution is estimated using a skew parabolic function. This is shown in

equation (2.8),

$$D_{gsp}(t;n,q) = (1 - |2t - 1|^n)[1 - q(2t - 1)] \tag{2.8}$$

where D_{gsp} is the generalized skew parabola, *t* is the independent variable, in this case length

along the contact patch, *n* is the shoulder coefficient, and *q* is the circumferential asymmetric co-

efficient. As *n* increases, the pressure distribution tends to flatten out around the midpoint. As *q*

increases, the pressure distribution tends to adjust rearward. This assumption represents the pres-

sure distribution well, and the model adjusts the backward shift of the contact patch as a function

of the SAT. The model, however, does not determine the shoulder exponent from the physical tire,

Table 2.1: *Governing equations of the CF/SAT model.*

Model component	Expression
Slip angle correction	$a_e = a - \frac{M_z}{G_{mz}}$
Circumferential asymmetry coefficient for pressure distribution within contact patch	$q = C_q M_z$
Location of steering axis within contact patch	$x_c = \frac{l}{2} - \frac{\zeta M_z}{l}$
Adhesion to sliding mode definition	$2k_{y0} \left(\frac{l_h}{l} \right) \left[\tan a_e - \varepsilon l F_y \left(1 - \frac{l_h}{l} \right) \right]$ $= \frac{n+1}{n} \mu_s F_z D_{gsp} \left(\frac{l_h}{l}; n, q \right)$
Lateral force output	$F_y(a) = 2k_{y0} \int_0^{\frac{l_h}{l}} \left[t \tan a_e - \varepsilon l F_y (1-t) \right] dt$ $+ \frac{n+1}{n} \mu_d F_z \int_{\frac{l_h}{l}}^{l} \left[D_{gsp}(t; n, q) \right] dt$
Aligning moment output	$M_z(a) = 12A_{s0} \int_0^{\frac{l_h}{l}} \left[t \tan a_e - \varepsilon l F_y (1-t) \right] \left(t - \frac{x_c}{l} \right) dt$ $+ \frac{n+1}{n} \mu_d F_z \int_{\frac{l_h}{l}}^{l} \left[D_{gsp}(t; n, q) + A_{x0} \frac{l_h}{l} \tan a_e \right] dt$

which is a shortcoming of this model.

2.3 Scale Modelling

Scale modelling is a technique that is highly utilized in the aerospace and marine industries due to the prohibitively high cost of constructing prototypes. While it is much less expensive to build a prototype ground vehicle, OEMs, motorsports, and academia alike can benefit from doing at least preliminary physical vehicle studies at a scale level. In order to develop and better understand the state of the art of scale vehicle modelling, the principle that allows for dynamic scale modelling, known as Buckingham Pi theory, must be introduced. Once this is accomplished, some of the current research in scale vehicle modelling will be discussed.

2.3.1 Buckingham-Pi

Through the use of dimensional analysis, a dynamic system can be redefined in terms of a series of non-dimensional parameters describing the behaviour of the system. Buckingham-Pi theory [3] is the method by which this non-dimensionalization is accomplished. There are two direct benefits to this approach. One is that the variable space that defines the system's behaviour is reduced. The other is that it allows for direct comparison of two dynamic systems that are governed by the same parameters, but are on vastly different scales.

The theory is based on the concept of dimensional homogeneity. If there is a physically meaningful function such that

$$f(q_1, q_2, ..., q_n) = 0 \tag{2.9}$$

where q_n represents a physical variable that affects the system, and these variables can be represented in terms of j independent physical units, such as mass, length, time, then the same system may be represented in $k = N - j$ non-dimensional terms, where each non-dimensional term is de-

scribed by equation (2.10).

$$\pi_i = q_1^{a1} q_2^{a2} ... q_n^{an} \tag{2.10}$$

The application of this stems from the concept of similitude. If the response of multiple systems on different scales can be defined by the same π_i, then the systems are said to be similar. If two dynamic systems have the same value for each of the pi parameters then similitude between the two systems is guaranteed. It is very important that all the pi parameters be matched, otherwise the scale system will have a response that may not match the full size system's response in some manners.

To better understand how to use this theory, an example system will be non-dimensionalized. The dynamic system analyzed will be that of an object falling through empty space under the influence of a gravitational field.

The first step is to identify each parameter that affects the dynamic response of the system. In this case the objects height, z, is a function of the elapsed time, t, the initial height, z_0, the initial velocity, w_0, and the gravitational acceleration of the field, g.

$$z = f(t, z_0, w_0, g) \tag{2.11}$$

The next step is to list the primary dimensions of each of the parameters. The results are shown below in equation (2.12).

$$z = \{L_n^1\}, \quad t = \{t^1\}, \quad z_0 = \{L_n^1\}, \quad w_0 = \{L_n^1 t^{-1}\}, \quad g = \{L_n^1 t^{-2}\} \tag{2.12}$$

The third step is to select the number of repeating parameters. The number of repeating parameters should match the number of primary dimensions that exist within the system. In this case there are two primary dimensions, time and length. The number of non-dimensional parameters, k, we should expect is equal to the number of parameters, N, minus the number of primary dimensions, j.

$$N = 5, \quad j = 2, \quad k = N - j = 3 \tag{2.13}$$

The fourth step is to select the repeating parameters to use to non-dimensionalize the remaining parameters. This choice is ultimately up to the analyst, but there are some guidelines. First the repeating parameters must encompass all of the primary dimensions used in the system. Also, the dependent variable is a poor selection as it will show up in each of the non-dimensional parameters, making analysis very cumbersome. If interested, please consult Çengal [4] for additional suggestions. For this example the initial height, z_0, and the initial velocity, w_0, were selected.

The final step is to form the non-dimensional parameters by combining the repeating parameters as products with the remaining parameters such that the primary dimensions are eliminated. These parameters are sometimes also referred to as pi parameters. In this example the resultant pi groups are,

$$\pi_1 = \frac{z}{z_0} \quad \pi_2 = \frac{w_0 t}{z_0} \quad \pi_3 = \frac{g z_0}{w_0^2} \tag{2.14}$$

For comparison purposes, the dimensional equation of motion for this system is given as,

$$z = \frac{g}{2} t^2 + w_0 t + z_0 \tag{2.15}$$

and the non-dimensional equation of motion is defined as,

$$\pi_1 = \frac{\pi_2^2 \pi_3}{2} + \pi_2 + 1 \tag{2.16}$$

The two equations are equivalent to each other, however, the non-dimensional equation allows for the direct comparison of the response of two systems on different scales. The equivalency of these two equations can be proven by replacing the pi parameters in equation (2.16) with their definitions in equation (2.14) and multiplying through by z_0. When this is done the result in equation (2.15) is obtained.

It is this theory that allows for the direct comparison of two similar dynamic systems of different scale. The next section will introduce some examples of current research into the application of this theory to scale vehicle modelling.

Table 2.2: *Pi parameters for the IRS scale vehicle model [2].* For variable definitions, please refer to the notation section.

Parameter	π_1	π_2	π_3	π_4	π_5	π_6	π_7
Expression	$\frac{a}{L}$	$\frac{b}{L}$	$\frac{R}{L}$	$\frac{C_{\alpha f}L}{mU^2}$	$\frac{C_{\alpha r}L}{mU^2}$	$\frac{I_z}{mL^2}$	$\frac{T}{mU^2}$

2.3.2 Scale Vehicles

The Illinois Roadway Simulator (IRS) at the University of Urbana-Champaign is one example of the current research being conducted in scale vehicle modelling. The scale vehicle for the IRS is based on the linear bicycle model described in section 2.1.1. The parameters for the bicycle model were non-dimensionalized using Buckingham Pi theory and a scale vehicle was constructed to match the dynamic performance of a full size vehicle. The non-dimensional bicycle model parameters used in this study are shown in Table 2.2. For vehicle state feedback, the IRS, which is shown in Figure 2.11, utilizes a sensing arm featuring three revolute joints. The sensing arm is capable of measuring vehicle motion along the planar principal axes, as well as the vehicle's roll, pitch, and yaw angles. Due to the tire design and small width of the track, the vehicle was limited to non-aggressive manoeuvres within the linear region of tire response in order to maintain dynamic similitude. Though limited, this study successfully demonstrated the ability to use scale vehicles for the testing of full scale vehicle dynamics [14].

The Pennsylvania State University Rolling Roadway Simulator, (PURRS), is a similar, but more advanced, scale vehicle than the IRS described earlier. This scale vehicle is also based on the linear bicycle model, with the addition of vehicle roll dynamics into the model. This increases the fidelity of the model and results in greater similitude between the full and scale vehicles. This model was again non-dimensionalized using the procedure described in section 2.3.1. The resultant non-dimensional parameters for the model are shown in Table 2.3. While the state feedback system was almost identical to the one developed by the University of Urbana-Champaign, it allowed additionally for the inclination of the road surface both in the pitch and roll directions. This allowed for a much greater range of test conditions. The scale vehicle itself was developed using pi parameters
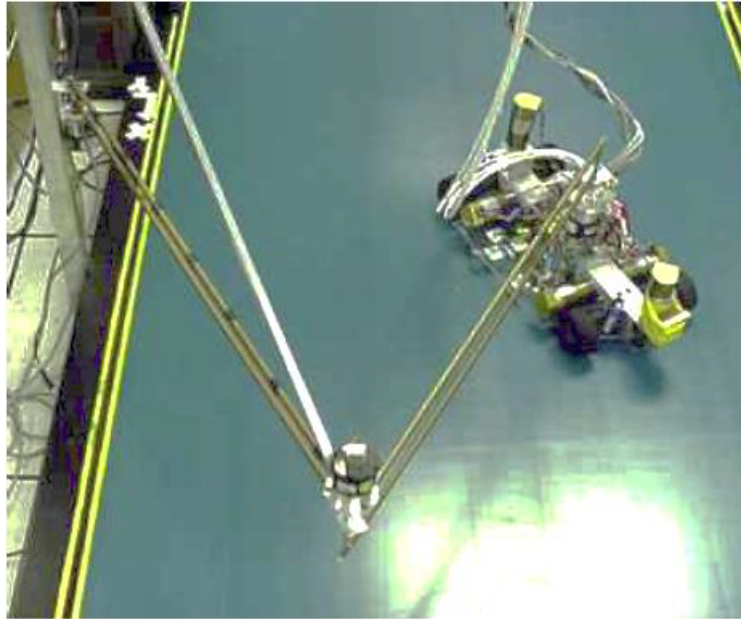
Figure 2.11: *The Illinois Roadway Simulator.* Reproduced from Liburdi [14]

that matched a 1992 Mercury Tracer. Testing accomplished with this testbed showed that there was good correlation between the scale and full size vehicles at low frequency inputs, but high error at high frequency inputs. This was attributed to the use of solid rubber tires on the test platform, reducing the effect of tire lag dynamics in the scale model [14].

2.3.3 Scale Tires

While the current work in scale vehicles allows for good correlation at low slip angle and input frequencies, the real benefit of scale vehicle testing is realized within the non-linear regime of tire response. In order to accomplish this, a tire that is scaled independently from the vehicle is necessary. Currently the only known research accomplished to this end was done by Polley [20] at the University of Urbana-Champaign.

Polley developed a small scale tire flat track test machine, shown in Figure 2.12, with the intention of testing the response of existing pneumatic radio controlled (RC) application tires. The

Table 2.3: *Pi parameters for the PURRS system [13].* For variable definitions, please refer to the notation section.

Parameter	Expression	Parameter	Expression
π_1	$\frac{a}{L}$	π_9	$\frac{I_{yy}}{mL^2}$
π_2	$\frac{b}{L}$	π_{10}	$\frac{m_s}{m}$
π_3	$\frac{C_{\alpha f}L}{mU^2}$	π_{11}	$\frac{h_s}{L}$
π_4	$\frac{C_{\alpha r}L}{mU^2}$	π_{12}	$\frac{I_{xz_s}}{mL^2}$
π_5	$\frac{I_{zz}}{mL^2}$	π_{13}	$\frac{I_{xx_s}}{mL^2}$
π_6	$\frac{h}{L}$	π_{14}	$\frac{K_\phi}{mU^2}$
π_7	$\frac{t}{L}$	π_{15}	$\frac{D_\phi}{mU^2}$
π_8	$\frac{I_{xx}}{mL^2}$		

Figure 2.12: *University of Urbana-Champaign Scale Tire Tester.* Reproduced from Liburdi [14]

only pneumatic tire found at that scale was the Dubro RC model aircraft tire. Using the developed testing machine, a dataset for the tire was collected and fit with a magic tire model. The results demonstrated that the lateral and aligning moment responses were similar to that of a full scale tire; however, a good set of longitudinal response data was unable to be collected due to excessive tire wear. An example of the lateral force response results is shown in Figure 2.13.

Although the curve shapes for this small scale tire were similar to that of a full scale tire, this tire is not appropriate for use in scale modelling. Using the collected data, Polley attempted to design a scale vehicle around the available scale tire. This resulted in a scale vehicle mass far exceeding the load capability of the tire. In order to build the scale vehicle, some of the non-dimensional parameters between the full and scale vehicles did not match. This results in non-similarity between the scale vehicle and the full size vehicle.

In order to accurately capture the full range of vehicle response in a scale vehicle, the tire must be scaled independently from the vehicle. The research conducted in the foregoing sections was accomplished as a means to this end.
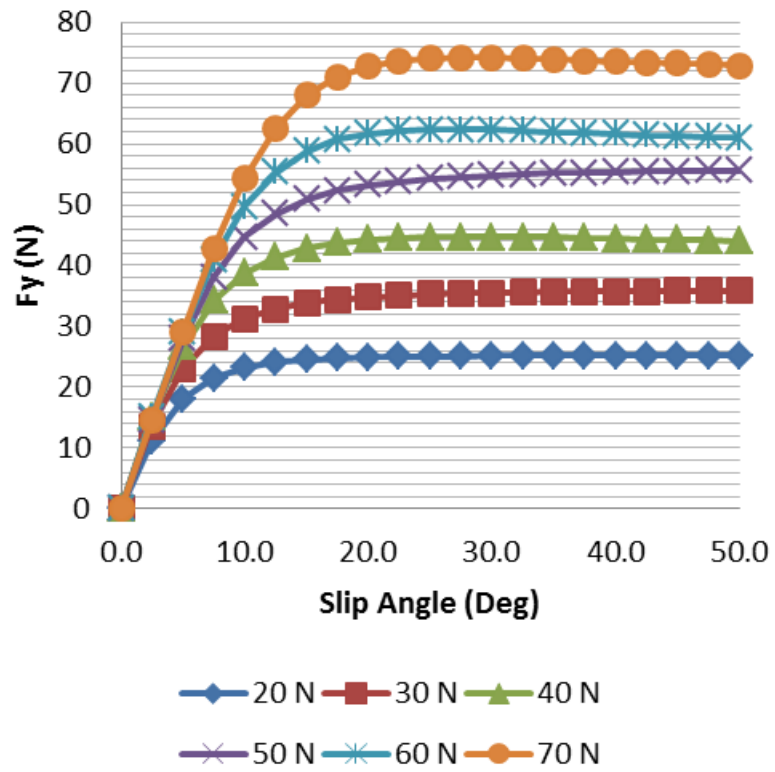
Figure 2.13: *Lateral force response of DU-BRO 5.00 T.V.*

Chapter 3

Scale Tire Modelling

In order to properly evaluate the performance characteristics required of a scale tire for use in vehicle dynamics, it must be capable of being defined by a mathematical model in terms of physically significant properties. This is mandatory to both assess the performance of the full size tire of interest, and provide a basis to non-dimensionalize the parameters for comparison of the full and scale tires. This requirement mandates that an analytical type model, as described in Section 2.2.3, is selected. While many of these types of models exist, one model, the CF/SAT model, lends itself quite well to this application.

3.1 CF/SAT model

The CF/SAT model was selected for several reasons. The parameters within the model that define tire performance, shown in Table 3.1, are based on real physical tire characteristics. There are some caveats to this statement, the details of which will be discussed in the subsequent section. The model was also selected because it only attempts to predict lateral force and self-aligning torque, reducing the set of parameters required to define a tire when compared with other models. This is desirable as a first attempt approach due to the highly complicated nature of tire response.

The ability of a tire to generate force in any one component direction is directly coupled with
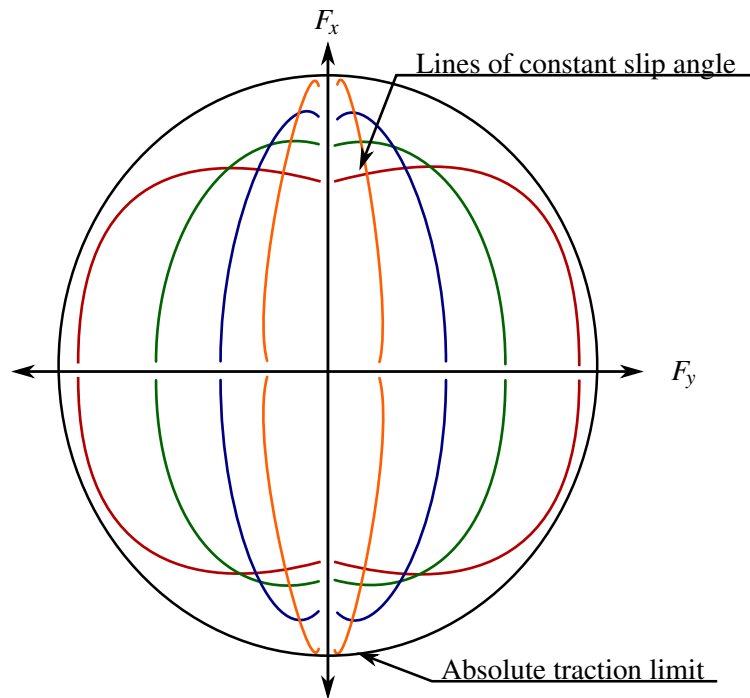
Figure 3.1: *Tire friction ellipse.* The friction ellipse represents the range space of a tire's force generation capabilities. The axes represent pure slip in the component directions. The absolute traction limit, represented by the outer most ring, shrinks and enlarges with changes in normal load. The inner lines represent tire force generation at a constant slip angle. The ability of a tire to generate force in a component direction is enhanced or mitigated by the combined load placed on the tire.

the force currently being generated in the opposing direction. This effect is outlined in Figure 3.1. While this model, and subsequently the approach presented as a whole, do not take this effect into account, the results are still very beneficial and give insight into the mechanisms within the tire that cause the observed behaviour. There are other nuances of this model, however, that present a challenge when applied to scale modelling.

Table 3.1: *CF/SAT model parameters [17].*

Parameter	Description
$w\,(\mathrm{m})$	Width of the contact patch
$R_0\,(\mathrm{m})$	Unladen tire radius
$l\,(\mathrm{m})$	Length of the contact patch
n	Shoulder coefficient for the skew parabolic function
$C_y\left(\frac{\mathrm{kN}}{\mathrm{m}^3}\right)$	Lateral spring constant of tread element
$\varepsilon\left(\frac{1}{\mathrm{kN\,m}}\right)$	Belt deflection compliance
$C_q\left(\frac{1}{\mathrm{kN\,m}}\right)$	Compliance of front inclination in contact pressure
$\zeta\left(\frac{\mathrm{m}}{\mathrm{kN}}\right)$	Contact-patch shift compliance
$A_{x0}\,(\mathrm{kN\,m})$	Self-aligning torque stiffness of a rigid ring model from longitudinal force
$EI_z\,(\mathrm{kN\,m}^2)$	Bending rigidity of the belt
μ_s	Static coefficient of friction
μ_d	Dynamic coefficient of friction
$F_z\,(\mathrm{kN})$	Normal load on the tire
$F_y\,(\mathrm{kN})$	Lateral force output
$M_z\,(\mathrm{kN\,m})$	Aligning moment output

3.1.1 Model Caveats and Shortcomings

While the CF/SAT does provide a good starting point for dimensional analysis, there are several shortcomings that make its use for this application a challenge. These issues and the manner in which they were treated will be discussed in the following sections.

Contact Patch Length

As shown in Table 3.1, the CF/SAT model requires the analyst to give the model the length of the contact patch. This is a challenge not only because it is difficult to measure directly, but it is also changing with tire load. As an improvement to the model a relationship was developed relating the overall vertical stiffness, C_z, and normal load, F_z, with the laden and unladen radius, R_e, and R_0, of the tire. This information is then used to determine the contact patch length, l, in the relationship given in equation (3.1)

$$R_e = R_0 - \frac{F_z}{C_z}$$
$$l = 2\sqrt{R_0^2 - R_e^2}$$
(3.1)

This model of the contact patch length assumes that the contact patch only expands in length, and not width, as the tire is loaded. The results obtained in Chapter 5 suggest the error introduced by this assumption are insignificant for the purposes of this approach. Figure 3.2 depicts the contact patch length model.

Normal Load Distribution

Determining the contact pressure distribution within the contact patch is a difficult problem to deal with both analytically and empirically. While there are methods of measuring the distribution using commercial products, these are generally for static pressure distributions and do not help clarify what is happening dynamically.

$$l = 2\sqrt{R_0^2 - R_e^2}$$
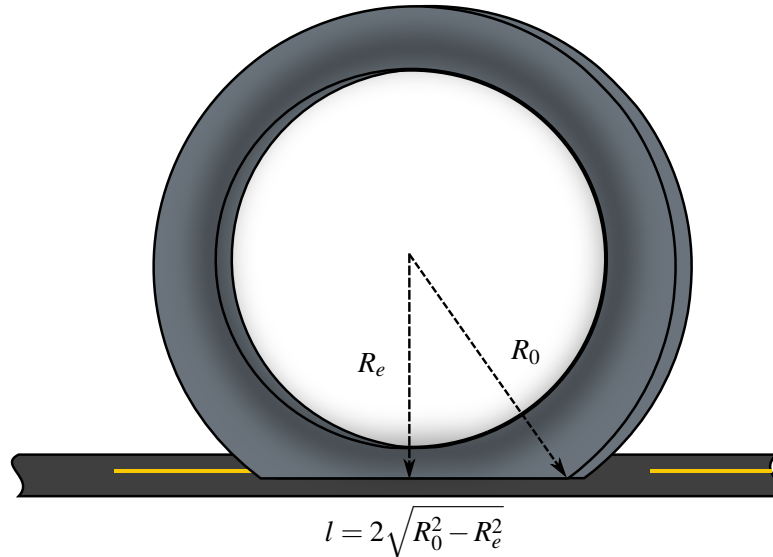
Figure 3.2: *Estimation of contact patch length.* Visual representation of contact patch length interpretation.

Finding an analytically method by which to determine the pressure distribution is a challenging issue due to variations between tire constructions, and surface effects. As a result of these challenges, Miyashita and Kabe use the general skew parabolic function to estimate the contact pressure distribution. This assumption is a significant improvement over the more commonly used quadratic parabola function as it allows for the forward inclination and backwards shift of the contact patch [17]. Figure 3.3 depicts the function and describes its use as an estimate for contact pressure distribution of a tire.

While this assumption may match the contact profile of the tire quite well, it does not describe what physical characteristics are responsible for the observed behaviour. The two parameters associated with the pressure distribution in the model are the shoulder coefficient, n and the circumferential asymmetric coefficient, q. The authors define q in terms of the self-aligning torque being generated; however, n is left undefined in terms of the tire's physical properties, making non-dimensionalization of this parameter for a specific tire impossible. To deal with this, optimally, an analytical relationship between the tire's physical parameters and the behaviour of the contact patch pressure distribution could be found; however, this topic is beyond the scope of this work. As a
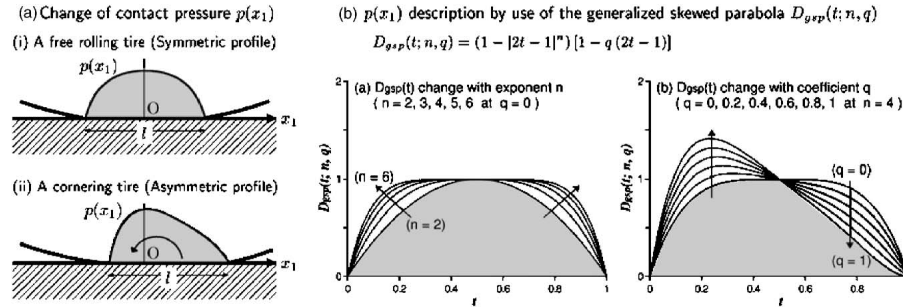
Figure 3.3: *Generalized skew parabolic function description[17].*(a) Describes the forward inclination of the contact pressure distribution. (b) Depicts the effect of variation of the shoulder coefficient and the circumferential asymmetric coefficient. Reproduced from Miyashita and Kabe [17]

result the shoulder coefficient was determined through regression analysis, as done by Miyashita and Kabe, in order to carry on with the study.

3.2 Model Verification and Non-Dimensionalization

The first step taken in the development of an appropriate non-dimensional scale tire model was to verify the results of the CF/SAT model. MATLAB® was used to evaluate the findings of Miyashita and Kabe. The MATLAB® M-code developed for this model is given in appendix A.

3.2.1 Model Output Comparison

To ensure that the MATLAB® model developed matches the behaviour of the model as described by Miyashita and Kabe, the output of the developed model was compared to the results provided in the literature. The tire parameters used for each of the comparison results are given in Table 3.2. The comparison results are outlined in Figures 3.4 - 3.6.

Table 3.2: *Model verification parameters* The model output results from the literature use these parameters. These results were compared with the output of the developed MATLAB® model.
[1] No value was reported for these parameters. As a result, an estimate was made using values reported in other sections of the literature.
[2] The model typically defines Ky_0 in terms of the length and width of the contact patch, as well as the lateral spring constant of a tread element. However, in the regression analysis in the literature, direct estimates of Ky_0 were reported. As a result, for this comparison, the value of Ky_0 was used directly instead of the relationship previously defined.

Parameter	Case A	Case B	Case C
w(m)	0.205	0.205	0.205
R_0(m)	0.31595	0.31595	0.31595
l(m)	0.0902	0.116	0.155
n	9.28	9.34	18.1
$C_y^{(1)} \left(\frac{kN}{m^3} \right)$	$6.47x10^{-4}$	$8.02x10^{-4}$	$6.7x10^{-4}$
$Ky_0^{(2)}$(kN)	54.7	111	177
$Ax_0^{(1)}$(kN m)	0	0	-0.38
$\varepsilon^{(1)}$	$5.78x10^{-2}$	$5.78x10^{-2}$	$5.78x10^{-2}$
$C_q \left(\frac{1}{kN\,m} \right)$	18.6	4.27	1.03
$\zeta \left(\frac{m}{kN} \right)$	$1.35x10^{-2}$	$1.78x10^{-2}$	$1.67x10^{-2}$
$EI_z^{(1)}$(kN m^2)	1.17	1.17	1.17
μ_s	1.93	1.62	1.24
μ_d	1.07	1.06	1.03
F_z(kN)	2.28	3.98	5.69

To compare the models, results for three different loading conditions on the same tire were used, as provided in Miyashita and Kabe [17]. The tire used for this study was a 205/55R16 of unknown make and model. As described earlier, the authors used regression analysis to fit the CF/SAT model to the empirical data gathered. The results of the fitting procedure were outlined in the literature and were used as the input to the MATLAB® model created for this study. Four of the parameters required for input to the model, however, were not provided. As a result, the parameter values were estimated from a previously published paper by the same authors [16], as well as through regression analysis. For case A and B only the lateral spring constant of a tread element, C_y, required modification to match the results found in the literature. Case C further required the A_{x_0} parameter to be fit due to the influence of longitudinal force on the self-aligning torque. This influence is outlined in Figure 3.9c.

The regression analysis required for C_y and A_{x_0} was accomplished through a manual fitting procedure. Through careful inspection of Figures 3.4 - 3.6 a small discrepancy between the results can be observed. This is most easily visualized through inspection of the composite of the two results. This discrepancy was determined to be solely a result of an incomplete data set provided in the literature. As a result, the MATLAB® model created was assessed to accurately represent the model portrayed in the literature.

(a) Literature results   (b) MATLAB® model results   (c) Composite of results
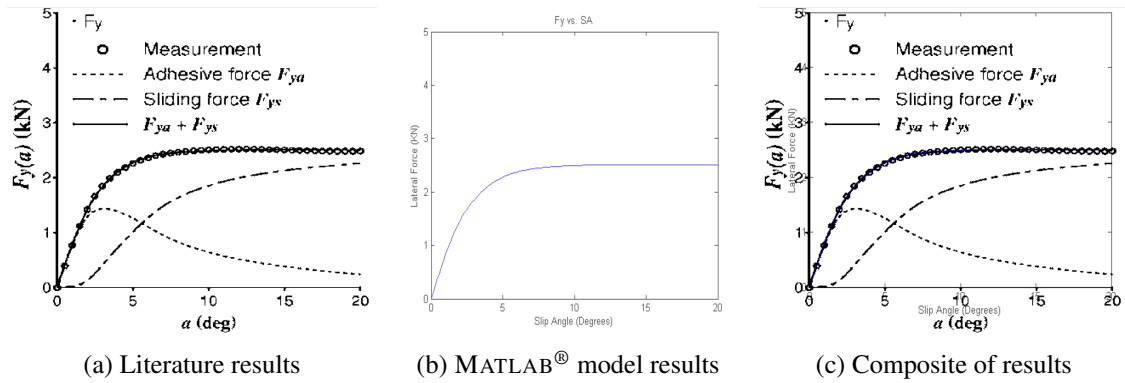
Figure 3.4: *C*F/SAT model comparison of literature and MATLAB®lateral tire force response results for case A.

(a) Literature results   (b) MATLAB® model results   (c) Composite of results
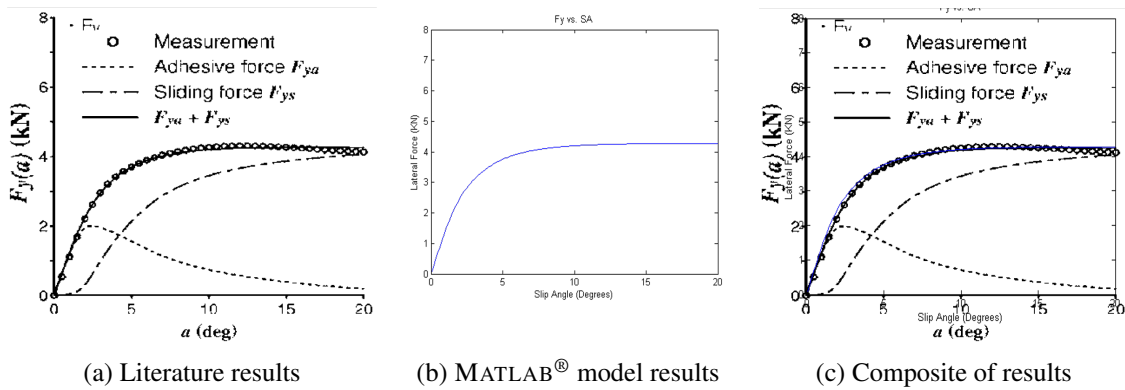
Figure 3.5: *C*F/SAT model comparison of literature and MATLAB®lateral tire force response results for case B.

(a) Literature results   (b) MATLAB® model results   (c) Composite of results
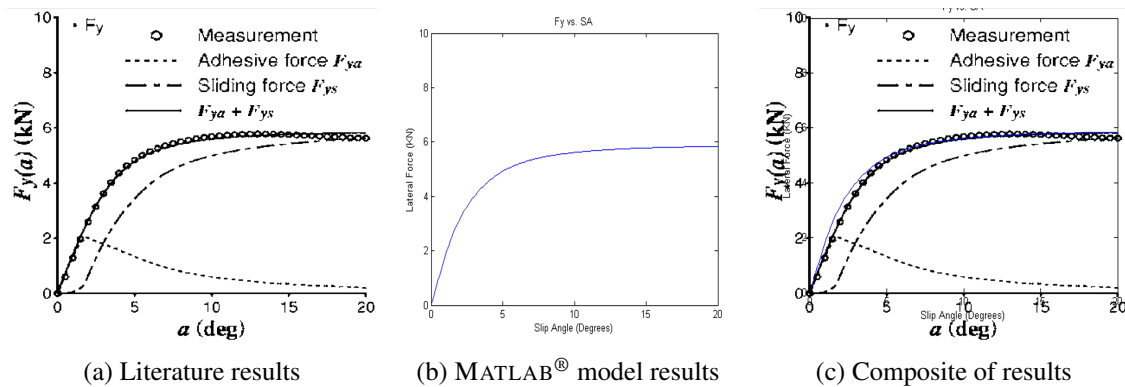
Figure 3.6: *C*F/SAT model comparison of literature and MATLAB®lateral tire force response results for case C.

(a) Literature results   (b) MATLAB® model results   (c) Composite of results
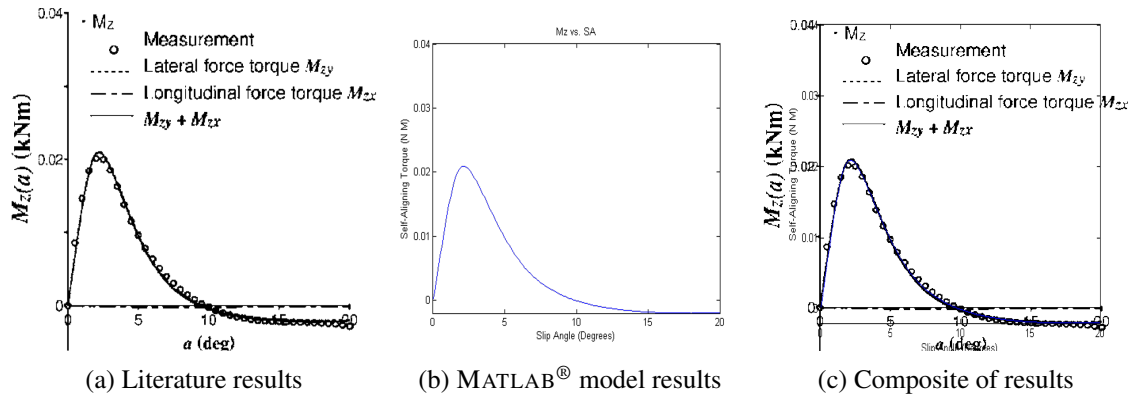
Figure 3.7: *C*F/SAT model comparison of literature and MATLAB®aligning torque response results for case A.

(a) Literature results   (b) MATLAB® model results   (c) Composite of results
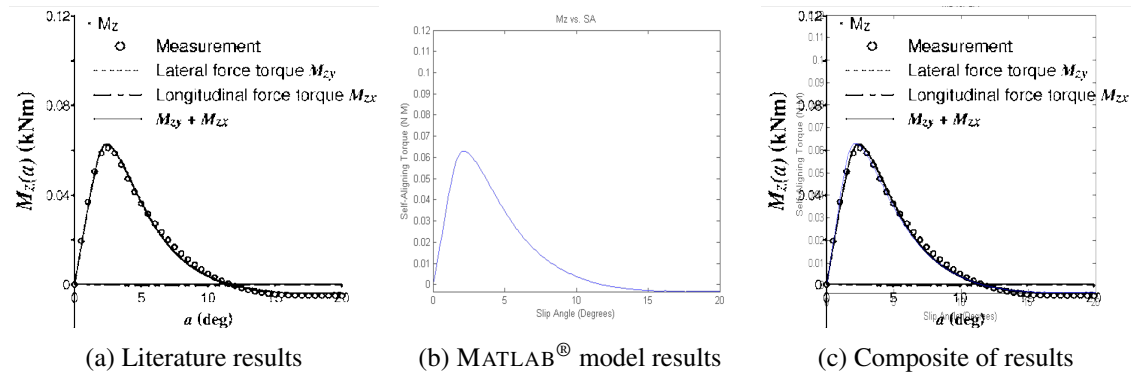
Figure 3.8: *C*F/SAT model comparison of literature and MATLAB®aligning torque response results for case B.

(a) Literature results   (b) MATLAB® model results   (c) Composite of results
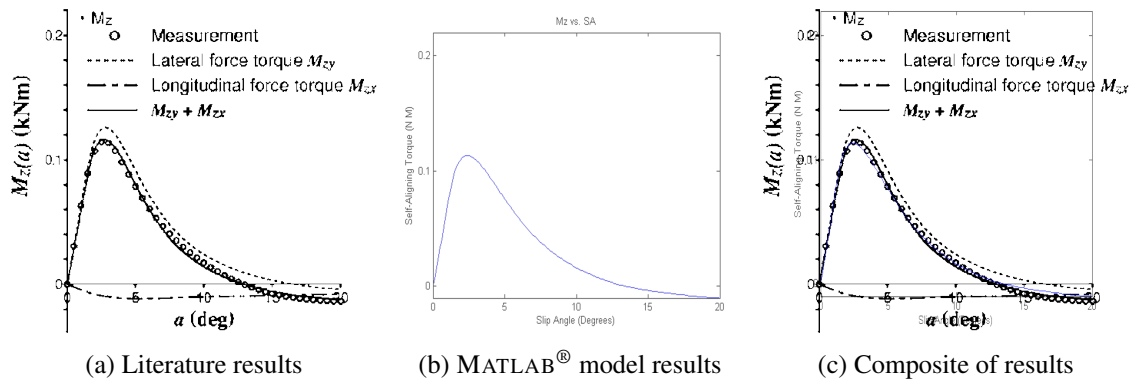
Figure 3.9: *C*F/SAT model comparison of literature and MATLAB®aligning torque response results for case C.

3.2.2 Model Sensitivity Analysis

Due to the large number and the complexity of the parameters within the model, some use of regression analysis is unavoidable. In order to better understand the relationship between each of the input parameters and the output of the model, a sensitivity analysis was completed. Case B parameters from the previous analysis were utilized as reference parameters. Each of these values were then adjusted independently to analyse their effect on the system response. Figures 3.10 - 3.12 show the results of this analysis.

Inspection of Figures 3.10a - 3.11b show the model is relatively insensitive to parameters C_q, ε, and EI_z in terms of both lateral force and aligning torque response. Furthermore, the model shows relative insensitivity to n and ζ in lateral force response, as can be seen in Figures 3.12c and 3.12e. It should be noted that Figure 3.11d indicates numerical instability of the model as the contact patch becomes too low. This information will be used in Section 3.3.1 to estimate CF/SAT parameters for the DU-BRO RC airplane tire used in Polley's study.
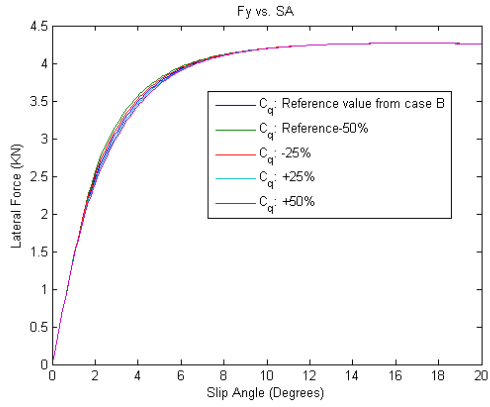
(a) C_q Lateral force sensitivity analysis.
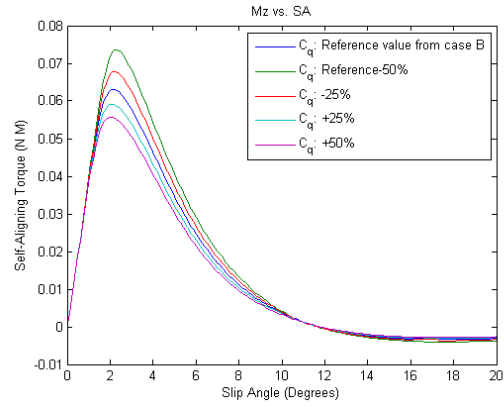
(b) C_q Aligning moment sensitivity analysis.
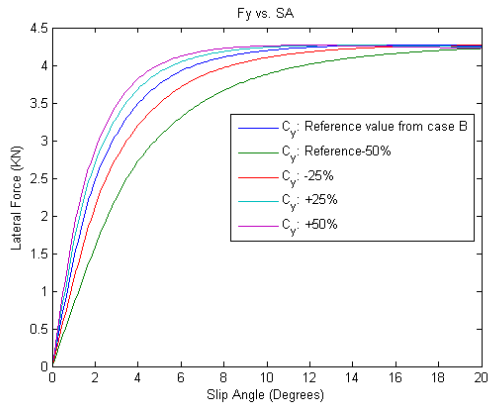
(c) C_y Lateral force sensitivity analysis.
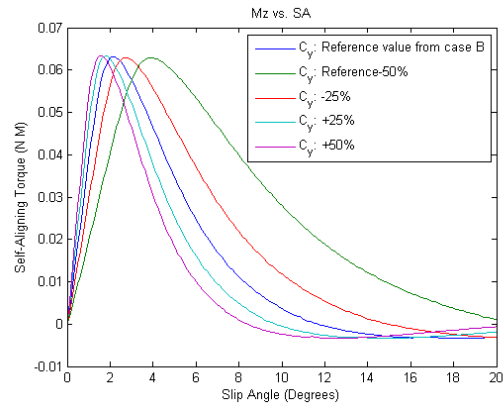
(d) C_y Aligning moment sensitivity analysis.
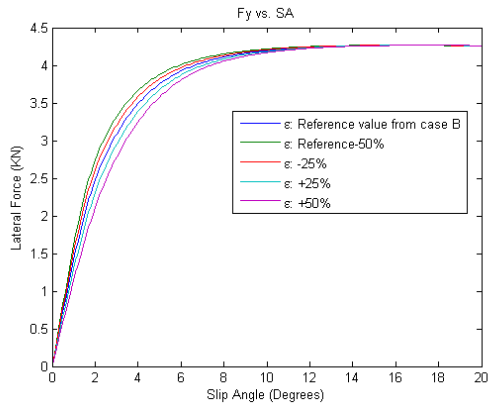
(e) ε Lateral force sensitivity analysis.
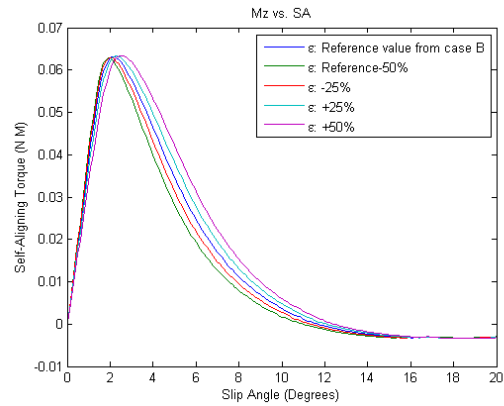
(f) ε Aligning moment sensitivity analysis.

Figure 3.10: *CF/SAT model parameter sensitivity analysis part I*
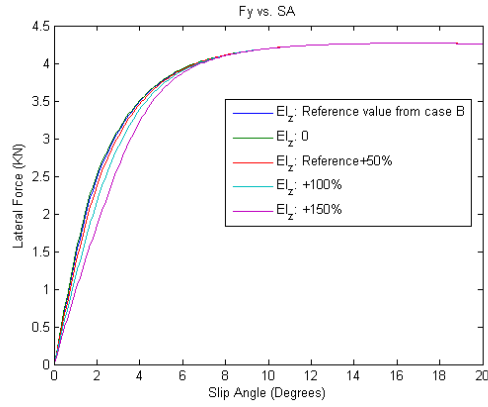
(a) *EI_z* Lateral force sensitivity analysis.
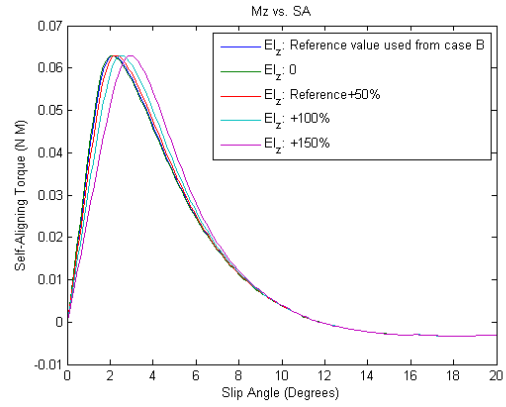
(b) *EI_z* Aligning moment sensitivity analysis.
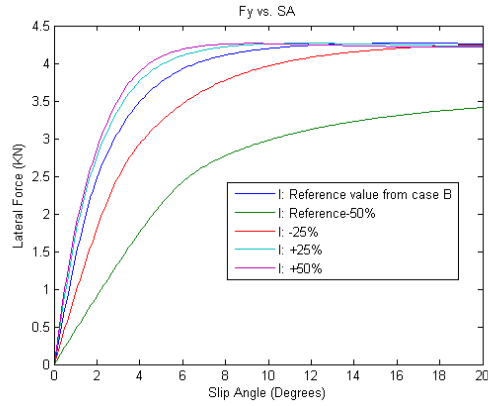
(c) *l* Lateral force sensitivity analysis.
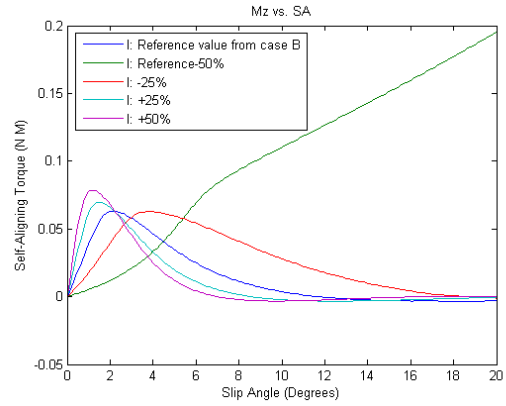
(d) *l* Aligning moment sensitivity analysis.
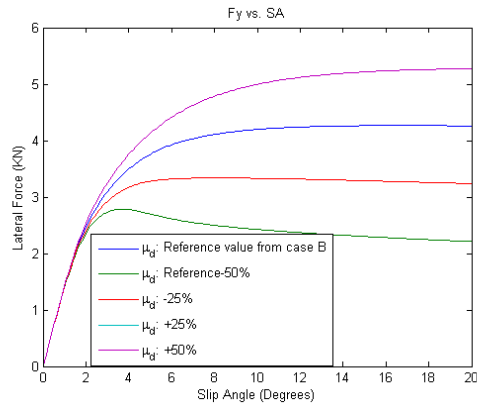
(e) μ_d Lateral force sensitivity analysis.
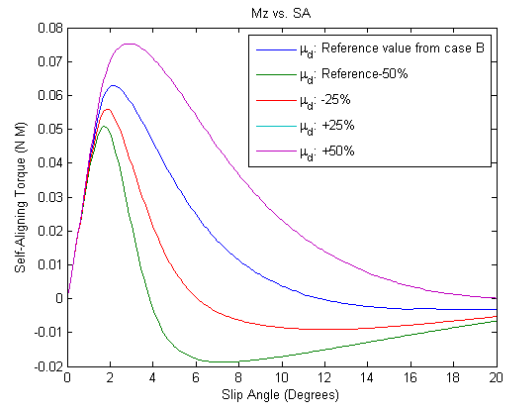
(f) μ_d Aligning moment sensitivity analysis.

Figure 3.11: *CF/SAT model parameter sensitivity analysis part II*
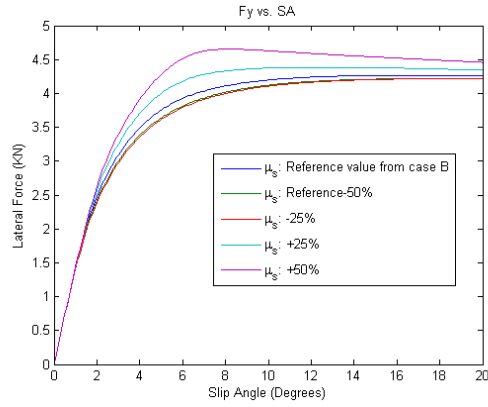
(a) μ_s Lateral force sensitivity analysis.
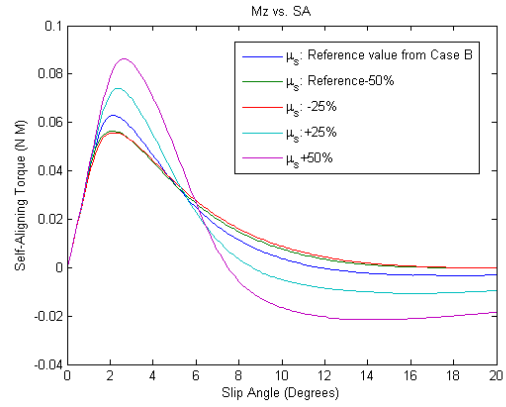
(b) μ_s Aligning moment sensitivity analysis.
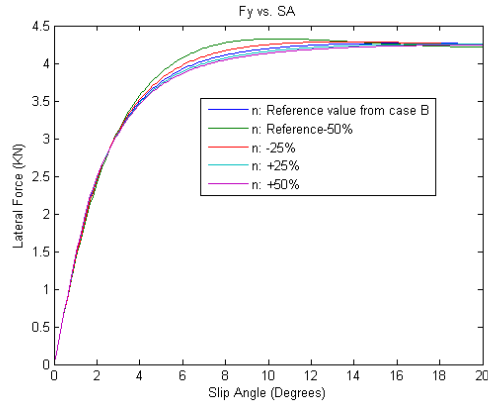
(c) *n* Lateral force sensitivity analysis.
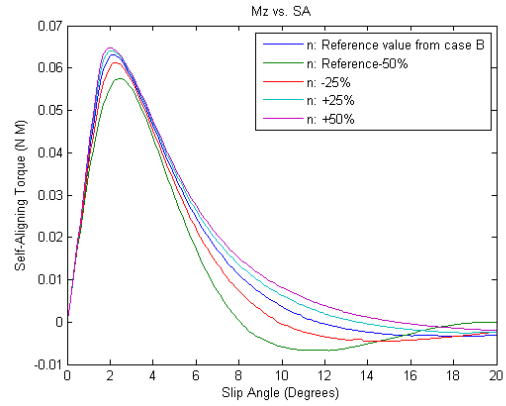
(d) *n* Aligning moment sensitivity analysis.
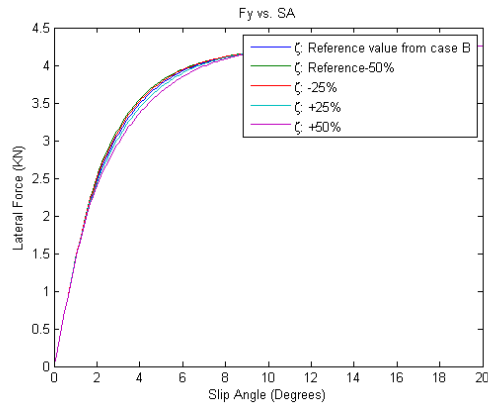
(e) ζ Lateral force sensitivity analysis.
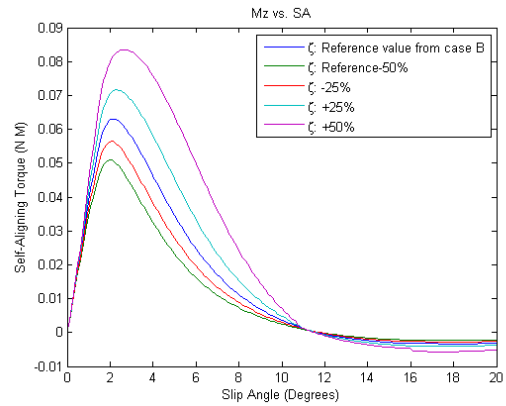
(f) ζ Lateral force sensitivity analysis.

Figure 3.12: *CF/SAT model parameter sensitivity analysis part III*

3.2.3 Non-Dimensionalization

Once the CF/SAT model had been verified and some of the shortcomings of the model had been addressed, the model was non-dimensionalized using the technique presented in 2.3.1. The normal load on the tire and the unladen radius of the tire were selected as repeating parameters. Assuming the analyst would desire to apply this tire to an existing scale vehicle, these parameters would give the analyst the greatest control over the scale and load bearing capability of the scale tire. With the repeating parameters selected, the remaining thirteen parameters were non-dimensionalized to give the non-dimensional CF/SAT model. The pi parameters for this model are outlined in Table 3.3.

The goal of this research is to allow for physical verification of vehicle dynamics in a fast and cost effective manner. If the analyst knows the values for each of the parameters of the CF/SAT model, then the required values for a scale tire can be determined using the pi parameters outlined in Table 3.3. For example, suppose an analyst has determined π_6 to have a value of 635.55 for the full size tire of interest. Since the pi parameters for both the full and scale tires must match for dynamic simultude, then to determine the required value for the scale vehicle's C_y, equation (3.2) needs to be evaluated. This is accomplished by selecting the desired unladen radius and load of the scale tire. To determine the remaining required parameters, the same analysis is simply repeated for each of the parameters at the selected normal load and unladen radius.

$$\left[\frac{C_y R_0^3}{F_z}\right]_{full} = 635.55 = \left[\frac{C_y R_0^3}{F_z}\right]_{scale} \tag{3.2}$$

While the ability to determine the required parameters of a scale tire is an excellent and necessary step towards a successful scale vehicle testbed, the information is meaningless without the ability to both determine the CF/SAT parameters of the full size tire in a cost effective manner, and correlate these parameters to the scale tire's physical construction. The remainder of this thesis is dedicated to a solution to the first of these two requirements.

Table 3.3: *Pi parameters for the Non-dimensional CF/SAT model*

Parameter	Expression	Parameter	Expression
π_1	$\frac{F_y}{F_z}$	π_9	$C_q F_z R_0$
π_2	$\frac{M_z}{F_z R_0}$	π_{10}	$\frac{\zeta F_z}{R_0}$
π_3	$\frac{w}{r_0}$	π_{11}	$\frac{A_{x_0}}{F_z R_o}$
π_4	μ_s	π_{12}	n
π_5	μ_d	π_{13}	$\frac{C_z R_0}{F_z}$
π_6	$\frac{C_y R_0^3}{Fz}$		
π_7	$\varepsilon F_z R_0$		
π_8	$\frac{E I_z}{F_z R_0^2}$		

3.3 Parameterization

One of the largest challenges to analytical modelling is the method by which the tire is parameterized. In order to preserve the utility of the approach presented, the physical parameters, which define tire response within the model, must be easily obtained. Unfortunately, in the work done by Miyashita and Kabe [17], the tire was parameterized through regression analysis performed on a set of empirical data obtained through dynamic tire testing on an MTS Flat-Trac® tire testing system. The cost associated with this method is prohibitively expensive, negating much of the benefit of performing scale vehicle testing. Furthermore, fitting a model to empirically derived data results in physical tire parameters that may no longer represent their intended meaning due to a multiplicity of inputs for a unique output. Figure 3.13 illustrates this more clearly. In order to ensure that the estimated tire parameters match the physical tire's characteristics, the number of parameters that

Parameters based on
regression analysis

Parameters based on
physical tire properties

Model input

CF/SAT model
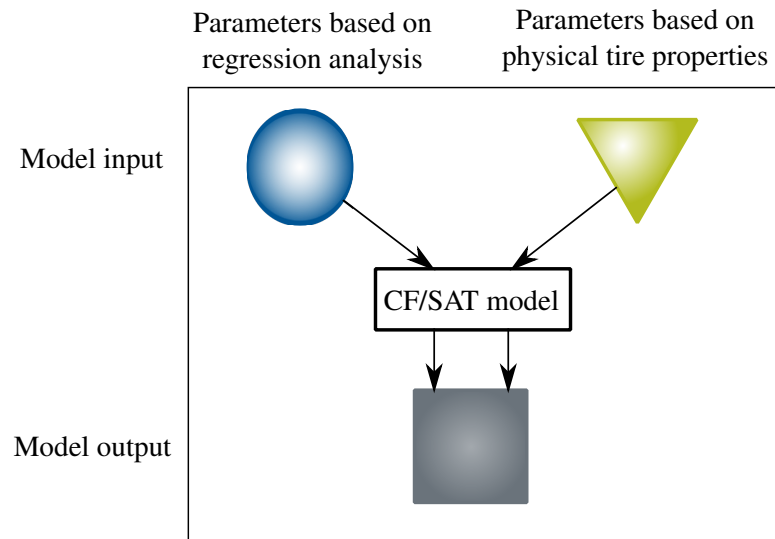
Model output

Figure 3.13: *Duplication of output for multiple inputs.* The circle and triangle represent different sets of input data to the CF/SAT model. One based on regression analysis and the other on the actual physical tire properties each parameter is intended to represent. The range space of the model is such that it is possible to reach the same result with multiple input configurations, however, the real tire can only be represented by one.

require regression analysis need to be reduced. Some form of empirical testing is a requirement for parameterization of a tire. Testing every tire individually in a full dynamic study, however, is impractical and results in very little applicability between tire constructions. It stands to reason that tire response is fundamentally determined by the manner in which the tire deforms. Due to this, the approach taken in this study was to perform a series of static load deflection tests on a tire and attempt to find a relationship between the tests performed and the parameters required for the CF/SAT model. Optimally, a consistent relationship between the load deflection tests and each of the CF/SAT parameters could be determined with some confidence such that future tire studies would no longer require verification through full scale dynamic studies.

To determine any relationships between static load tests and tire response, both a set of deflection curves and results of a full scale dynamic study are required. Due to the cost associated with full scale dynamic testing of tires, the results are typically highly guarded by the customer of such services. Furthermore, the construction of a machine to statically test a full size tire would come

at quite an expense. In keeping with the nature of the study, it was decided that attempting to find these results in a scale tire would be a cost effective and equally valid approach for a first attempt. Dynamic testing data was obtainable for the DU-BRO RC airplane tire through the study done by Polley [20]. Initial estimates for the CF/SAT model parameters for this tire were made using the data through regression analysis. The information discussed in Section 3.2.2 was also used to aid in the fitting analysis that will be discussed in Section 3.3.1. Static load data was obtained from a purpose built load testing machine. The development of this machine is outlined in Chapter 4. The results of this testing, as well as the relationships between these results and the CF/SAT parameters discovered are outlined in Chapter 5.

3.3.1   DU-BRO CF/SAT Model Parameter Estimation

Using the data provided by Polley, a set of CF/SAT parameters were estimated through the use of regression analyses. This was a necessary step to compare pure regression techniques to load deflection relationships in their ability to parameterize a tire for the CF/SAT model. The first challenge to overcome is to find a reasonable estimate for the initial values for each of the parameters. This was accomplished by using the non-dimensional relationships found earlier and the full scale CF/SAT parameters from Miyashita and Kabe.

First the free radius of the tire was measured, and empirical data from Polley was gathered at each normal load desired. Once this was achieved, the pi parameters for the CF/SAT model were calculated using the full scale tire parameters. With this information, the initial parameters for the DU-BRO RC airplane tire were estimated using the technique described in Section 3.2.3. Table 3.4 shows the resulting pi parameter values for the full scale tire, as well as the initial estimate for the DU-BRO CF/SAT model parameters.

The CF/SAT model was then fit to the results obtained by Polley through a manual curve fitting procedure. In order to simplify the analysis the curve fitting was limited to modification of the shoulder coefficient, n, vertical tire stiffness, C_z, the lateral stiffness of a tread element, C_y, and

Table 3.4: *Full size tire pi parameter values and initial CF/SAT model parameter estimates for the DU-BRO tire.*

Pi Parameter	Result	DU-BRO Parameter	Result
$\frac{w}{R_0}$	0.6488	w	0.0225
μ_s	1.62	μ_s	1.3
μ_d	1.06	μ_d	1.06
$\frac{C_y R_0^3}{F_z}$	635.5451	C_y	$1.7375x10^5$
$\varepsilon F_z R_0$	0.0727	ε	16.3515
$\frac{EI_z}{F_z R_0^2}$	2.9449	EI_z	$8.312x10^{-4}$
$C_q F_z R_0$	5.3694	C_q	$1.208x10^3$
$\frac{\zeta F_z}{R_0}$	0.2242	ζ	0.2032
$\frac{A_{x_0}}{F_z R_0}$	0	A_{x_0}	0
n	9.34	n	9.34
$\frac{C_z R_0}{F_z}$	34.482	C_z	38.022

Table 3.5: *Resultant CF/SAT parameters from manual curve fitting for the DU-BRO 5.00 T.V. tire.*

Parameter	Normal load			
	70N	50N	30N	20N
w	0.0225	0.0225	0.0225	0.0225
μ_s	1.3	1.3	1.3	1.3
μ_d	1.05	1.08	1.17	1.25
C_y	$8.6875x10^4$	$6.6397x10^4$	$5.4731x10^4$	$4.7161x10^4$
ε	16.3515	22.8921	38.1535	57.2302
EI_z	$8.312x10^{-4}$	$5.9372x10^{-4}$	$3.5623x10^{-4}$	$2.3749x10^{-4}$
C_q	$1.208x10^3$	$1.6912x10^3$	$2.8186x10^3$	$4.2279x10^3$
ζ	0.2034	0.2848	0.4746	0.7119
A_{x_0}	0	0	0	0
n	2.2	3.8	4.5	4.5
C_z	71.942	42.553	23.310	13.928

the dynamic coefficient of friction, μ_d. The tire width, w, free radius, R_o, normal load, F_z, and the static coefficient of friction, μ_s were either directly measured from the tire or estimated from the research done by Polley. The remaining parameters were left unmodified from the original dimensional analysis due to the relative insensitivity of the model to these parameters, as outlined in Section 3.2.2. Table 3.5 gives the resulting parameters of the curve fitting analysis. The results obtained from the fitting procedure are compared to the results obtained by Polley in Section 5.3.

Chapter 4

The Windsor Automotive Tire Tester

The need to evaluate the performance characteristics of a tire is mandatory for all varieties of tire modelling. This research aims to develop a method to assess tire performance in terms of the parameters required for use of the CF/SAT model. Since the goal of this research is to develop scale tires, the need for a cost effective solution is even more imperative than for full scale tire research. The approach taken was to collect a series of static load deflection curves to determine relationships between this data and the parameters for the CF/SAT model. To accomplish this, a custom testing apparatus entitled the Windsor Automotive Tire Tester (WATT) was developed. Section 4.1 outlines the design and construction of the WATT, Section 4.2 details the sensor and electronic design, and Section 4.3 describes the calibration and test process as well as the performance capabilities of the apparatus.

4.1 Mechanical Design

The WATT is a 2-axis load deflection testing apparatus that was used to collect vertical and lateral deflection data of the DU-BRO T.V. series of tires. The complete assembly is depicted in Figure 4.1. The system is comprised of six main components; the frame, lateral load sensing block, lateral carrier block, vertical load sensing block, vertical carrier block, and the tire fork. Each component
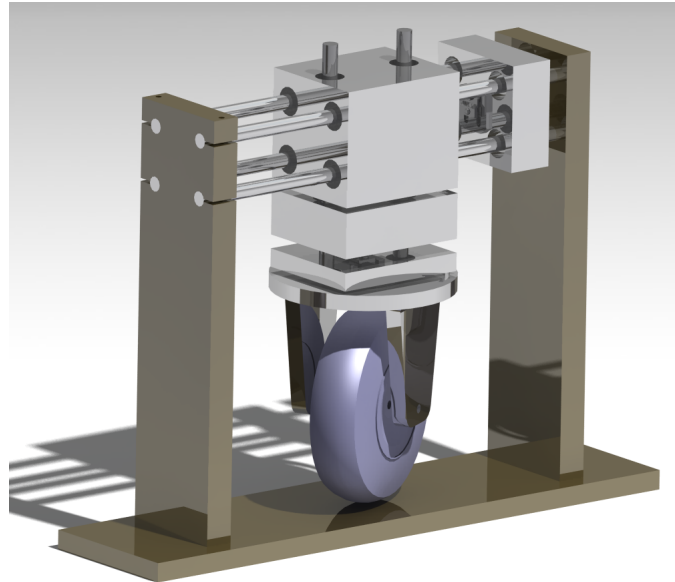
Figure 4.1: *WATT CAD assembly.* Final CAD design of the Windsor Automotive Tire Tester. All design work was completed in CATIA®.

performs a specific function to allow the determination of the loads on the tire with minimal error.

4.1.1   Frame

The frame's primary function is to hold the assembly together and provide a test surface for the testing apparatus. The base and stanchions of the frame are comprised of hardened 1020 steel due to its low cost and hardness. The base plate features a slot with which to locate the stanchions accurately and increase their bending rigidity. The alignment of the stanchions is critical to prevent binding of the carrier assemblies. The frame must be very stiff in order to prevent deflection of the test assembly, which would cause error in the measurements taken. Four guide rods are pressed into the frame to support the lateral load sensing block and the lateral carrier block. An acme thread drive screw and nut are located on the right stanchion to allow the analyst to control the lateral displacement of the tire during testing. This feature can be seen in Figure 4.5.
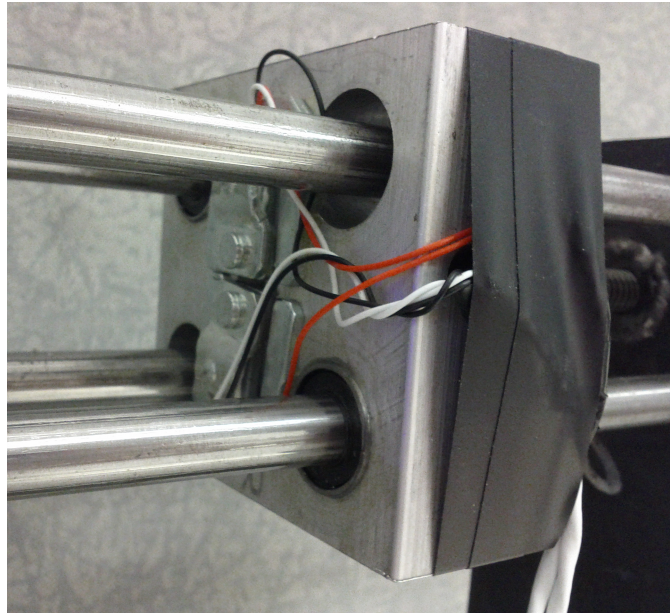
Figure 4.2: *WATT lateral load sensing block.* The load cells are placed in series with the load screw to allow direct measurement of the lateral force exerted on the tire.

4.1.2   Lateral Load Sensing Block

The lateral load sensing block features a strain gauge type load sensor for force measurement along the lateral axis of the testing apparatus. These sensors are discussed in greater detail in Section 4.2. This component additionally features 4 LM10UU linear bearings to allow for motion along the lateral access with minimal friction. These bearings are a mandatory feature of this system in order to minimize the effect of friction on the measurements taken. This block is driven into the lateral carrier block to cause deflection in the tire along this axis. This component is depicted in Figure 4.2.

4.1.3   Lateral Carrier Block

The lateral carrier block's primary purpose is to support the entire vertical assembly, as well as transfer the load placed on the lateral sensing block to the tire. This component also features six LM10UU linear bearings to reduce friction within the assembly. This block and the remaining components are comprised of 6061 T6 aluminium due to its reduced weight over steel components

Figure 4.3: *WATT vertical load sensing block.* The two load cells in the figure are placed in line with the load placed by the drive screw, allowing direct measurement of the applied vertical tire load.

and relatively low cost. An Acme thread drive screw and nut are also located in this component to allow the analyst to control the vertical load and deflection of the tire during testing.

4.1.4   Vertical Load Sensing Block

In similar fashion to the lateral load sensing block, this component is intended to measure the vertical load on the tire in the assembly. It features two linear bearings and a load sensor to accomplish this task. These features can be seen in Figure 4.3 The block is driven into the vertical carrier block to measure the additional load placed on the tire in the normal direction. While it is possible to place zero lateral load on the test tire, due to the design of the machine, the minimum load that can be achieved vertically is equivalent to the weight of this and all the remaining components. This weight amounts to a minimum normal load of 19.5 N.

Figure 4.4: *WATT wheel fork assembly.*

4.1.5   Vertical Carrier Block

The vertical carrier block's primary purpose is to support the entire vertical axis and transfer both the vertical and lateral loads to the tire. The block features two steel rods to support these functions. These rods are press fit into the block. The block also features a counter sunk hole to allow a 10mm bolt to be used to mount the fork and wheel assembly to the testing apparatus.

4.1.6   Tire Fork Assembly

The fork assembly, shown in Figure 4.4, has the primary task of supporting and transferring loads to the tire. A 6mm steel rod is used as an axle for the wheel and the tire is centred along the axle through the use of bushings. A hole through the center of the fork is used to mount the fork to the vertical carrier block. The fork also features a ring on the top surface to locate a needle thrust bearing. This feature will allow the fork to rotate along the vertical axis, allowing for easier modification of the WATT in future applications when a moment sensing system has been developed.
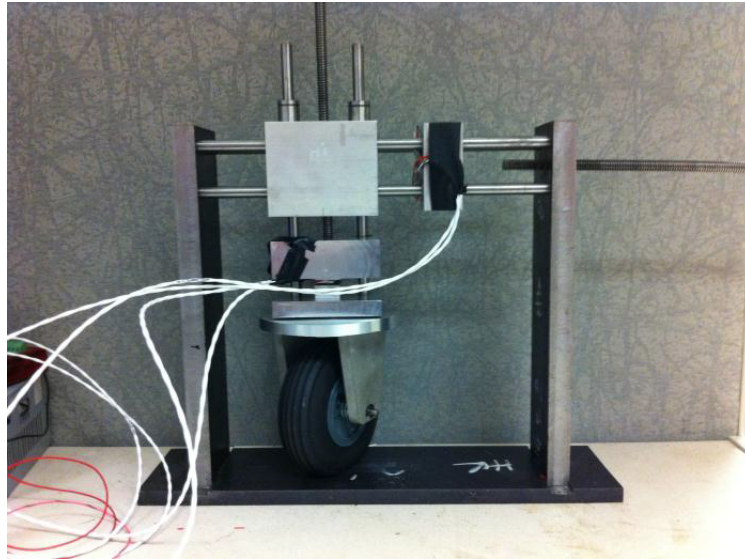
Figure 4.5: *WATT final assembly*

4.2 Electronic Design

The complete electronic package is comprised of three main subsystems that were utilized to measure and record the loads placed on the tire in real time. The electronic system was comprised of four strain gauge type load sensors, a signal conditioning unit, and a LabJack U12® data acquisition system.

4.2.1 Load Sensors

Low-cost-off-the-shelf load sensors were utilized for this machine. The scale was equipped with four load cells, and was rated for a 320 pound load capacity. It was estimated this translated into a load capacity of about 80 pounds for each load cell. Each load sensor was comprised of two active strain gauges. This arrangement allows for greater sensitivity of the sensor as well as implicit temperature regulation. The load sensor is depicted in Figure 4.6.

The typical arrangement of a load cell with two active strain gauges is with one strain gauge on the top surface and one on the bottom surface of a cantilevered beam. This is because the

Figure 4.6: *WATT internal construction of the load cells.* Each cell features two active strain gauges oriented on the top surface.

resistance of the gauges must be divergent from one another with load, otherwise changes in load would change each resistance proportionally, preventing any way of measuring the load. This type of arrangement is depicted in Figure 4.7. This load cell, however, features both strain gauges on the top surface of a beam. Initially it was believed these cells were designed with only one active gauge by placing the second gauge perpendicular to load. This would result in one gauge maintaining a constant resistance with any load on the cell. Through careful disassembly of the load cell, it was realized both gauges are oriented such that they are active. The tab shown in Figure 4.6 was rotated 180 degrees to allow for viewing of the strain gauges. When the load tab is in the normal position, any load placed on the tab results in a combined end load and moment on the sensing beam. This combined loading condition results in a compressive strain on the top surface of the beam from the end of the beam where the tab is mounted to the center, and a tensile strain from the center to the opposite end of the beam. Figure 4.8 depicts the load cell undergoing exaggerated strain. The combined end loading of the beam results in differential loading on the strain gauges allowing both gauges to be placed on the top surface. This arrangement dramatically improves manufacturability, without compromising performance.
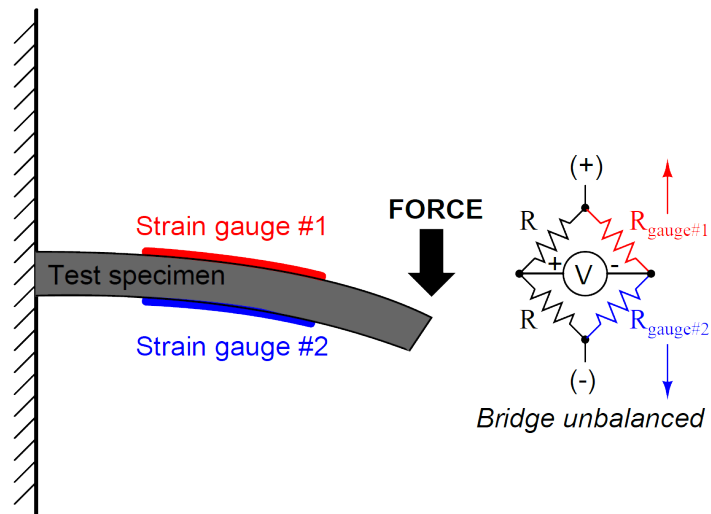
Figure 4.7: *Typical half bridge strain gauge arrangement.* This figure depicts the typical arrangement of a load cell with two active strain gauges. To measure the strain using a Wheatstone the load must be in opposing loading conditions. This figure depicts the strain gauges arranged with two inactive legs to complete the bridge. In the set-up used for the WATT, an additional load cell was utilized for the second half of the bridge, increasing the sensitivity of the system.
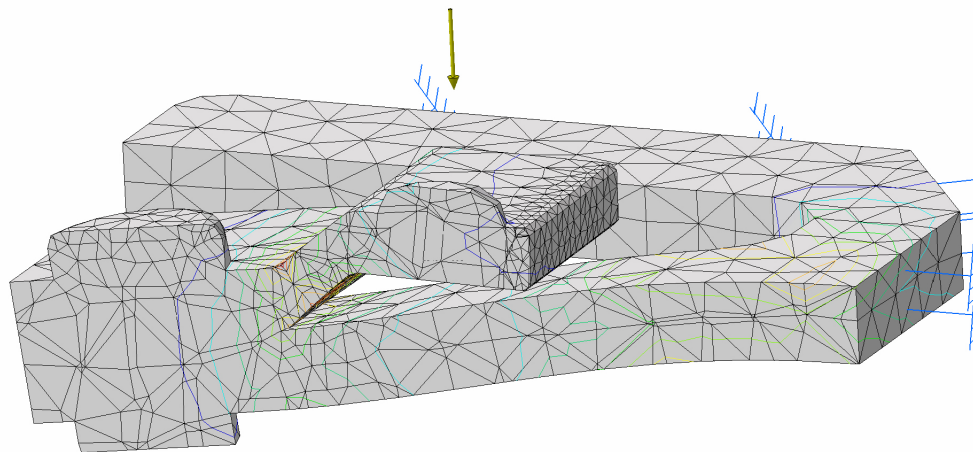
Figure 4.8: *Load cell deformation from applied force.* The figure was produced using CATIA's built in finite element analysis software. The strain gauge was clamped around the perimeter of the base and a 70N distributed load was placed on the center of the load tab. This was done to illustrate the change in loading condition on the top surface of the beam from compressive to tensile.

Full-bridge strain gauge circuit
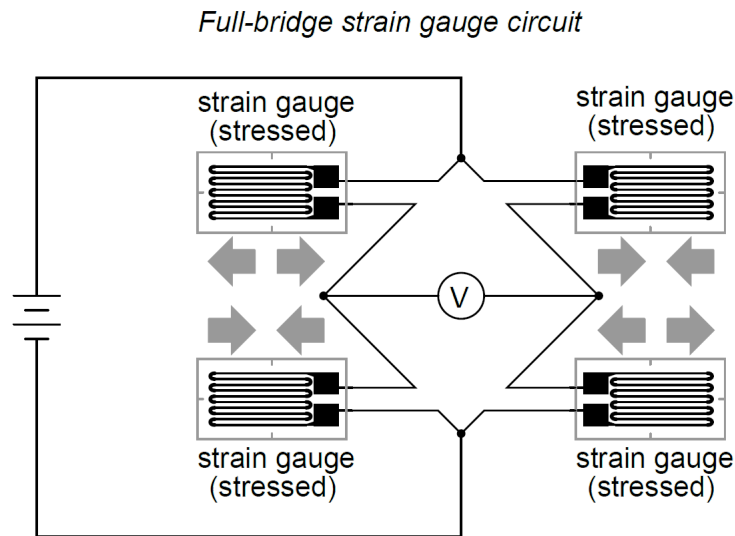
Figure 4.9: *WATT Full active Wheatstone bridge arrangement.* The use of two load cells, and therefore four active strain gauges, increases system sensitivity and inherently compensates for temperature fluctuation.

Two load cells were utilized for each axis, which further increased the sensitivity of the system and reduced noise in the signal. Each load cell represented half of a Wheatstone bridge and, when combined to make a full bridge, could be utilized to measure the load on the cell. Figure 4.9 shows the arrangement of the load cells in the Wheatstone bridge. A twelve volt applied voltage was used for bridge excitation, and when each cell was loaded, a bridge imbalance occurred allowing measurement of the applied strain by the change in voltage across the bridge.

The change in resistance of the strain gauge with load is quite small, only a fraction of a percent with full load. As a result of this the particular arrangement used in this system generates less than 2 mV maximum. To generate a measurable signal from this system some conditioning is required.

4.2.2 Signal Conditioning

The first issue when dealing with small signal outputs is noise. The electromagnetic interference (EMI) present in a typical lab environment is much too high for the signal output of the bridge used
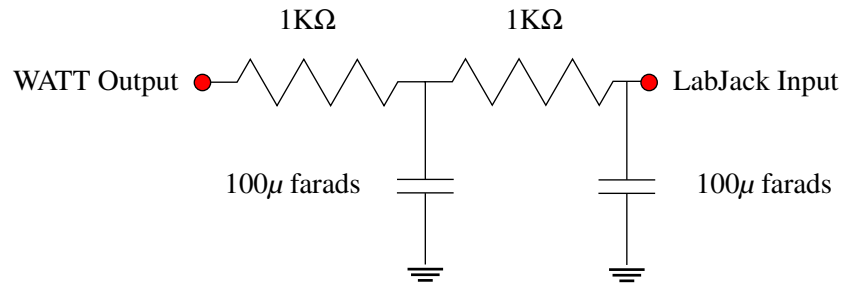
Figure 4.10: *Diagram of the WATT second-order low pass filter.* The second order low pass filter utilized in the WATT attenuates signals from the load cells dramatically when the input frequency is beyond the cut-off frequency.

(a) Filtered input signal

(b) Unfiltered input signal
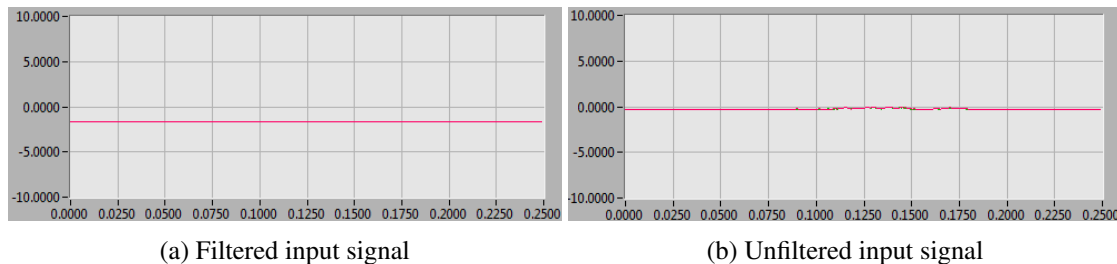
Figure 4.11: *Filtered and unfiltered input signal comparison.* Variation in the signal from the load sensors results when the input signal is unfiltered. This effect is caused by ambient electromagnetic interference.

in this experiment. Sources such as cell phones, wireless routers and the like are unavoidable. To reduce the effect of this noise an aluminium braided shielded wire was used for the signal line. This was grounded at one end only to avoid a ground loop from inducing noise.

Even with this arrangement, the system still exhibited issues with high frequency noise. To eliminate the remaining noise a second order passive low pass filter was utilized. This filter is depicted in Figure 4.10. Since the system is intended to measure static tire load deflection, the cut-off frequency for this filter was set quite low, 1.59 Hz. The measured signal frequency is much lower than this, so there is little performance impact from this arrangement. Figure 4.11 compares the signal input with and without the low pass filter.

The second component required for signal conditioning is amplification of the signal. For this an integrated circuit instrumentation amplifier, the TEXAS INSTRUMENTS INA128, was utilized.

The INA128 allows for gains of up to 10000:1 with very low offset voltage, and temperature drift, with the ability to adjust the system output sensitivity. The WATT utilizes two of these amplifiers, one for each axis, both set for a gain of 895 $\left(\frac{V}{V}\right)$. For more details on the TEXAS INSTRUMENTS INA128 please refer to the data sheet [11].

4.2.3 Data Acquisition

For real-time signal processing a LabJack®U12 data acquisition system was utilized. Initially the design intent was to use the Arduino Uno micro controller prototyping board for data acquisition. A simple software front end was written for the Arduino to convert and display the loads measured by the WATT; however, this system was abandoned due to issues with repeatability.

The LabJack® U12 hardware features a vast array of input and output options. The U12 incorporates eight analogue inputs featuring a twelve bit analogue to digital converter. It also features four configurable digital input/outputs, two analogue outputs, and various voltage source options. For more details on this system please refer to the U12 user's guide [12]. The WATT utilizes two of the single ended analogue inputs from the U12 for data transmission to the acquisition system. The capabilities of the U12 are far beyond what is needed by the WATT; however, this system was readily available at no extra cost and was therefore utilized as a replacement for the Arduino unit.

The software front end utilized was developed by LabJack® and is referred to as LJscope. The software allows for real-time measurement of the output signals from the WATT, and displays the signal as a function of time in the top window of the viewer. The software interface is depicted in Figure 4.12. The bottom window of the viewer displays frequency information of the incoming signals.

4.3 Testing and Calibration

Once the machine was constructed, the electronics package needed to be calibrated in order to determine the relationship between applied load and voltage output for each of the axes. This was
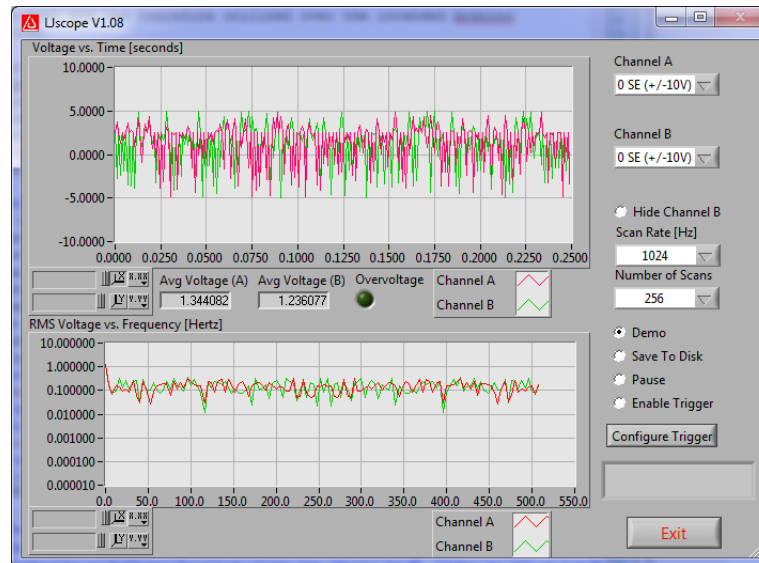
Figure 4.12: *LJ scope user interface.* This software front-end displays both voltage of the input signal as well as the frequency. The average voltage of the input signal over the displayed time span is shown below the top window.

accomplished by isolating each axis on a bench and loading them with a series of known weights and recording the voltage output at each load. This procedure was repeated three times for each axis to ensure repeatability and accurate calibration of the WATT. The results of this calibration are shown in Figure 4.13.

Looking at goodness of fit values for each of the calibration curves in Figure 4.13, it can be seen that the z-axis performed much better than the y-axis in terms of repeatability. This is a result of the weights available for calibration. The z-axis load sensor block was much easier to calibrate due to the two in-line posts that support the assembly, which lend themselves much better to the available slotted calibration weights. The four post y-axis sensor block, however, was much more challenging to centre the weights over, since the four posts used to support the y-axis interfered with the weights. As a solution to this, one post of the z-axis carrier block was used to support the lateral sensor block. The arrangement used is depicted in Figure 4.14. Due to the offset calibration weight and single bearing, much more load was present in the system than normal, resulting in increased friction. This friction in turn induced some error in the load cell calibration of the lateral axis. Despite this, the
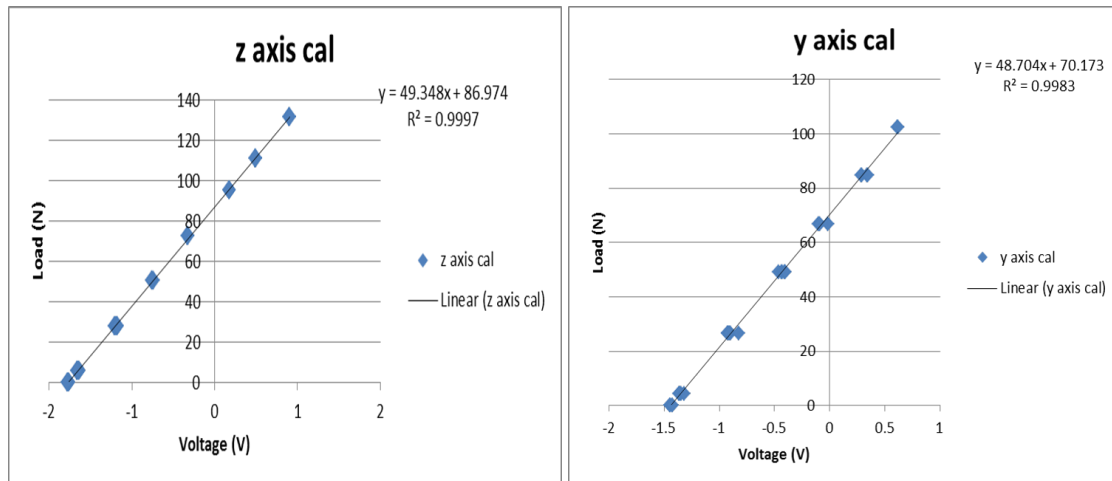
(a) Vertical axis calibration data   (b) Lateral axis calibration data

Figure 4.13: *WATT load cell calibration results.* Combined results of all calibration testing for each axis. Linear regression results were used to find a transfer function between sensor voltage output and applied load. These regression results are displayed in the upper right hand corner of the figure.

calibration results are still satisfactory.

Using the calibration data obtained, a transfer function was found to convert the voltage output to the data acquisition system to the actual load on the sensor. This was done through the use of the built in linear regression analysis tool in Microsoft® Excel. Using the data obtained from this analysis and the data sheet for the INA128, the performance capabilities of the WATT were determined. These results are compiled in Table 4.1. With the construction, calibration and verification of the WATT complete, the DU-BRO tire was then tested.

Figure 4.14: *Lateral axis load cell calibration set-up.* Due to the four posts present in the lateral axis, a single post of the vertical axis carrier block was utilized to support the lateral load sensing block during calibration.

Table 4.1: *System specifications of the WATT.* Compiled testing results and system specifications for the WATT.

Parameter	Specification
Maximum measurable load (N)	130
Lateral load resolution (N)	0.5
Signal gain $\left(\frac{V}{V}\right)$	895
Vertical load sensitivity $\left(\frac{N}{V}\right)$	49.348
Lateral load sensitivity $\left(\frac{N}{V}\right)$	48.704
Filter cut-off frequency (Hz)	1.59
Bridge excitation voltage (V)	12
Amplifier supply voltage (V)	24

4.3.1 Test Procedure

In order to reduce operator error introduced during the testing process, the following general test procedure was observed. For both the vertical and lateral deflection testing, the same general testing procedure was used, with small variations between tests. These variations were intended to highlight different aspects of the results obtained. The specific variations on this test procedure for each experiment are highlighted in the corresponding test sections in Chapter 5.

1. Initialize the tire by removing applied load from the load screws and weight loads to remove any residual deflection from hysteresis effects.

2. Initialize each axis by setting each load block up against the respective carrier block without applying load from the screw.

3. Measure the initial distance from the stanchion, for the lateral axis, or the lateral carrier block, for the vertical axis, to the respective load cell block.

4. Measure the unladen load reading from LJ scope

5. Begin loading the desired axis while maintaining a constant load on the opposing axis. stop after a small distance and record both the load and distance deflected.

6. Repeat until desired load is obtained.

7. Measure the fully deflected distance and begin unloading the tire slowly. Stop after a small distance and record both the load and distance deflected.

8. Repeat until load screw is fully removed from the load cell block.

9. Measure final position.

Chapter 5

Results and Discussion

The following sections will present and discuss the results of the studies done with the WATT on the DUBRO 5.00 T.V. tire. The first section, 5.1, will present the general static load deflection behaviour measured by the WATT. The second section, 5.2, will discuss the relationships used to find a correlation between the load deflection behaviour and the CF/SAT model parameters. The final section, 5.3, will compare the results of the CF/SAT model from the parameterization using the developed relationships to the regression analysis performed in Section 3.3.1, as well as, the magic tire model developed by Polley.

5.1 Tire Load Deflection Behaviour

The DUBRO 5.00 T.V. tire was tested in both the lateral and vertical directions independently. Independently loading each axis allows for the derivation of CF/SAT parameters responsible for tire behaviour solely along the corresponding axis. During the vertical deflection tests, no lateral load was placed on the tire. During the lateral deflection tests, a constant normal load was maintained as the tire was loaded laterally. Adjustment of the vertical load screw was mandatory to maintain normal load, due to tire deflection. Several tests were conducted at various normal loads in the lateral direction.

5.1.1 Vertical Deflection Behaviour

In the vertical direction, six separate tests were conducted. The first test measured tire deflection with increasing load only. The tire was loaded and tested following the procedure in Section 4.3.1 until the normal load exceeded 100 N. Once this was achieved, the tire was reinitialized and loaded again a minimum of one hour later. The time between each load cycle was inconsistent during this test. A total of four loading cycles were completed for the first test. The second test was to measure tire deflection behaviour starting in a loaded position and decreasing the load on the tire. The tire was quickly loaded to about 150 N and incrementally unloaded until the load screw was released from the load block. This test was only conducted for a single load cycle. This was because it was observed during the second load cycle in test two that the normal load on the tire at high load and constant deflection was rapidly diminishing. A third test that loaded the tire and unloaded the tire in the same load cycle was completed. The same effect observed in test two was seen in test three. Before further testing was conducted, these results were investigated. Once the observed results were verified to be a tire phenomenon and not an error introduced by the WATT, four additional tests were conducted following a similar procedure to test three. For tests four to seven, the tire was loaded and measured incrementally up to about 120 N. It was then held at a fixed displacement for two minutes. After the two minutes were complete the tire was incrementally unloaded and measured. Each of these tests and the observations made at high normal loads will be discussed in more detail in the following sections.

Vertical Load Test One

Figure 5.1 shows the results obtained for the first vertical load test on the DUBRO 5.00 T.V. tire. The first test seemed to show a fairly linear relationship between tire deflection and normal load with increasing load. Microsoft® Excel's built in linear regression tool was utilized to fit a line to the results obtained in test one. The Goodness of fit value obtained from this analysis was 0.9919, indicating the results indeed approximate a linear relationship. The slope of this curve would there-
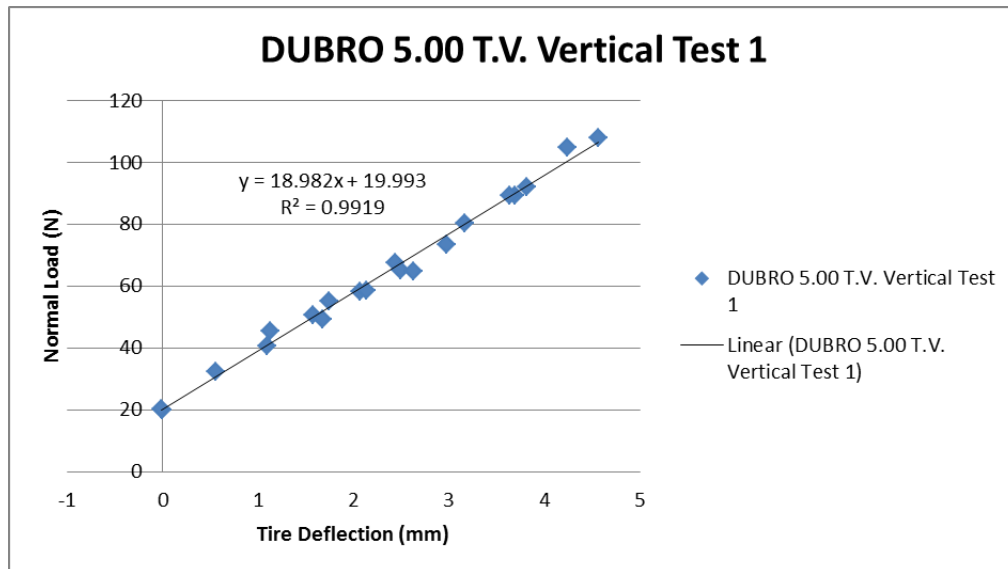
Figure 5.1: *DUBRO 5.00 T.V. vertical deflection results for test one.*

fore give the average vertical stiffness of the tire. With these promising results an effective tire stiffness with decreasing load was then pursued.

Vertical Load Test Two and Three

To capture the tire's behaviour with decreasing load the same procedure used in test one was to be applied to test two, except with decreasing load. The result of the first load cycle of testing indicated a much less linear relationship than observed in test one. This was attributed to a rapidly decreasing observed normal load with fixed vertical displacement of the tire. It was initially believed this was a product of the test equipment. The use of inexpensive load cells and heat rejection from the higher current as a result of a significantly more imbalanced bridge at high loads was believed to result in temperature effects in the measurement. Instead of continuing testing on more load cycles with this procedure, a third test was conducted, slowly loading the tire and measuring the results, followed by slowly unloading the tire and measuring the results. It was believed this would give the system time to normalize the temperature of the load cell; however, the same effect of rapidly decreasing load with time at high normal loads was observed. The results obtained from these tests are provided in
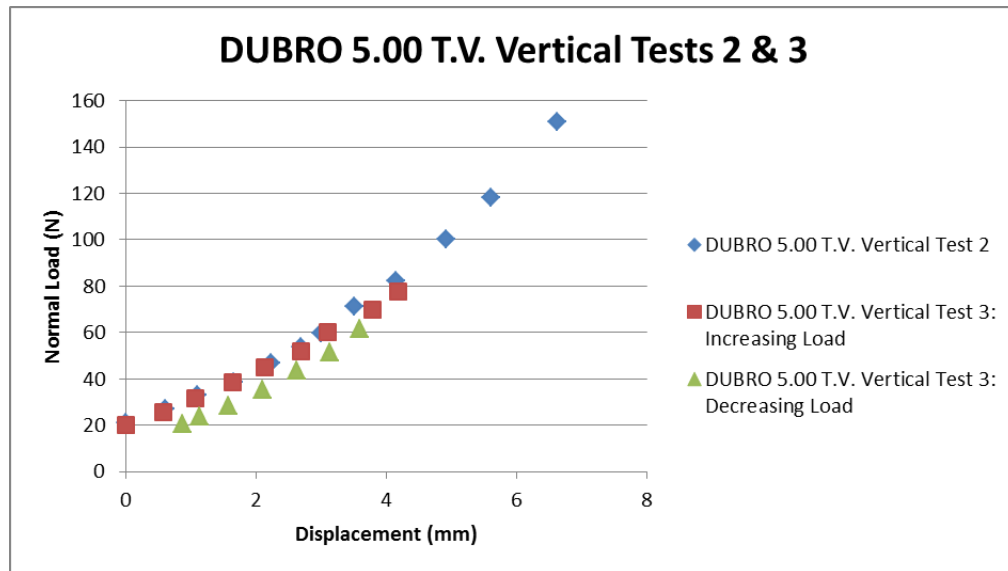
Figure 5.2: *DUBRO 5.00 T.V. vertical deflection results for test two and three.*

Figure 5.2. These results were not utilized due to improper management of the observed behaviour at a fixed displacement with high normal load.

High Normal Load Tire Behaviour

Before further testing could be conducted, the source of the observed results needed to be understood. To accomplish this, the tire was loaded to a high load and the displacement was maintained over five minutes. The normal load was recorded incrementally over the time period. This was done three times to ensure the observed results were repeatable. The results of this test are shown in Figure 5.3. To determine whether these observations were a result of the WATT or a tire phenomenon the same procedure was repeated without the tire. The tire fork was driven directly into the base of the WATT. These results are shown in Figure 5.4. As can be seen in Figure 5.4 there is some time dependence on the measurement observed by the WATT as suspected. The change in the observed measurement, however, only account for about 1-2% of the initial value. After 1 minute the measurement decreases less than 0.5%. In the observations made by the WATT with the DUBRO 5.00 T.V. tire, the change in load over the observed time span was between 10-15%. This indicates
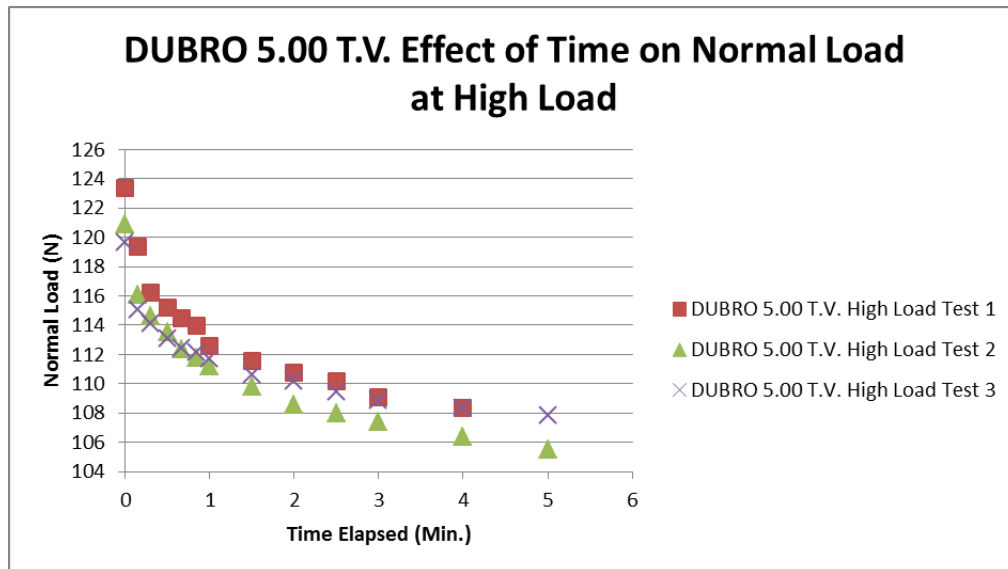
Figure 5.3: *DUBRO 5.00T.V. effect of time on normal load at high loads.*

the time dependency of the normal load is an effect inherent in the tire and not the measurement equipment.

One property of vulcanized rubber material, such as that used in the DUBRO tire, is that of stress softening. As the material is stretched the force required to maintain the strain induced in the material declines with time. This effect is also known as the Mullins effect, named after the discoverer [18]. This effect results in both reduced force to maintain constant strain in the material over time, as well as reduced material stiffness during subsequent loading cycles of the material. After an extended period of time the majority of the material stiffness returns. In the tests conducted in this study the effect manifested itself as both a reduced normal load with fixed deformation over time at high normal loads, as well as reduced vertical tire stiffness with subsequent load cycles. The latter manifestation is illustrated further in the next section. In Bever [5], several possible sources for this effect are cited.

1. Breaking and remaking of cross links during extension.

2. Residual load orientation of network chains persisting after recovery.
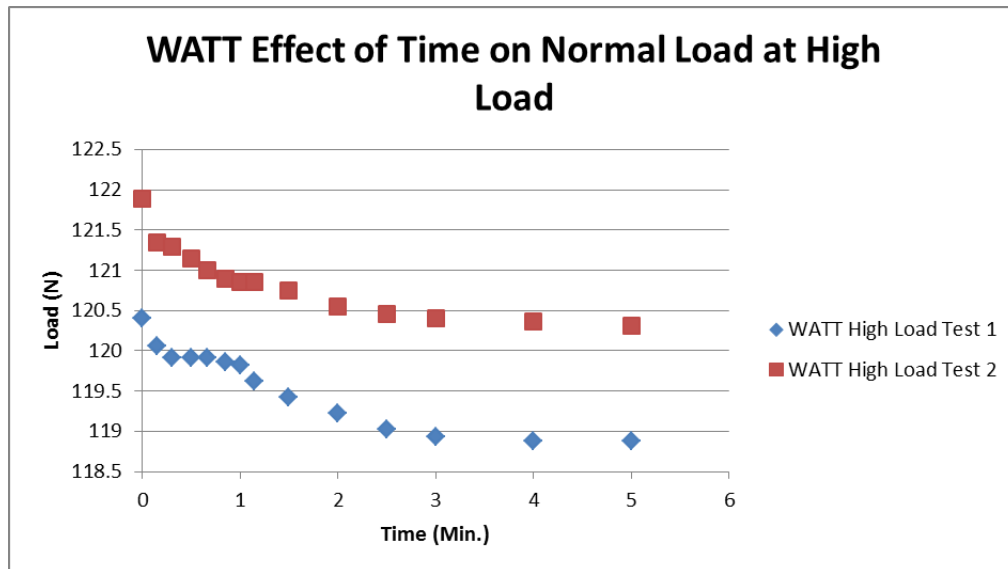
Figure 5.4: *WATT effect of time on normal load at high loads.*

3. Breaking of network chains.

The normal load on the tire continued to decrease over the time period it was analyzed in this study, however, eventually the tire must reach some equilibrium point. The time required for this to occur was not established within this body of work. A rolling tire will undergo a similar effect as observed during the sequential load cycles of these tests, due to the loading and unloading of tire sections as they enter and exit the contact patch. This will affect how the tire behaves in a dynamic setting, however, to what extent this will affect response is unknown. As a result, the remaining tests were conducted by carefully controlling the time the tire spent at high load to produce more repeatability within the tests.

Vertical Load Tests Four Through Seven

Once the behaviour observed in the previous tests had been understood, a final set of tests was developed to capture vertical tire deflection behaviour such that the influence of these effects would be manifested in a repeatable manner across the remaining tests. To accomplish this, the tire was again loaded and incrementally measured up to the peak normal load. The tire was then allowed to
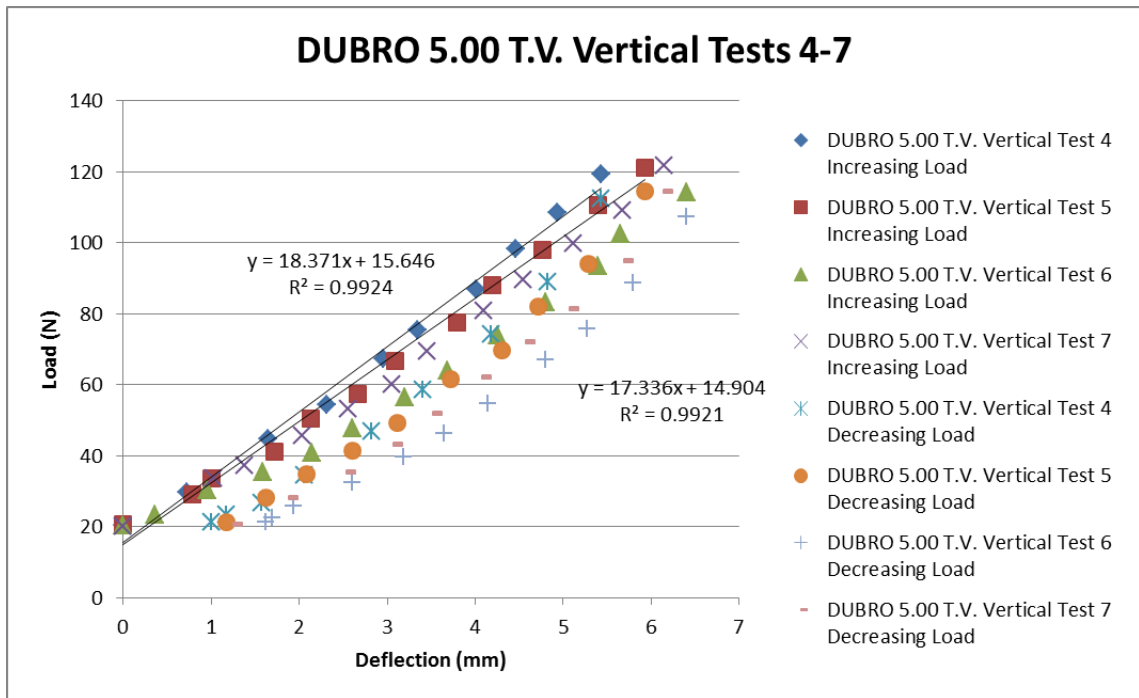
Figure 5.5: *DUBRO 5.00 T.V. vertical deflection results for test four through seven.*

rest at full load for two minutes. This period of time was selected because the majority of the stress softening and sensor effects within the WATT would have occurred. After this period, the tire was incrementally unloaded and measured. The tire was allowed to rest at a 20 N normal load for five minutes between tests four through six. Test seven was completed 60 minutes after test six. The results are shown in Figure 5.5

By controlling the time the tire was allowed to rest at both high and low loads, a predictable effect on the tire's behaviour with vertical load can be demonstrated. As described in Section 5.1.1, the stress softening effect of the tire material is visible in Figure 5.5. A drop in normal load is seen between each individual test's increasing and decreasing load curves over the two minute span, for which it was held at a fixed deflection at high load. The normal load required to maintain tire deflection at peak normal load consistently dropped 5.5-6% for each of the tests.

The effect of the stress softening property of the material is also seen in the reduction of the overall vertical tire stiffness between subsequent tests. To demonstrate this, a linear curve fit was

made for tests four and five. The reduction in the slope of this curve is due to stress softening. In tests four through six, the fixed five minute interval resulted in reduced overall stiffness with each test. A larger reduction of stiffness was observed between test five and six than between test four and five. After the tire was allowed to rest at low normal load for 60 minutes, a recovery of the tire's overall stiffness was observed in test seven.

5.1.2 Lateral Deflection Behaviour

Once the tire's behaviour in the vertical direction was understood, it was then tested for lateral response. Five tests were conducted in total, each at a different normal load. Because the tire deforms as it is loaded laterally, the normal load screw had to be adjusted during the testing to maintain a constant normal load on the tire. As a result, the normal load on the tire varied within +/- 2% of the nominal normal load, with larger variations occurring at higher normal loads.

Due to the nature of the testing, sliding of the tire during the loading phase is unavoidable. As a result, the reference used for the loading phase cannot be used for the unloading phase. To resolve this, it is assumed the tire returns to a state of zero deflection once the lateral load on the tire had been completely eliminated. As the normal load on the tire increases, this assumption can be observed to diverge farther from reality. Despite this fact, however, the assumption allows for comparison of the stiffness of the tire between the loading and unloading phase even if the actual displacement of the tire during unloading is unknown.

In the lateral direction, the deflection response of the tire displayed much more non-linearity than observed in the vertical direction across all of the tests. As the tire was loaded laterally, the force response of the tire would actually decrease occasionally with increased lateral displacement. The response seemed to resemble that of snap-through buckling. This could, perhaps, be caused by a buckling of the sidewall as the tire is deflected laterally. This snap through buckling effect, where the lateral response decreases with increased displacement, can be observed in every test, except the 70 N load, to occur at two distinct locations prior to full saturation of the tire's contact patch. This

is likely due to each sidewall buckling at a separate instance, resulting in the observed reduction in lateral response. In test five, however, there are three locations where this seems to occur. It is believed this is due to a buckling event from each of the side walls and a separation of the tire bead from the wheel at very high displacement. The specific results for each of these tests will be discussed in more detail in the following sections.

Lateral Load Test One: 20 N

The first test was conducted at a normal load of 20 N. Figure 5.6 shows the results obtained from this test. As expected, the response of the tire to lateral deflection occurred in a very non-linear fashion. The snap through buckling effect discussed earlier in Section 5.1.2 can be observed to occur at around 2 mm of displacement and 5 mm of displacement. The tire reached its peak lateral load, 23 N, at around 6.5 mm of displacement. It is at this point the tire began to slide along the surface. Continued deflection beyond this point simply resulted in oscillation between about 19 and 23 N. During the unloading phase of each test, 0.5 mm of deflection was initially removed from the last position of the loading phase. This resulted in a significant reduction of lateral load on the tire, from 22 N to 6 N for test one. As a result of this, there were limited data points collected during the unloading phase of this test. Despite this, the test data is still viable since the objective of these tests is to estimate stiffness of the tire during each phase individually and data points at high displacement need to be rejected due to sliding. Microsoft® Excel was used to fit a line to the test results in order to estimate an overall lateral stiffness. Data after a 6.5 mm displacement was ignored. This resulted in an estimated stiffness of 2.57 and 3.38 N/mm for the loading and unloading phases, respectively.

Lateral Load Test 2: 30 N

The second test was conducted at a normal load of 30 N. Figure 5.7 displays the results observed during this test. The buckling effect can again be observed to occur at about 3.5 mm and 9 mm of deflection. In this case the snap through effect seemed to coincide near the peak of lateral force,
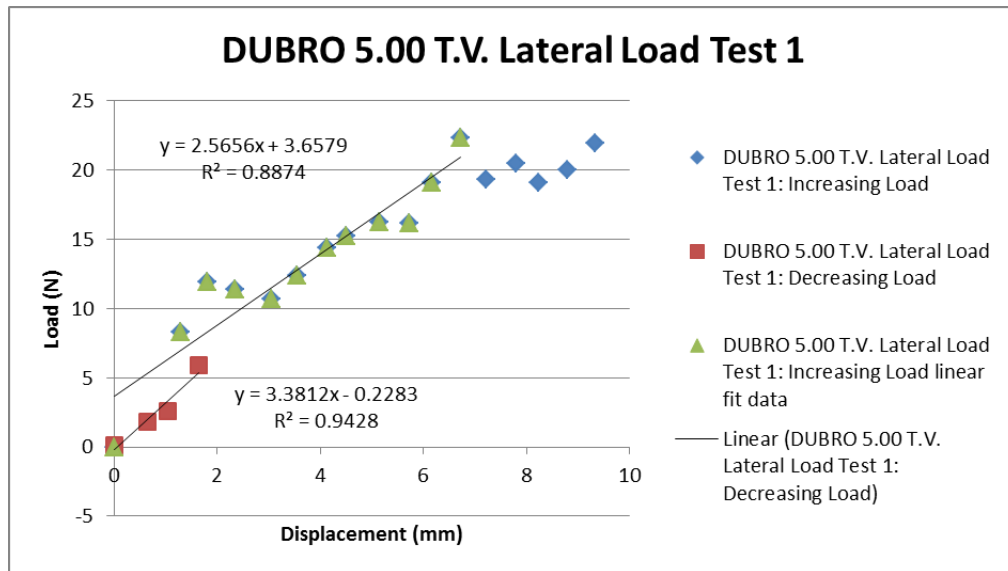
Figure 5.6: *DUBRO 5.00 T.V. lateral deflection results for test one.*

also occurring at 9 mm of deflection. The maximum observed load during this test was about 25 N. It was again observed with continued deflection beyond this point the tire force oscillated between 23 and 25 N. During the unloading phase the majority of the load on the tire was released during the initial 0.5 mm of reduced deflection. After this point, the tire unloaded in a much more linear fashion than during the loading phase. Ignoring the data points obtained after the tire began sliding, beyond 9 mm of deflection, a lateral tire stiffness was estimated using Microsoft® Excel's built in linear regression tool. This resulted in an estimated stiffness of 2.72 and 2.27 N/mm for the loading and unloading phases, respectively.

Lateral Load Test 3: 40 N

A third test was conducted at a 40 N normal load. These results are depicted in Figure 5.8. Through inspection it can be observed that snap through buckling occurred in this test configuration at a deflection of 4 mm and 10.5 mm. A much less defined peak was observed in this test than encountered in previous tests. This could be a result of tire slippage prior to capturing the peak load measurement. The observed maximum force was 31 N occurring at 13 mm of deflection. This oscillated
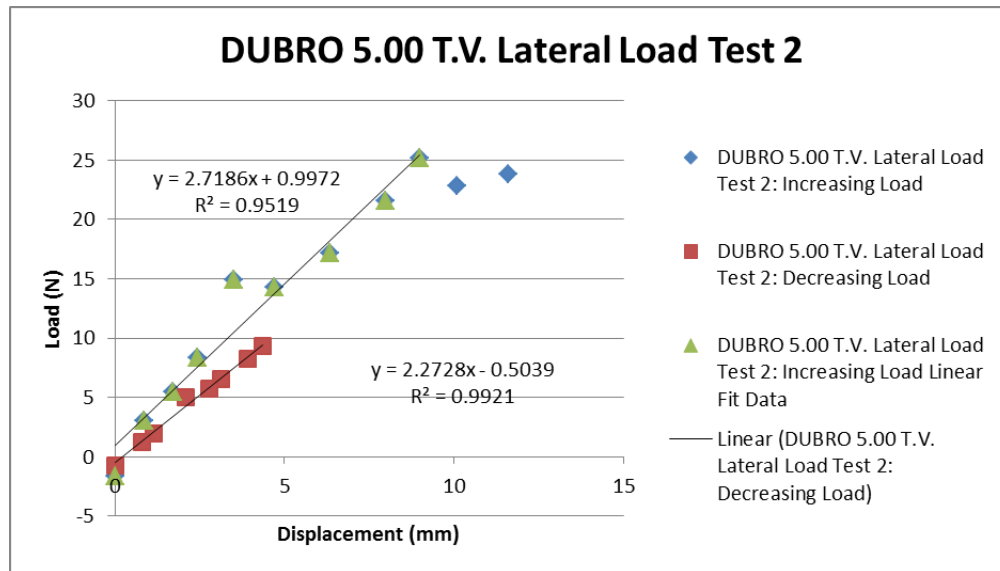
Figure 5.7: *DUBRO 5.00 T.V. lateral deflection results for test two.*

between 28 and 31 N with increased loading. For a third time it was observed that the majority of the load in the tire was released during the initial unloading segment. After this large decrease, the tire unloaded somewhat linearly from about 16 N of load. Using linear regression a tire stiffness was estimated during each of the phases ignoring data occurring after the observed peak at 13 mm. The estimated stiffness at 40 N of normal load was found to be 2.05 and 2.14 N/mm for loading and unloading of the tire, respectively.

Lateral Load Test 4: 50 N

The fourth test was conducted at a normal load of 50 N. These results are depicted in Figure 5.9. As can be seen in the graph the peak lateral load of 36 N occurs at 15 mm of deflection. Further loading resulted in oscillation between 32 and 36 N of force. The snap buckling effect was observed to occur at a displacement of 6 mm and 10 mm during this load cycle. During the unloading phase the lateral load decreased initially to a value of 17 N and steadily declined over 9.5 mm of unloading. The loading and unloading overall lateral stiffness of the tire was estimated to be 2.14 and 1.85 N/mm for this cycle, respectively.
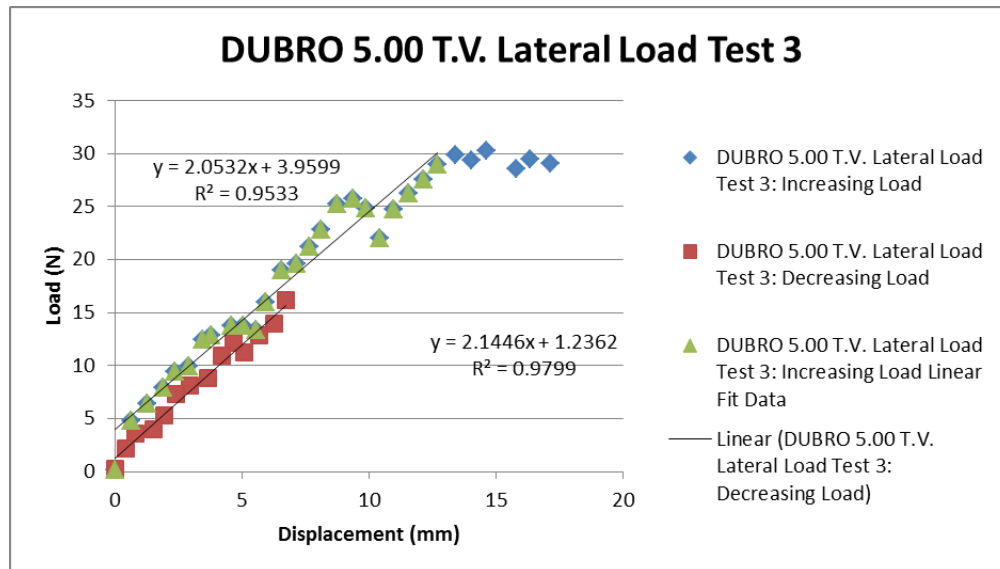
Figure 5.8: *DUBRO 5.00 T.V. lateral deflection results for test three.*

Lateral Load Test 5: 70 N

The final test conducted was performed with a normal load of 70 N. Although the research con-
ducted by Polley included results obtained at this normal load, it appears to be beyond the load
capacity of the tire at high lateral loads. Large deflections at this normal load resulted in separation
of the tire bead from the edge of the wheel. This can be seen in Figure 5.10. It is believed this
resulted in higher than anticipated lateral load results due to compression of material on the trailing
edge of the wheel. Vertical deflection was increased dramatically over the course of the test, to
maintain normal load with the stretching of the tire, causing material to compress as it attempts to
exit the contact patch.

The results for this test are shown in Figure 5.11. The peak lateral force observed during this
test was 52 N, occurring at 22 mm of deflection. Continued deflection beyond this value resulted in
lateral load oscillation between 42 and 49 N. The snap-through effect is observed to occur at 6 mm
and 12 mm of deflection. A third region of reduced lateral load with increased deflection is seen at
17 mm of deflection. It is believed this is a result of the separation of the tire from the wheel at this
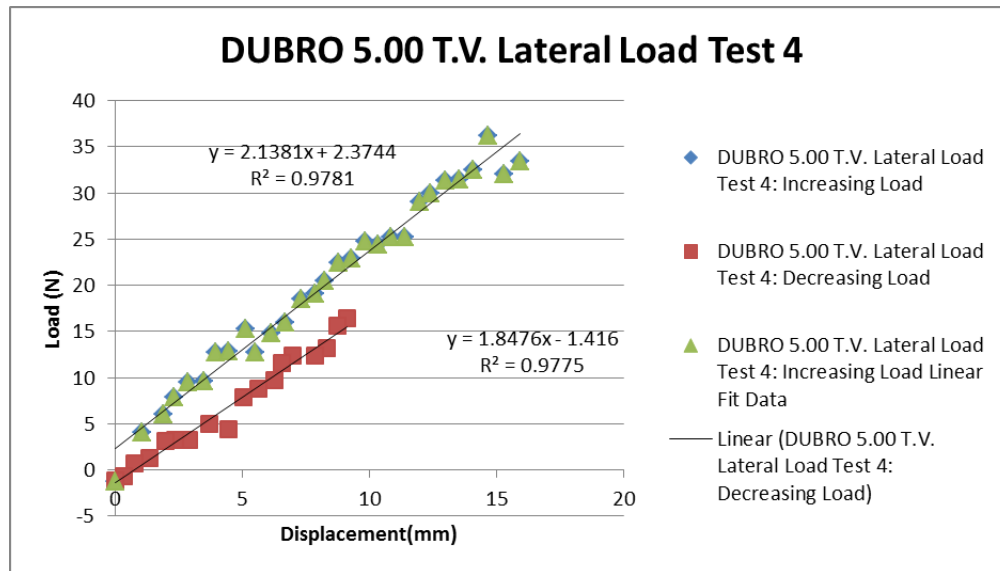
Figure 5.9: *DUBRO 5.00 T.V. lateral deflection results for test four.*

point.

During unloading the observed lateral load dropped dramatically initially and reduced less linearly than observed in the previous tests, starting from about 21 N. Once the lateral load had been fully removed a significant deflection remained in the tire prior to the removal of the normal load. This deflection is depicted in Figure 5.12. Due to the tire wheel separation, the tire material seemed to be caught between the wheel and the test surface, unable to return to it's initial position. This resulted in a significantly higher than expected estimated overall lateral stiffness for the tire in both the loading and unloading case. The estimated stiffness was found to be 2.31 and 2.26 N/mm, respectively.

5.2 Parameterization Relationships

The load deflection results obtained in Section 5.1.2 were then used to estimate some of the CF/SAT model parameter values for the DUBRO 5.00 T.V. tire. The most obvious and simplest parameter to estimate is the overall vertical stiffness of the tire, C_z. This was a simple choice as it is the only

Figure 5.10: *DUBRO 5.00 T.V. tire wheel separation at large deflection under 70 N normal load.*

parameter within the model that relates the tire to vertical deflection. Parameterization of the tire in the lateral direction is a much more difficult challenge.

The CF/SAT model uses several parameters to define the lateral deflection response of the tire. Namely, the lateral spring constant of a tread element, C_y, belt deflection compliance, ε, and the bending rigidity of the belt, EI_z. One of the features lacking on the DUBRO tire that is present on a full size tire is a belt. As a result of this, it was decided that the data collected on the lateral deflection response of the tire would be used to estimate the parameter C_y directly. The remaining parameters for the CF/SAT model were either estimated directly from the research done by Polley, or determined by scaling the parameters used in the work by Miyashita using the non-dimensional parameters developed in Section 3.2.3. The following sections will detail the relationships used to estimate the selected CF/SAT parameters from the load deflection data obtained in Section 5.1.
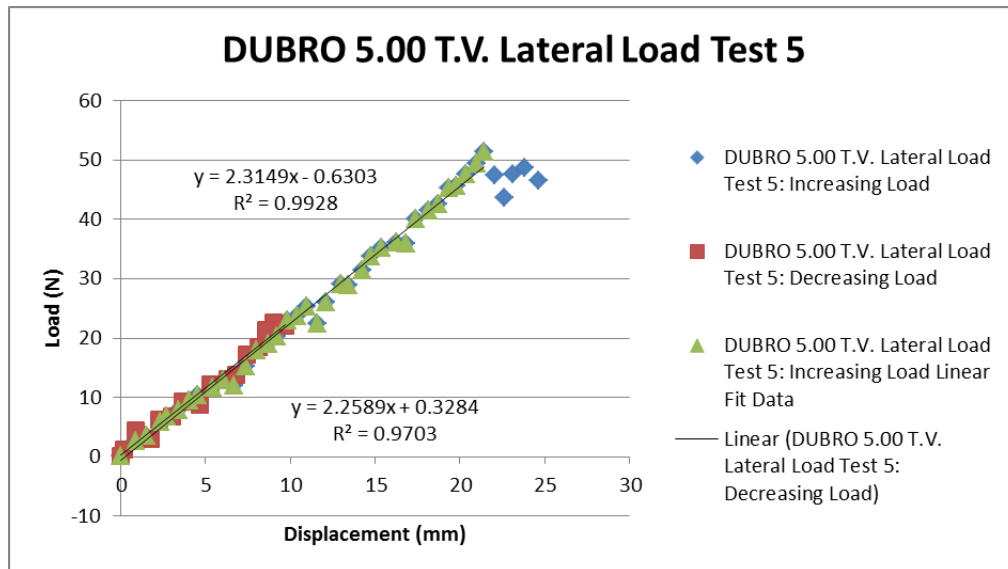
Figure 5.11: *DUBRO 5.00 T.V. lateral deflection results for test five.*

5.2.1   Overall Vertical Tire Stiffness

The tire's overall vertical stiffness was estimated from the slope of the regression analysis done in the vertical deflection testing of the tire. Only the data obtained during the loading phase of the cycle was used. This was because of the inconsistencies encountered during the unloading phase due to the effects discussed in Section 5.1.1. Of the tests performed, only test one, four and five were used to estimate the vertical stiffness of the tire. This was done to limit the influence of the poorly managed hysteresis effects encountered during testing. A better estimate may result from a more controlled testing procedure if the influence of these effects is better understood in regards to dynamic tire performance. Without this knowledge, the results may be unfairly weighted towards a lower vertical stiffness. Unfortunately, a full treatment of the hysteresis encountered is beyond the scope of this study. Despite these challenges, an estimate for C_z was made that differed dramatically from the results obtained through pure regression analysis, but still resulted in good correlation between the CF/SAT model and the results obtained by Polley. These results are discussed in more detail in Section 5.3. Using the average of these slopes, C_z was approximated to be 18.229 N/mm.

Figure 5.12: *DUBRO 5.00 T.V. residual tire deflection with full removal of lateral load during 70 N normal load test.*

5.2.2 Lateral Stiffness of a Tread Element

The relationship between the lateral spring constant of a tread element, C_y, and the lateral deflection relationship is not as simple as the relationship used for the vertical tire stiffness. Looking at the units used in the CF/SAT model for this parameter, it was discovered the parameter is defined as a force over a volume or a stiffness over an area. Using the slope of the regression fit to the data obtained in Section 5.1, an estimate of an overall lateral stiffness was made. Several relationships were explored to try and relate the overall lateral stiffness to the CF/SAT model in terms of the units described within the model. Since there were three parameters defined by length within the model from which to select from and which parameter was an appropriate selection was not obvious, the stiffness was divided by the sum of squares of each of these lengths. The initial result did not give good correlation, however if the estimated stiffness is multiplied by 0.981×10^2, then an excellent correlation was obtained at *each normal load*. If this result was obtained for a single normal load case, then it could easily be dismissed as coincidence. However, since good correlation is obtained

at every normal load, except the 70 N which is explained in Section 5.3.2, it is unlikely to be merely happen stance. This is particularly true because the value of the contact patch length, which is used to determine this parameter, is changing with each normal load in relation to the obtained vertical stiffness C_z. This relationship is depicted in equation (5.1), where k_y is the estimated overall lateral tire stiffness in $\frac{kN}{m^3}$.

$$C_y = \frac{0.981 \times 10^2 k_y}{l^2 + w^2 + r_0^2} \tag{5.1}$$

While the reasoning behind why this relationship gives such accurate results is unknown, the dependency of this value on a second estimated parameter, as well as, its applicability across different normal loads make it hard to believe it is mere coincidence. The results obtained using the relationships described above will be compared with the results obtained by Polley, as well as the results obtained through pure regression analysis in Section 5.3.

5.3 CF/SAT Parameterization Results

Using the data obtained from Polley, the results of the manual curve fitting procedure, and the relationships described in Section 5.2, the ability of the CF/SAT model to predict the performance of the DUBRO 5.00 T.V. was determined. The magic tire model results from Polley are assumed to represent the actual tire performance accurately. The manual curve fitting of the CF/SAT model to these results is shown to assess the validity of the use of regression analysis in determining the parameters of this model for any given tire. The results obtained from the static tire deflection testing and their corresponding relationships are compared at each normal load to both Polley's data and the manual curve fit.

The load-deflection data was used to estimate both the overall vertical stiffness, C_z and the lateral spring constant of a tread element, C_y. The remaining parameters were estimated in an identical way to the manual curve fitting procedure. These parameters were estimated through

dimensional analysis of the full size parameters provided in Miyashita using the non-dimensional relationships obtained in Section 3.2.3 and data from Polley. As such, the parameters not defined by these relationships match those used in the manual curve fitting analysis. It should be noted that the parameters that are similar between these two approaches were never modified in either case; they were estimated from the full size data and left unchanged both during the manual fitting of the model and the estimation of the parameters from the static load tests. This is important because it would be quite easy to manipulate the data to achieve the observed results; however, this would render the relationships discovered insignificant. The results given in the following section were purely a result of the relationships ascertained. Table 5.1 gives the values used for the CF/SAT parameters with the model estimates from the load deflection data. It can be observed that no modifications of the parameters was required in order to maintain the accuracy of the discovered relationships by comparing these values with Table 3.5

5.3.1 20, 30, and 50 N Normal Load Results

Figure 5.13 compares the results for the 20, 30, and 50 N normal loads found by Polley to the manual curve fit, and load deflection relationship parameterization methods for the CF/SAT model. It can be seen that the results show excellent correlation between all three of these approaches in each of the three cases. The largest variation between Polley's results and the CF/SAT model using the load deflection data is 2.74%, 1.93% and 17.43% for the 20, 30, and 50 N tests respectively. While the 17.43% result seems quite high for the 50 N load case, it occurs at a low slip angle which over inflates the percent error when compared to the absolute error. The average difference between the results more accurately represents the overall error, which is only 1.042%, 1.170% and 3.481% for each of the tests. This result indicates the relationships used to estimate the C_z and C_y parameters for the CF/SAT model for this dataset are valid.

The values for C_z and C_y for the measured parameters and the curve fit parameters are shown in Table 5.1 and Table 3.5 respectively. Looking at these values it can be seen that the measured value
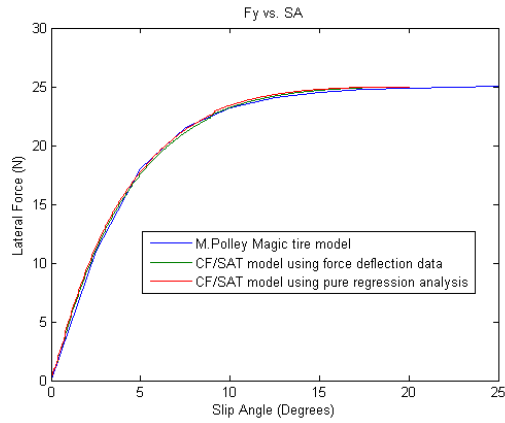
(a) 20 N normal load
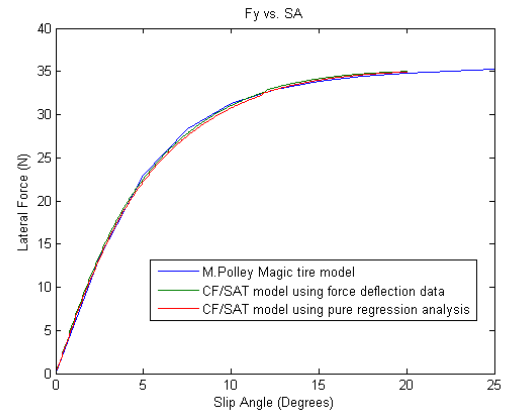
(b) 30 N normal load
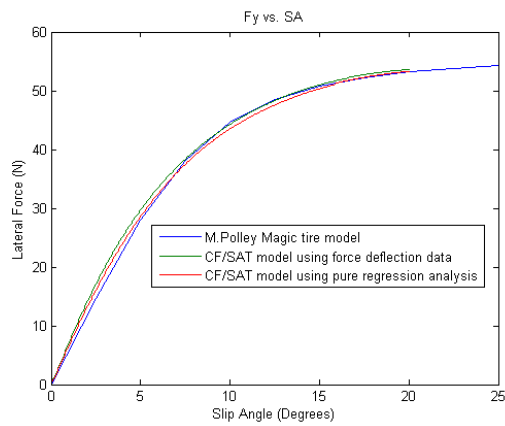
(c) 50 N normal load

Figure 5.13: *DUBRO 5.00 T.V. CF/SAT model results comparison.*
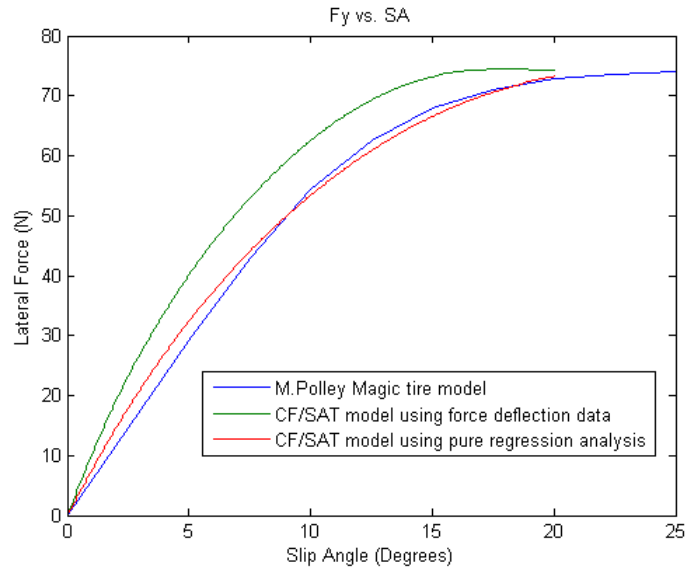
Figure 5.14: *DUBRO 5.00 T.V. CF/SAT model results comparison for 70 N normal load.*

of C_z varies as much as 294.2% from the estimated curve fit value, and the measured value of C_y

varies as much as 65.38% from the value estimated through the manual curve fit. This indicates that

while regression analysis is capable of determining parameters that force the model to match the

desired results, these parameters are not founded on the physical tire properties, and therefore lose

their meaning entirely. Since the values determined from the deflection data match the results ob-

tained from physical tire testing and consistently predict tire performance using the CF/SAT model,

then it is highly likely these values accurately reflect the intended physical interpretation as defined

in the CF/SAT model.

5.3.2   70 N Normal Load

Figure 5.14 shows the comparison of Polley's magic tire model to both the manual curve fit and

physically estimated parameters for the CF/SAT model for the 70 N test. In this case, it can be seen

the model estimates using the physically derived data correlate very poorly to the results obtained

by Polley and the manual curve fit. Since the relationships derived resulted in excellent correlation

at each of the normal loads previous to this test, it is likely not an error in the relationship, but in the test data obtained. As discussed in Section 5.1.2, the tire was separating from the wheel during the testing. It is unlikely this is the intended mode of operation for the tire and it is, therefore, assumed the tire was operating beyond its maximum recommended load. Since the effects of the observed behaviour on the load-deflection results obtained are unknown, it is reasonable to believe that the poor correlation of the physically estimated CF/SAT model to the results obtained by Polley is a possible result of this behaviour. Complete dismissal of this result, however, is imprudent, and further testing is required to understand how this behaviour affected the CF/SAT model results. Despite this, the excellent correlation observed in the previous three trials indicates a plausible relationship between the CF/SAT model parameters and the load deflection data was obtained.

Table 5.1: *Resultant CF/SAT parameters from load deflection estimates for the DU-BRO 5.00 T.V. tire.* Each parameter was either estimated directly from Polley, scaled values from Miyashita and Kabe using the developed non-dimensional parameters, or measured from the static load-deflection relationships. The source of each of the values is given in the last column.

Parameter	Normal load				Source of parameter
	70N	50N	30N	20N	
w	0.0225	0.0225	0.0225	0.0225	Measurement
μ_s	1.3	1.3	1.3	1.3	Polley
μ_d	1.05	1.08	1.17	1.25	Scaled
C_y	$3.8007x10^4$	$3.3119x10^4$	$4.5653x10^4$	$5.7301x10^4$	Measurement
ε	16.3515	22.8921	38.1535	57.2302	Scaled
EI_z	$8.312x10^{-4}$	$5.9372x10^{-4}$	$3.5623x10^{-4}$	$2.3749x10^{-4}$	Scaled
C_q	$1.208x10^3$	$1.6912x10^3$	$2.8186x10^3$	$4.2279x10^3$	Scaled
ζ	0.2034	0.2848	0.4746	0.7119	Scaled
A_{x_0}	0	0	0	0	Scaled
n	2.2	3.8	4.5	4.5	Scaled
C_z	18.229	18.229	18.229	18.229	Measurement

Chapter 6

Conclusions and Recommendations

The physical verification of vehicle dynamic models and control algorithms presents a challenge to researchers, both in terms of the resources available and cost associated with these types of studies. This is of particular concern to academia due to limited facilities and funding when compared to OEM efforts. The work presented in this thesis was aimed at alleviating some of the issues currently facing scale modelling approaches to physical vehicle dynamic studies. Particular emphasis was placed on the treatment of the tire due to a general lack of focus on this issue in previous studies.

The method by which this was accomplished was to first define the tire's behaviour in terms of a mathematical model in order to allow non-dimensional characterization of the tire. The CF/SAT model was selected and non-dimensionalized to serve this purpose. The non-dimensionalized CF/SAT model would allow direct comparison of the response between tires of differing scale. In order for this approach to remain viable, however, a method of characterizing an individual tire with this model was required without adding substantial cost, in terms of time and capital, to the approach. An exploratory study was then conducted to establish whether it was possible to define a tire in terms of the required model parameters without the use of a full battery of dynamic tire tests.

To limit the cost of this introductory analysis, a scale tire, the DUBRO 5.00 T.V. tire, was utilized to probe whether a simple set of static tire load-deflection tests could be used to characterize

a tire in terms of the CF/SAT model. The Windsor Automotive Tire Tester was then designed and constructed for the purpose of collecting static load-deflection data on the scale tire. This data was then analyzed and compared to the parameters that define tire performance within the CF/SAT model. A set of relationships were then developed to allow parameterization of the tire from the static tests.

6.1 Contributions

Three major contributions result from this work. The first of which is the non-dimensional CF/SAT model. The second is the Windsor Automotive Tire Tester, and the third is the set of parameterization relationships determined through the testing done with the WATT.

The results obtained from the non-dimensionalization of the CF/SAT model are discussed in section 3.3. This non-dimensionalized version of the original model allows the analyst to compare the dynamic response of two tires directly. By applying this non-dimensionalization to the tire independently from the non-dimensionalization of the vehicle, the findings of the scale vehicle model are no longer coupled with the tire's behaviour. This will allow for comparison of two different vehicles using the same tire, or even the comparison of the same vehicle with different tires. It also allows the analyst the ability to apply non-linear vehicle models without the need to operate within the linear regime of vehicle dynamics due to the tire. This will greatly broaden the applicability of the results obtained through scale vehicle studies and further reduce the need for full scale vehicle testing.

The WATT is a load-deflection testing machine specifically designed to statically perform tire testing on small scale tires. In its current configuration, it is capable of measuring both vertical and lateral load-deflection relationships for a tire. The cost associated with the construction of this testing apparatus is very low, allowing inexpensive replication at other facilities. This is important in order to allow continued research in this field to be easily accessible, as well as to allow tire characterization with little capital investment.

The most significant contribution of this work is the parameterization relationships discovered, which correlate the static test data to the CF/SAT parameters. Tire characterization, for scale studies or otherwise, is a prohibitively expensive endeavour. The relationships discovered here, detailed in section 5.2, indicate that it is possible to characterize a tire for mathematical modelling through the use of static load-deflection tests. Although this study was only exploratory in nature, the results indicate that more detailed research into static parameterization relationships is not only warranted, but is likely to deliver the desired results.

6.2 Future Work

The contributions made in this study, while significant, are hardly a complete picture of the desired outcome, a method by which to develop a scale tire for vehicle dynamics research. Much more work is required to find a means to this end. Despite this, the required work is justified not only to fulfill this specific goal, but also due to the many fringe benefits which result from this research. The most significant of these is the ability to determine tire response without the need of full scale dynamic testing.

6.2.1 Non-Dimensional CF/SAT Model

While some of the shortcomings of this model, for the purpose of a non-dimensional approach, discussed in section 3.1.1, have been alleviated, the issues surrounding the contact patch pressure distribution remain. In the CF/SAT model, the contact patch pressure distribution is defined empirically by a general skew parabolic distribution. This gives no information on the physical tire properties responsible for this response, making tire characterization based on analytical properties impossible. In order to allow for full physical non-dimensional characterization of this model, the relationship must be redefined in terms of measurable physical parameters. This will require the use of a large number of tires and a rather complex testing apparatus to find a consistent relationship between the pressure distribution and the pertinent tire properties, if one exists at all.

6.2.2 WATT

The WATT was successful at finding the required information for developing parameterization relationships for the vertical and lateral response of the tire. In order to determine relationships for the aligning moment response of the tire, further instrumentation is required. The ability to measure the aligning moment response of the tire during these static load tests is required to indicate if there are any relationships between the results and the CF/SAT model parameters. Some design elements were incorporated into the WATT to allow for this measurement; however, they were not utilized due to the inability to source an inexpensive method to measure the moment response of the tire. This could be done in a more expensive manner for the initial study; however, such an investment would diminish the benefit of the approach as a whole if a cheaper solution is not realized for implementation of the methodology.

6.2.3 Tire Parameterization

The most significant amount of research is required for greater understanding of static tire parameterization; however, the largest benefits can be realized from this work. The work done in this study on the topic was exploratory in nature; as a result, much more testing is required to determine the precision and accuracy with which these results can be obtained. Although the number of tests performed were statistically insufficient, and therefore the certainty of the relationships discovered cannot be ensured, the goal was to determine if, at minimum, an approximate relationship could be developed. It is imprudent to invest the time and capital into a full series of tests without any knowledge whether the desired outcome is possible. Despite this, the results are quite remarkable and warrant further research to determine, statistically, the value of these relationships.

Once this has been accomplished, this research should be conducted on a set of full size tires to determine if the relationships discovered, or ones similar to them, exist in full size tires. The tests will also require the use of a large variety of full size tire constructions to ensure any relationships discovered can be stated generally, allowing any desired tire to be defined in terms of the CF/SAT

model using a fixed set of tests and relationships. The scale and cost of such a research project would be substantial; however, if successful, the outcome would result in significant cost reduction of tire modelling for both researchers and industry.

6.3 Final Remarks

The research conducted in this thesis is very promising both in terms of scale modelling and tire modelling as a whole. Though more investigation is required to fully establish an approach for the development of a small scale tire for vehicle dynamics research, the results obtained in this study are a segue to both this realization and a method by which to ascertain tire response without the use of full scale dynamic tire testing.

References

[1] BELLIS, M. History of tires. `http://inventors.about.com/library/inventors/bltires.htm`, November 2012.

[2] BRENNAN, S. Modeling and control issues associatied with scaled vehicles. Master's thesis, University of Illinois at Urabana-Champaign, 1999.

[3] BUCKINGHAM, E. On physically similar systems: Illustrations of the use of dimensional equations. *Bureau of Standards 4*, 4 (1914), 345–376.

[4] ÇENGAL, Y., AND CIMBALA, J. *Fluid Mecahnics: Fundamamentals and Applications*. Mcgraw-Hill, 2006.

[5] DE BEVER, A. Dynamic behaviour of rubber and rubberlike materials. Tech. rep., WFW, 1992.

[6] DE WIT, C. C., OLSSON, H., ASTROM, K. J., AND LISCHINSKY, P. Dynamic friction models and control design. In *American Control Conference* (San Francisco, California, 1993), p. 19201926.

[7] DRESSEL, A. Tire pneumatic trail. `http://en.wikipedia.org/wiki/File:Tire_pneumatic_trail.png`, November 2012.

[8] DUGOFF, H., FANCHER, P., AND SEGEL, L. An analysis of tire traction properties and their influence on vehicle dynamics performance. *Society of Automotive Engineers* (1970).

[9] FIALA, E. Seitenkraft am rollenden luftreifen. *VDI 96* (1954).

[10] GILLESPIE, T. *Fundamentals of Vehicle Dynamics*. Society of Automotive Engineers, 1992.

[11] INSTRUMENTS, T. Ina128 ina129 precision, low power instrumentation amplifiers. Tech. rep., Texas Instruments, 2005.

[12] LABJACK. Labjack u12 user's guide. Tech. rep., LabJack, 2003.

[13] LAPAPONG, S., GUPTA, V., CALLEJAS, E., AND BRENNAN, S. Fidelity of using scaled vehicles for chassis dynamics studies. *Vehicle System Dynamics* (2008), 1–29.

[14] LIBURDI, A. Development of a scale vehicle dynamics testbed. Master's thesis, University ofWindsor, 2010.

[15] MILIKEN, W., AND MILIKEN, D. *Race Car Vehicle Dynamics*. Society of Automotive Engineers, 1995.

[16] MIYASHITA, N., AND KABE, K. A new analytical tire model for cornering simulation. part 1: Cornering power and self-aligning torque power. *Tire Science and Technology 34*, 2 (2006), 84–99.

[17] MIYASHITA, N., AND KABE, K. A new analytical tire model for cornering simulation. part 2: Cornering force and self-aligning torque. *Tire Science and Technology 34*, 2 (2006), 100–118.

[18] MULLINS, L., AND TOBIN, N. Stress softening in rubber vulcanizates part 1. use of a strain amplification factor to describe the elastic behaviour of filler reinforced vulcanizes rubber. *Journal of Polymer Science 9* (1965), 3011–3021.

[19] PACEJKA, H., AND BAKKER, E. The magic tyre model. *Vehicle System Dynamics 21*, sup001 (1992), 1–18.

[20] POLLEY, M. Size effects on steady state pneumatic tire behaviour: An experimental study. Master's thesis, University of Illinois at Urbana-Champaign, 2001.

[21] REZA, R. *Vehicle Dynamics Theory and Application*. Springer, 2008.

[22] RIEVELEY, R. *The Effect of Direct Yaw Moment on Human Controlled Vehicle Systems*. PhD thesis, University of Windsor, 2010.

[23] WADDELL, W., BHAKUNI, R., BARBIN, W., AND SANDSTROM, P. *Pneumatic Tire Compounding*. Goodyear Tire and Rubber Company, undated, pp. 596–611.

Appendix A

CF/SAT M-Code

A.1   User Main File

```
clc
clear all
close all
%------------------------------------------------------------------------
slip = 20;
res = 2.5;
%{
datset 1 full size tire modelled using original CF/SAT model
dataset 2 full size tire modelled using modifed CF/SAT model
dataset 3 Scale tire modelled using modified CF/SAT model
        tire parameters are calcualted from desired radius and normal
        load and pi parameters for the full size tire from dataset 2
dataset 4 Dubro tire response, using estimated parameters from polley
dataset 5 Dubro tire response, using estimated parameters from tire load ...
    deflection relationships
dataset 6-9 Original CF/SAT mode lused for sensitivity analysis
```

```
cf_sat(slip,resolution,dataset,pi parameters) calcualtes a tires lateral ...
    force
and aligning torque response for slip angles fr0m 0 to the value of slip
%}
[output1,press1,deflec1,x1,pi_param1,pi_out1,params1] = cf_sat(slip,res,1);
[output2,press2,deflec2,x2,pi_param2,pi_out2,params2] = cf_sat(slip,res,2);
[output3,press3,deflec3,x3,pi_param3,pi_out3,params3] = cf_sat(slip,res,3,...
    pi_param2);
[output4,press4,deflec4,x4,pi_param4,pi_out4,params4] = cf_sat(slip,res,4,...
    pi_param2);
[output5,press5,deflec5,x5,pi_param5,pi_out5,params5] = cf_sat(slip,res,5,...
    pi_param2);
% [output6,press6,deflec6,x6,pi_param6,pi_out6,params6] = cf_sat(slip,res,6);
% [output7,press7,deflec7,x7,pi_param7,pi_out7,params7] = cf_sat(slip,res,7);
% [output8,press8,deflec8,x8,pi_param8,pi_out8,params8] = cf_sat(slip,res,8);
% [output9,press9,deflec9,x9,pi_param9,pi_out9,params9] = cf_sat(slip,res,9);
polleyslip = xlsread('polley_tire_data','O41:O49');
polleylatforce = xlsread('polley_tire_data','S41:S49');%S is 50N data P is 20...
    N
polleyaligntor = xlsread('polley_tire_data','self aligning moment data','M8:...
    M18');


%-------------------------------------------------------------------------
% slipangle = 5; %slip angle of interest for pressure distibution
% figure('name','Fy vs. SA','numbertitle','off')
% plot(0:res:slip,output1(:,1),0:res:slip,output6(:,1),0:res:slip,output7...
    (:,1),0:res:slip,output8(:,1),0:res:slip,output9(:,1))
% title('Fy vs. SA')
% % axis([0,20,-inf,10])
% % set(gca,'Xtick',0:5:20)
% % set(gca,'Ytick',0:2:10)
```

```matlab
% legend('l: Reference value from case B','l: Reference-50%', 'l: -25%','l: ...
    +25%','l: +50%')
% xlabel('Slip Angle (Degrees)')
% ylabel('Lateral Force (KN)')


figure('name','Scale tire Fy vs. SA','numbertitle','off')
plot(polleyslip,polleylatforce,0:res:slip,output5(:,1)*1000)%, 0:res:slip,...
    output4(:,1)*1000)
legend('M.Polley Magic tire model','CF/SAT model using force deflection data'...
    ,'CF/SAT model using pure regression analysis')
title('Fy vs. SA')
xlabel('Slip Angle (Degrees)')
ylabel('Lateral Force (N)')


% figure('name','Mz vs. SA','numbertitle','off')
% plot(0:res:slip,output1(:,2),0:res:slip,output6(:,2),0:res:slip,output7...
    (:,2),0:res:slip,output8(:,2),0:res:slip,output9(:,2))%*1000,polleyslip,...
    polleyaligntor)
% title('Mz vs. SA')
% % axis([0,20,-inf,0.22])
% % set(gca,'Xtick',0:5:20)
% % set(gca,'Ytick',0:0.1:0.22)
% legend('l: Reference value from case B','l: Reference-50%', 'l: -25%','l: ...
    +25%','l: +50%')
% xlabel('Slip Angle (Degrees)')
% ylabel('Self-Aligning Torque (N M)')


% figure('name','Pressure Distribution')
% plot(x3(slipangle/res+1,:)*1000,press3(slipangle/res+1,:)*0.14504,x2(...
    slipangle/res+1,:)*1000,press2(slipangle/res+1,:)*0.14504)
% title('Pressure Distribtion')
% xlabel('longitudnal position (mm)')
% ylabel('Pressure (Psi)')
```

```
%
% figure('name','Lateral Belt Deflection')
% plot(x3(slipangle/res+1,:)*1000,deflec3(slipangle/res+1,:)*1000,x2(...
    slipangle/res+1,:)*1000,deflec2(slipangle/res+1,:)*1000)
% title('Lateral Belt Deflection')
% xlabel('longitudnal position (mm)')
% ylabel('lateral deflection(mm)')
```

A.2 CF/SAT Main File

```
function [output,press,deflec,pos,pi_param,pi_out,params] = cf_sat(slip,res,...
    dataset,pi_param_full)
i=1;
j=1;
k = 1;
%-------------------------------------------------------------------------
%Finds the lateral and moment forces
switch dataset
    case {1}
        disp('Using dataset with original CF_SAT method')
        for slipangle = 0:res:slip
            fy(j,1) = 0; %KN
            mz(j,1) = 0; %KN
                for i = 2:100
                    params(j) = tire_params_1(slipangle,fy(j,i-1),mz(j,i-1));
                    [fy(j,i)] = cf(slipangle,fy(j,i-1),mz(j,i-1),params(j));
                     mz(j,i) = sat(slipangle,fy(j,i),mz(j,i-1),params(j));
                        if abs(fy(j,i)-fy(j,i-1)) < 0.001 && abs(mz(j,i)-mz(j...
                            ,i-1)) < 0.001
                            output(j,1) = fy(j,i);
                            output(j,2) = mz(j,i);
```

```matlab
                    for x = 0:0.01*params(j).l:params(j).l
                            press(j,k) = pressuredist(x,params(j));
                            deflec(j,k) = beltdeflec(x,params(j));
                            pos(j,k) = x-params(j).l/2;
                            pi(j,:) = pi_params_orig(params(j));
                            k=k+1;
                    end
                    pi_out(j,1) = pi(j,1);
                    pi_out(j,2) = pi(j,2);
                break
                else
                continue
                end
        end
        j=j+1;
        k=1;
    end
 pi_param(:,1) = pi(1,3:13);
     case {2}
 disp('Using dataset with modified CF/SAT method')
for slipangle = 0:res:slip
    fy(j,1) = 0; %KN
    mz(j,1) = 0; %KN
        for i = 2:100
            params(j) = tire_params_2(slipangle,fy(j,i-1),mz(j,i-1));
            fy(j,i) = cf(slipangle,fy(j,i-1),mz(j,i-1),params(j));
             mz(j,i) = sat(slipangle,fy(j,i),mz(j,i-1),params(j));
                if abs(fy(j,i)-fy(j,i-1)) < 0.001 && abs(mz(j,i)-mz(j...
                    ,i-1)) < 0.001
                    output(j,1) = fy(j,i);
                    output(j,2) = mz(j,i);
                    for x = 0:0.01*params(j).l:params(j).l
                            press(j,k) = pressuredist(x,params(j));
```

```matlab
                            deflec(j,k) = beltdeflec(x,params(j));

                            pos(j,k) = x-params(j).l/2;

                            pi(j,:) = pi_params(params(j));

                            k=k+1;

                    end

                    pi_out(j,1) = pi(j,1);

                    pi_out(j,2) = pi(j,2);

                break

                else

                continue

                end

        end

        j=j+1;

        k=1;

    end

    pi_param(:,1) = pi(1,3:13);

case {3}

    display('Using scale tire dataset')

    for slipangle = 0:res:slip

        fy(j,1) = 0; %KN

        mz(j,1) = 0; %KN

            for i = 2:100

                params(j) = tire_params_3(slipangle,fy(j,i-1),mz(j,i-1),...
                    pi_param_full);

                [fy(j,i)] = cf(slipangle,fy(j,i-1),mz(j,i-1),params(j));

                 mz(j,i) = sat(slipangle,fy(j,i),mz(j,i-1),params(j));

                    if abs(fy(j,i)-fy(j,i-1)) < 0.001 && abs(mz(j,i)-mz(j...
                        ,i-1)) < 0.001

                        output(j,1) = fy(j,i);

                        output(j,2) = mz(j,i);

                        for x = 0:0.01*params(j).l:params(j).l

                                press(j,k) = pressuredist(x,params(j));

                                deflec(j,k) = beltdeflec(x,params(j));
```

```matlab
                            pos(j,k) = x-params(j).l/2;
                            pi(j,:) = pi_params(params(j));
                            k=k+1;
                    end
                    pi_out(j,1) = pi(j,1);
                    pi_out(j,2) = pi(j,2);
                break
                else
                continue
                end


            end
            j=j+1;
            k=1;
        end
        pi_param(:,1) = pi(1,3:13);
case {4}
        display('Using estimated CF/SAT model for 5.00T.V. Dubro tire')
        for slipangle = 0:res:slip
            fy(j,1) = 0; %KN
            mz(j,1) = 0; %KN
                for i = 2:100
                    params(j) = tire_params_4(slipangle,fy(j,i-1),mz(j,i-1),...
                        pi_param_full);
                    [fy(j,i)] = cf(slipangle,fy(j,i-1),mz(j,i-1),params(j));
                     mz(j,i) = sat(slipangle,fy(j,i),mz(j,i-1),params(j));
                        if abs(fy(j,i)-fy(j,i-1)) < 0.001 && abs(mz(j,i)-mz(j...
                            ,i-1)) < 0.001
                            output(j,1) = fy(j,i);
                            output(j,2) = mz(j,i);
                            for x = 0:0.01*params(j).l:params(j).l
                                    press(j,k) = pressuredist(x,params(j));
                                    deflec(j,k) = beltdeflec(x,params(j));
```

```matlab
                            pos(j,k) = x-params(j).l/2;
                            pi(j,:) = pi_params(params(j));
                            k=k+1;
                    end
                    pi_out(j,1) = pi(j,1);
                    pi_out(j,2) = pi(j,2);
                break
                else
                continue
                end


        end
        j=j+1;
        k=1;
    end
    pi_param(:,1) = pi(1,3:13);
    case {5}
     display('Using measured CF/SAT model for 5.00T.V. Dubro tire')
    for slipangle = 0:res:slip
        fy(j,1) = 0; %KN
        mz(j,1) = 0; %KN
            for i = 2:100
                params(j) = tire_params_5(slipangle,fy(j,i-1),mz(j,i-1),...
                    pi_param_full);
                [fy(j,i)] = cf(slipangle,fy(j,i-1),mz(j,i-1),params(j));
                 mz(j,i) = sat(slipangle,fy(j,i),mz(j,i-1),params(j));
                    if abs(fy(j,i)-fy(j,i-1)) < 0.001 && abs(mz(j,i)-mz(j...
                        ,i-1)) < 0.001
                        output(j,1) = fy(j,i);
                        output(j,2) = mz(j,i);
                            for x = 0:0.01*params(j).l:params(j).l
                                press(j,k) = pressuredist(x,params(j));
                                deflec(j,k) = beltdeflec(x,params(j));
```

```matlab
                                pos(j,k) = x-params(j).l/2;
                                pi(j,:) = pi_params(params(j));
                                k=k+1;
                        end
                        pi_out(j,1) = pi(j,1);
                        pi_out(j,2) = pi(j,2);
                    break
                    else
                    continue
                    end


        end
        j=j+1;
        k=1;
    end
    pi_param(:,1) = pi(1,3:13);


    case {6}
    disp('Using dataset with original CF_SAT method sensitivity analysis'...
        )
    for slipangle = 0:res:slip
        fy(j,1) = 0; %KN
        mz(j,1) = 0; %KN
            for i = 2:100
                params(j) = tire_params_6(slipangle,fy(j,i-1),mz(j,i-1));
                [fy(j,i)] = cf(slipangle,fy(j,i-1),mz(j,i-1),params(j));
                 mz(j,i) = sat(slipangle,fy(j,i),mz(j,i-1),params(j));
                    if abs(fy(j,i)-fy(j,i-1)) < 0.001 && abs(mz(j,i)-mz(j...
                        ,i-1)) < 0.001
                        output(j,1) = fy(j,i);
                        output(j,2) = mz(j,i);
                        for x = 0:0.01*params(j).l:params(j).l
                                press(j,k) = pressuredist(x,params(j));
```

```matlab
                                deflec(j,k) = beltdeflec(x,params(j));
                                pos(j,k) = x-params(j).l/2;
                                pi(j,:) = pi_params_orig(params(j));
                                k=k+1;
                        end
                        pi_out(j,1) = pi(j,1);
                        pi_out(j,2) = pi(j,2);
                    break
                    else
                    continue
                    end
            end
            j=j+1;
            k=1;
    end
 pi_param(:,1) = pi(1,3:13);
     case {7}
disp('Using dataset with original CF_SAT method sensitivity analysis'...
     )
for slipangle = 0:res:slip
    fy(j,1) = 0; %KN
    mz(j,1) = 0; %KN
        for i = 2:100
            params(j) = tire_params_7(slipangle,fy(j,i-1),mz(j,i-1));
            [fy(j,i)] = cf(slipangle,fy(j,i-1),mz(j,i-1),params(j));
             mz(j,i) = sat(slipangle,fy(j,i),mz(j,i-1),params(j));
                if abs(fy(j,i)-fy(j,i-1)) < 0.001 && abs(mz(j,i)-mz(j...
                    ,i-1)) < 0.001
                    output(j,1) = fy(j,i);
                    output(j,2) = mz(j,i);
                    for x = 0:0.01*params(j).l:params(j).l
                            press(j,k) = pressuredist(x,params(j));
                            deflec(j,k) = beltdeflec(x,params(j));
```

```matlab
                            pos(j,k) = x-params(j).l/2;
                            pi(j,:) = pi_params_orig(params(j));
                            k=k+1;
                    end
                    pi_out(j,1) = pi(j,1);
                    pi_out(j,2) = pi(j,2);
                break
                else
                continue
                end
        end
        j=j+1;
        k=1;
    end
 pi_param(:,1) = pi(1,3:13);
    case {8}
disp('Using dataset with original CF_SAT method sensitivity analysis'...
    )
for slipangle = 0:res:slip
    fy(j,1) = 0; %KN
    mz(j,1) = 0; %KN
        for i = 2:100
            params(j) = tire_params_8(slipangle,fy(j,i-1),mz(j,i-1));
            [fy(j,i)] = cf(slipangle,fy(j,i-1),mz(j,i-1),params(j));
             mz(j,i) = sat(slipangle,fy(j,i),mz(j,i-1),params(j));
                if abs(fy(j,i)-fy(j,i-1)) < 0.001 && abs(mz(j...
                    ,i-1)) < 0.001
                    output(j,1) = fy(j,i);
                    output(j,2) = mz(j,i);
                    for x = 0:0.01*params(j).l:params(j).l
                            press(j,k) = pressuredist(x,params(j));
                            deflec(j,k) = beltdeflec(x,params(j));
                            pos(j,k) = x-params(j).l/2;
```

```matlab
                                    pi(j,:) = pi_params_orig(params(j));

                                    k=k+1;
                        end
                        pi_out(j,1) = pi(j,1);
                        pi_out(j,2) = pi(j,2);
                break
                else
                continue
                end
        end
        j=j+1;
        k=1;
    end
 pi_param(:,1) = pi(1,3:13);
    case {9}
disp('Using dataset with original CF_SAT method sensitivity analysis'...
    )
for slipangle = 0:res:slip
    fy(j,1) = 0; %KN
    mz(j,1) = 0; %KN
        for i = 2:100
            params(j) = tire_params_9(slipangle,fy(j,i-1),mz(j,i-1));
            [fy(j,i)] = cf(slipangle,fy(j,i-1),mz(j,i-1),params(j));
             mz(j,i) = sat(slipangle,fy(j,i),mz(j,i-1),params(j));
                if abs(fy(j,i)-fy(j,i-1)) < 0.001 && abs(mz(j,i)-mz(j...
                    ,i-1)) < 0.001
                    output(j,1) = fy(j,i);
                    output(j,2) = mz(j,i);
                    for x = 0:0.01*params(j).l:params(j).l
                            press(j,k) = pressuredist(x,params(j));
                            deflec(j,k) = beltdeflec(x,params(j));
                            pos(j,k) = x-params(j).l/2;
                            pi(j,:) = pi_params_orig(params(j));
```

```
                                                k=k+1;
                                            end
                                            pi_out(j,1) = pi(j,1);
                                            pi_out(j,2) = pi(j,2);
                                        break
                                        else
                                        continue
                                        end
                            end
                        j=j+1;
                        k=1;
            end
             pi_param(:,1) = pi(1,3:13);
                    otherwise
                error('Please select a valid case')
end
return
```

A.3   Cornering Force Function

```
function [Fy] = cf(slipangle,fy,mz,params)
Fy = 2*params.Kyo*quadgk(@(t) shearforce(t,params),0,params.lh/params.l)+((...
    params.n +1)/params.n)*params.Mu_d*params.Fz*quadgk(@(f) Dgsp(f,params.n,...
    params.q),params.lh/params.l,1);
end
```

A.4   Aligning Moment Function

```
function [Mz] = sat(slipangle,fy,mz,params)
```

```
Mz = 12*params.Aso*quadgk(@(t) shearmoment(t,params),0,params.lh/params.l)+((...
    params.n +1)/params.n)*params.Mu_d*params.Fz*params.l*quadgk(@(f) ...
    Dgspmoment(f,params),params.lh/params.l,1)+params.Axo*(params.lh/params.l)...
    *tan(params.ae);
end
```

A.5   Belt Deflection Function

```
function [y] = beltdeflec(x,params)
y = params.eps.*params.l^2.*params.Fy.*(x/params.l).*(1-(x/params.l));
end
```

A.6   Contact Patch Pressure Distribution Due to Lateral Force

```
function [D] = Dgsp(t,n,q)
D = (1-abs(2.*t-1).^n).*(1-q.*(2.*t-1));
end
```

A.7   Contact Patch Pressure Distribution Due to Aligning Torque

```
function [D] = Dgspmoment(t,params)
D = ((1-abs(2.*t-1).^params.n).*(1-params.q.*(2.*t-1))).*(t-(params.xc/...
    params.l));
end
```

A.8   Calculation of the Location for Transition from Grip to Sliding

```matlab
function [eq] = grip2slip(lhf,params)
eq = 2*params.Kyo*lhf/params.l*(tan(params.ae)-(params.eps*params.l*params.Fy...
    *(1-lhf/params.l)))-(((params.n+1)/params.n)*params.Mu_s*params.Fz*Dgsp(...
    lhf/params.l,params.n,params.q));
end
```

A.9   Pi Parameter Calculation Function

```matlab
%Sean Maloney CF/SAT model
%Tire parameters
function [pi] = pi_params(params)
%Repeated parameters
r0 = params.r0; %Tire radius in meters
Fz = params.Fz; %vertical load in KN
%----------------------------------------------------------
pi(1) = params.Fy/Fz;
pi(2) = params.Mz/(Fz*r0); %Width of contact patch in meters
pi(3) = params.w/r0;
pi(4) = params.Mu_s;
pi(5) = params.Mu_d;
pi(6) = params.Cy*r0^3/Fz;
pi(7) = params.eps*Fz*r0;
pi(8) = params.EIz/(Fz*r0^2);
pi(9) = params.Cq*Fz*r0;
pi(10) = params.zeta*Fz/r0;
pi(11) = params.Axo/(Fz*r0);
pi(12) = params.n;
pi(13) = params.Cz*Fz/r0;
end
```

A.10   Shear Force Calculation

```
function [Fshear] = shearforce(t,params)
Fshear = t*tan(params.ae)-(params.eps*params.l*params.Fy*t.*(1-t));
end
```

A.11 Shear Moment Calculation

```
function [Mshear] = shearmoment(t,params)
Mshear = (t.*tan(params.ae)-(params.eps*params.l*params.Fy.*t.*(1-t))).*(t-(...
    params.xc/params.l));
end
```

A.12 Input Files

A.12.1 Modified CF/SAT Model Input File

```
%Sean Maloney CF/SAT model
%Tire parameters
function [params] = tire_params_2(a,Fy,Mz)
%----------------------------------------------------------
params.n = 9.34; %Shoulder exponent for tire pressure distrobution
% ^
%/|\
% |
% |
%perhaps this should be a function of pressure?
%------------------------------------------------------------------------------
%Tire properties

%These are easily estimated directly
params.w = 0.205; %Width of contact patch in meters
```

```matlab
params.r0 = 0.31595; %Tire radius in meters

params.Fz = 3.98; %vertical load in KN

%for finding effective radius

%params.press = 18; %pressure in psi inteded for finding effective radius

params.Cz = -0.0023; %vertical stiffness M/KN


%How to estimate these?

params.Cy = 8.02*10^4; %Lateral spring constant of tread element

params.eps = 5.78*10^-2; %deflection compliance of belt

params.Cq = 4.27; %Compliance of front inclination in contact pressure

params.zeta = 1.78*10^-2; %Compliance of contact-patch shift

params.Axo = 0; %longitudinal force torque stiffness

params.EIz = 1.17; %Bending ridgity of the belt
%-------------------------------------------------------------------------
%Tire properties that should be functions of other properties

%params.l = 0.0902;  Length of contact patch in meters, should be a function ...
    of tire pressure

%normal load,tire radius, aspect ratio


params.Mu_s = 1.62; %static coefficent of friction

params.Mu_d = 1.06; %dynamic coefficent of friction

% perhaps considering revising to account for simliairty to non

% dimensionalized lateral force
%-------------------------------------------------------------------------


%Resultant properties

params.arad = deg2rad(a); %converts degree input to radians


%testing results of updating contact patch length by normal load deflection

params.re = params.Cz*params.Fz+params.r0;

params.l = 2*sqrt((params.r0^2-params.re^2));


params.Fy = Fy;
```

```matlab
params.Mz = Mz;

params.q = params.Cq*params.Mz;

params.xc = params.l/2 - (params.zeta*params.Mz/params.l);

params.Kyo = params.Cy*params.w*params.l^2/2;

params.Aso = params.Cy*params.w*params.l^3/12;

params.ky = ((4^(4/5)*((params.EIz)^(3/4))*params.eps)^-4); %elastic modulus ...
    of the sidewall

params.G_mz = params.ky*pi()*params.re^3; %rotational stiffness of sidewall

params.ae = params.arad - (Mz/params.G_mz);

if grip2slip(0.001,params) < 0

[params.lh] = fzero(@(lhf) grip2slip(lhf,params),[0.001,params.l]);

else

    params.lh = 0;

end


end
```

A.12.2 manual DUBRO fit CF/SAT Model Input File

```matlab
%Sean Maloney CF/SAT model
%Tire parameters for Dubro tire
function [params] = tire_params_4(a,Fy,Mz,pi_param)
%-----------------------------------------------------------
params.n = 3.8; %modified %for 70N use 2.2 for 50N use 3.8 for 30N use 4.5 ...
    for 20N use 4.5
%Affects curvature


%------------------------------------------------------------------------
%These are easily estimated directly
params.w = 22.5/1000; %measured
params.r0 = 0.0635; %measured
params.Fz = 50/1000; %from polley
```

```matlab
params.Cz = (pi_param(11)*params.r0./params.Fz)*0.64;  %modified 70N use 0.53...
    50N use 0.64 use 0.7 30N 0.78 for 20N
%How to estimate these?
params.Cy = (pi_param(4)*params.Fz/params.r0^3)*0.535; %modified %70N use 0.5...
    use 0.535 for 50N 0.735 for 30N 0.95 for 20N
params.eps = pi_param(5)/(params.Fz*params.r0); %estimated from known full ...
    size tire
params.Cq = pi_param(7)/(params.Fz*params.r0); %estimated from known full ...
    size tire
params.zeta = pi_param(8)*params.r0/params.Fz; %estimated from known full ...
    size tire
params.Axo = pi_param(9)*(params.Fz*params.r0);%estimated from known full ...
    size tire
params.EIz =pi_param(6)*(params.Fz*params.r0^2); %estimated from known full ...
    size tire
%-------------------------------------------------------------------------
params.Mu_s = 1.3; %estimate from polley
params.Mu_d = 1.08; %modified 1.05 for 70N 1.08 for 50N 1.17 for 30N 1.25 for...
    20N
%-------------------------------------------------------------------------

%Resultant properties
params.arad = deg2rad(a); %converts degree input to radians

%testing results of updating contact patch length by normal load deflection
params.re = params.Cz*params.Fz+params.r0;
params.l = 2*sqrt((params.r0^2-params.re^2));

params.Fy = Fy;
params.Mz = Mz;
params.q = params.Cq*params.Mz;
params.xc = params.l/2 - (params.zeta*params.Mz/params.l);
params.Kyo = params.Cy*params.w*params.l^2/2;
```

```matlab
params.Aso = params.Cy*params.w*params.l^3/12;

params.ky = ((4^(4/5)*((params.EIz)^(3/4))*params.eps)^-4); %elastic modulus ...
    of the sidewall

params.G_mz = params.ky*pi()*params.re^3; %rotational stiffness of sidewall

params.ae = params.arad - (Mz/params.G_mz);

if grip2slip(0.001,params) < 0

[params.lh] = fzero(@(lhf) grip2slip(lhf,params),[0.001,params.l]);

else

    params.lh = 0;

end


end
```

A.12.3   Static Testing Parameterization of DUBRO tire for CF/SAT Model Input File

```matlab
%Sean Maloney CF/SAT model

%Tire parameters for Dubro tire

function [params] = tire_params_5(a,Fy,Mz,pi_param)


%20 PARAMS GOOD

% 30 PARAMS GOOD

%40 PARAMS NEED FITTING

%50 params good

%70 params not good

%-----------------------------------------------------

params.n = 3.8; %modified %for 70N use 2.2 for 50N use 3.8 for 30N use 4.5 ...
    for 20N use 4.5

%Affects curvature


%----------------------------------------------------------------------

%Tire properties
```

```
%These are easily estimated directly

params.w = 22.5/1000; %measured

params.r0 = 0.0635; %measured

params.Fz = 50/1000; %from polley

params.Cz = -0.0548;

  %modified 70N use 0.53 50N use 0.59 use 0.7 30N 0.78 for 20N

%How to estimate these?

%params.Cy = pi_param(4)*params.Fz/params.r0^3*0.58; %modified %70N use 1.02 ...

    use 1.14 for 50N 1.4 for 30N 1.7 for 20N


params.eps = pi_param(5)/(params.Fz*params.r0); %estimated from known full ...

    size tire

params.Cq = pi_param(7)/(params.Fz*params.r0); %estimated from known full ...

    size tire

params.zeta = pi_param(8)*params.r0/params.Fz; %estimated from known full ...

    size tire

params.Axo = pi_param(9)*(params.Fz*params.r0);%estimated from known full ...

    size tire

params.EIz =pi_param(6)*(params.Fz*params.r0^2); %estimated from known full ...

    size tire

%-------------------------------------------------------------------------

params.Mu_s = 1.3; %estimate from polley

params.Mu_d = 1.08; %modified 1.05 for 70N 1.08 for 50N 1.17 for 30N 1.25 for...

    20N

%-------------------------------------------------------------------------


%Resultant properties

params.arad = deg2rad(a); %converts degree input to radians


%testing results of updating contact patch length by normal load deflection

params.re = params.Cz*params.Fz+params.r0;

params.l = 2*sqrt((params.r0^2-params.re^2));
```

```matlab
%params.Cy = (2.9734*98.1)/(params.l^2+params.w^2+params.r0^2); % 20N actual ...
    average stiffness
%params.Cy = (2.4957*98.1)/(params.l^2+params.w^2+params.r0^2); % 30N actual ...
    average stiffness
%params.Cy = 205/(params.l^2+params.w^2+params.r0^2); % 40N estimated average
%stiffness
params.Cy = (1.992*98.1)/(params.l^2+params.w^2+params.r0^2); %actual average...
     stiffness 50N
%params.Cy = (2.286*98.1)/(params.l^2+params.w^2+params.r0^2); %70N actual ...
    average stiffness
%params.Cy = 160/(params.l^2+params.w^2+params.r0^2); %fitted 70N


params.Fy = Fy;
params.Mz = Mz;
params.q = params.Cq*params.Mz;
params.xc = params.l/2 - (params.zeta*params.Mz/params.l);
params.Kyo = params.Cy*params.w*params.l^2/2;
params.Aso = params.Cy*params.w*params.l^3/12;
params.ky = ((4^(4/5)*((params.EIz)^(3/4))*params.eps)^-4); %elastic modulus ...
    of the sidewall
params.G_mz = params.ky*pi()*params.re^3; %rotational stiffness of sidewall
params.ae = params.arad - (Mz/params.G_mz);
if grip2slip(0.001,params) < 0
[params.lh] = fzero(@(lhf) grip2slip(lhf,params),[0.001,params.l]);
else
    params.lh = 0;
end


end
```

Vita Auctoris

Name: Sean M. Maloney

Born: Natick, Massachusetts, United States of America, 1986

Education: 2003-2004 Norristown Area Highschool, Norristown, Pennsylvania, United States of America

2006-2010 Honours Bachelor of Applied Science with Automotive Option, Mechanical Engineering, University of Windsor, Windsor, Ontario, Canada